ADAPTIVE OPTICS

GUIDE

OKO Technologies

Polakweg 10-11, 2288 GG, Rijswijk ZH,
The Netherlands

ISBN: 90-8559-164-3

Third edition, April 2008

http://www.okotech.com

Polakweg 10-11, 2288 GG Rijswijk ZH, the Netherlands
PO Box 581, 2600AN Delft, the Netherlands

Editors: M. Loktev, O. Soloviev, G. Vdovin
E-mail: oko@okotech.com

Printed in the Netherlands

Contents

1

INTRODUCTION

This document describes the basic principles of wavefront measurement and correction using the current production line of OKO Technologies (Flexible Optical BV), including Micromachined Membrane Deformable Mirrors (MMDM), Piezoelectric Deformable Mirrors (PDM), liquid crystal (LC) adaptive lenses and Shack-Hartmann wavefront sensors.

1.1 Active and adaptive optics

OKO Technologies produces components for *active* and *adaptive optics* applications. We shall start from explaining these key terms.

To provide accommodation and focusing in a wide range, optical systems need to have adjustable design. In the majority of systems adjustment is done mechanically, by varying the configuration of the system. Another adjustment method is to use adjustable, or *active*, optical components. An example of such an active optical element in nature is the crystalline lens of the human eye, whose focusing power can be changed by the eye muscles. In optical instruments, however, active components are not yet applied very often, but there is a growing interest. Moreover, they have a potential to become the key element in future optical systems.

Active elements can fulfil another function - they can compensate for aberrations in the optical system, keeping them in the required range of tolerances for the whole range of operation. *Aberrations* are wavefront errors that lead to reduced resolution or power efficiency of the system. They are caused by imperfections of the optical elements and external conditions, such as turbulence of the ambient media and thermal effects. Aberrations can largely be compensated in the optical design, but their contribution is definitive in large-

aperture high-resolution systems, systems for imaging in highly aberrated media, and laser systems which are highly sensitive to energy losses. In these cases active compensation of aberrations is crucially important, and here we often use the term *"adaptive optics"*.

Adaptive optics (AO) is a rapidly developing branch of applied optics [1] whose purpose is to increase the resolution of optical systems by active compensation of phase aberrations. Although there is no consensus about the use of the terms *"active optics"* and *"adaptive optics"*, the use of the last term normally assumes use of a higher bandwidth (> 10 Hz) and the presence of a wavefront sensor coupled with an active optical element in a feedback loop.

1.2 Wavefront measurement

"Wavefront" is a key term in adaptive optics. We shall use the following definition. The electric field vector of a monochromatic light wave can be represented in the form

$$\mathbf{E}(\mathbf{r},t) = \mathbf{E}(\mathbf{r})\mathbf{e}^{i(\mathbf{kr}+\varepsilon(\mathbf{r}))}\mathbf{e}^{-i\omega t}, \tag{1.1}$$

where k is the wave vector, which is perpendicular to the electric field and has a modulus related to the wavelength λ as $k = 2\pi/\lambda$; ω is the angular frequency related to the temporal frequency ν as $\omega = 2\pi\nu$; $\mathbf{E}(\mathbf{r})$ describes the amplitude, and $\varphi(\mathbf{r}) = \mathbf{kr} + \varepsilon(\mathbf{r})$ the phase of the oscillating field $\mathbf{E}$. The surfaces joining all points of equal phase are known as *wavefronts*. The wavefront surface can be described by the equation $\varphi(\mathbf{r}) = \varphi_0$, where φ_0 is a constant.

The distribution of the optical phase in a certain plane, such as the pupil plane of an optical system, provides a good approximation of the wavefront in many cases. This is the reason why the measurement of the optical phase distribution is often referred to as *"wavefront measurement"* or *"wavefront sensing"*. However, this does not apply for strong aberrations, especially if these are accompanied by significant amplitude modulation and wavefront dislocations; in this situation both the amplitude and phase distributions should be analyzed.

A short overview of the most popular wavefront measurement methods - interferometric methods and Shack-Hartmann test - is given below.

1.2.1 Interferometric analysis

Interferometric methods are widely used in optical shop testing. Standard interferometric optical setup uses two (or more) coherent light beams. The first one (main beam) contains information about the object being analyzed; the object is either reflective or transparent. The second beam, which has a flat or spherical wavefront, is used as a reference. Let us suppose that the electric

fields of these light beams are identically oriented and have equal magnitudes E_0 but different phases in the measurement plane,

$$\begin{aligned} \mathbf{E}_1(\mathbf{r},t) &= \mathbf{E}_0(\mathbf{r})\mathbf{e}^{-i\omega t}, \\ \mathbf{E}_2(\mathbf{r},t) &= \mathbf{E}_0(\mathbf{r})\mathbf{e}^{i\varphi(\mathbf{r})}\mathbf{e}^{-i\omega t}. \end{aligned} \tag{1.2}$$

The phase difference φ results from the path-length difference ΔL between the waves and can be written as

$$\varphi = 2\pi\frac{\Delta L}{\lambda}, \tag{1.3}$$

where λ is the wavelength of light. Now, the net electric field has magnitude

$$\mathbf{E}_{net}(\mathbf{r},t) = |\mathbf{E}_1 + \mathbf{E}_2| = 2E_0\cos\left(\frac{\varphi(\mathbf{r})}{2}\right)\mathbf{e}^{i\varphi(\mathbf{r})/2}\mathbf{e}^{-i\omega t}. \tag{1.4}$$

Photo-detectors, such as photodiodes and CCD cameras, can detect only intensity of the light field, which is the time average of E^2. If we write individual intensities as $I_0 = E_0^2/2$ then the net intensity from the two light waves can be expressed as

$$I_{net}(\mathbf{r}) = 4I_0\cos^2\left(\frac{\varphi(\mathbf{r})}{2}\right) = 4I_0\cos^2\left(\frac{\pi\Delta L(\mathbf{r})}{\lambda}\right). \tag{1.5}$$

The intensity distribution $I_{net}(\mathbf{r})$ can be used to obtain information about the phase distribution $\varphi(\mathbf{r})$ or the wavefront difference $\Delta L(\mathbf{r})$. Extraction of phase from this intensity distribution is usually meant under wavefront reconstruction in interferometry. In general case the problem of phase reconstruction is ill-posed, and there are numerous techniques to get rid of ambiguity in the reconstruction.

Interferometric methods cover a wide range of measurement problems from shape to roughness measurements and may provide accuracy up to subnanometer range. However, as the most reliable methods are either calculation intensive or require multiple measurements, they are difficult to use for the real-time wavefront analysis.

1.2.2 Hartmann test

Among many approaches to test the quality of optical components in the industry and to get the real time wavefront information in adaptive optics, *Hartmann test* has its own distinct place. Hartmann (and *Shack-Hartmann*) tests are simple and can be explained in terms of pure geometrical optics.

The wavefront to be reconstructed is sampled by a screen with many subapertures (in Hartmann test) or by a dense array of lenslets (Shack-Hartmann

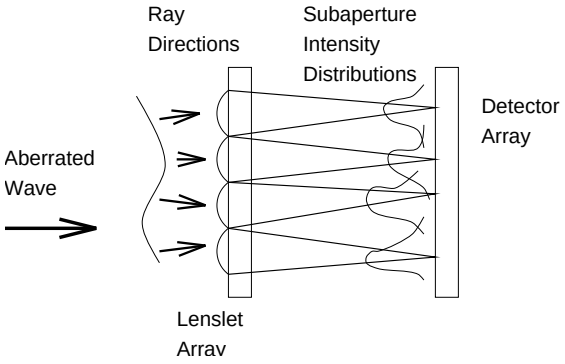

Figure 1.1: *Principle of Shack-Hartmann test*

test) - see Figure 1.1. Each sub-aperture (lenslet) produces a light spot on the screen or position sensitive detector. Position of the light spot is associated with the local slope of the incoming wavefront, averaged over the sub-aperture (lenslet) area. After all local slopes of the wavefront are registered, one can reconstruct the shape of the wavefront. Shack-Hartmann method has the advantages of gathering more light power per spot and covering the whole sensing area.

The results of the test are very robust and easy to interpret. This advantage made the Shack-Hartmann sensor the most popular tool for real-time wavefront measurements in adaptive optics. It is also suitable for shape measurements in optical shop testing. OKO Technologies offers both Shack and Shack-Hartmann sensors and *"FrontSurfer"* software for wavefront reconstruction. The sensor consist of a custom-made Hartmann mask or lenslet array coupled to a high-resolution CCD or CMOS camera.

1.3 Wavefront correction

The wavefront shape can be corrected by modifying the optical phase profile. The core principle used in the *wavefront correction* is *phase conjugation*. For wavefront correction the correcting phase profile should be optically conjugated to the measured phase aberration. Correction with the conjugated phase profile results in an ideal flat wavefront. However, if the wavefront cannot be precisely determined or precisely replicated by the relay optics, or if diffraction effects dominate, the phase conjugation cannot be precisely employed.

Operation of phase modulation devices is based on control of the optical path difference (OPD), which can be written as $\mathrm{OPD} = n\Delta z$, where n is the refractive index, and Δz is the physical distance travelled by the wave. OPD is

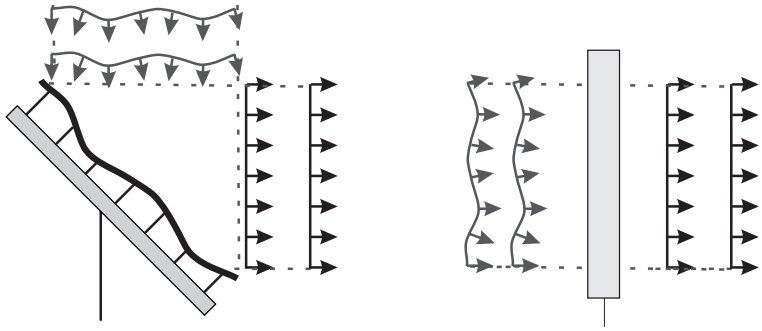

Figure 1.2: *Principle of wavefront correction in deformable mirrors (on the left) and LC phase modulators (on the right).*

related to the phase φ as $\varphi = 2\pi \cdot \mathrm{OPD}/\lambda$.

Deformable mirrors, which is the primary technology for wavefront correctors, modulate Δz, operating in the reflective mode - see Figure 1.2 on the left. *Liquid crystal (LC) phase modulators* represent a low-cost alternative to mechanically driven mirrors; their operation is based on modulation of n of the LC layer under the applied electric field in transparent or reflective mode (Figure 1.2 on the right).

Wavefront correctors are traditionally subdivided into two classes according to the implemented compensation technique - *zonal* and *modal*. Zonal correctors such as segmented piston and tip-tilt mirrors allow individual control of a phase over a set of subapertures providing step-wise phase compensation, whereas modal ones such as deformable mirrors use a set of smooth functions (modes, or influence functions) to approximate the required phase function.

Modal-type deformable mirrors are presented in a series of modifications: membrane, bimorph and continuous faceplate mirrors with different geometries of actuators and boundary conditions. OKO Technologies produces membrane mirrors based on micromachining technology and continuous faceplate mirrors with piezoelectric actuators. These mirrors shall be further referred to as micromachined membrane deformable mirrors (*MMDMs*) and piezoelectric deformable mirrors (*PDMs*), respectively.

Besides, OKO Technologies offers liquid crystal correctors of low-order aberrations - adaptive cylindrical and spherical LC lenses.

1.4 Closed-loop wavefront control

The majority of adaptive optical systems are based on the traditional phase-conjugate scheme [1]. Its operation can be explained using a simplified example

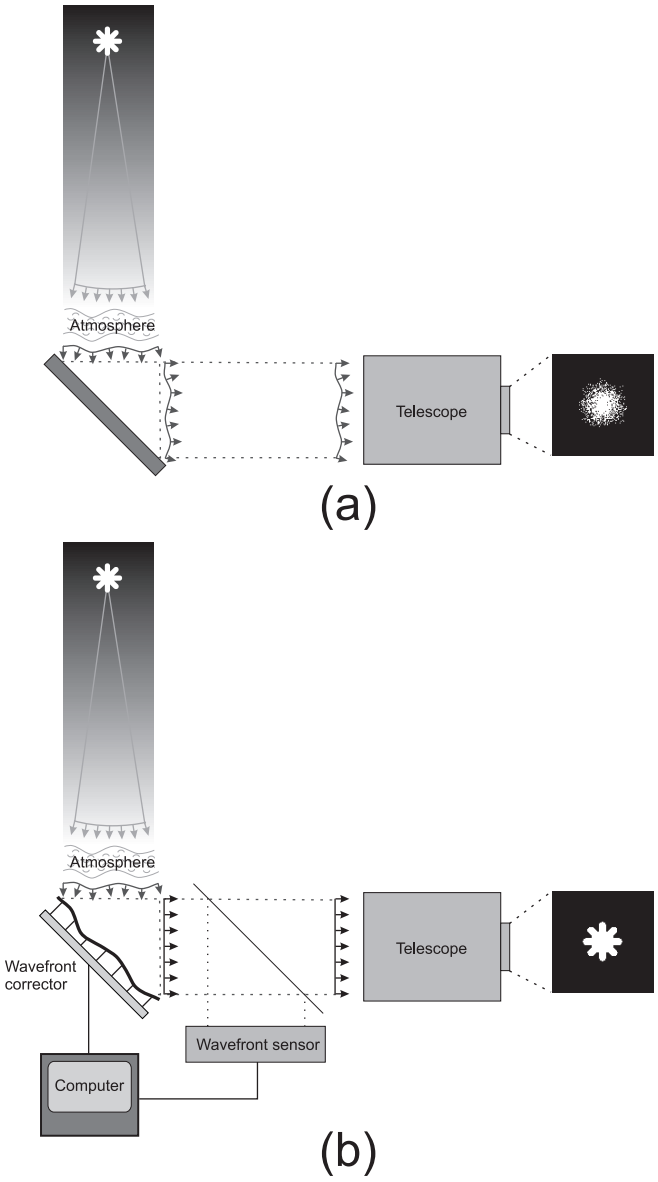

Figure 1.3: *Image blurring induced by atmospheric wavefront distortions in astronomy (a); operation of the adaptive optical system (b).*

from astronomy. A light wave coming from a distant star forms an image of this star in a telescope. Passing through the atmosphere, the light wave is affected by fluctuations in density of the atmosphere due to turbulence, distorting the front of the wave (Fig. 1.3(a)). Due to this kind of distortion, a blurred image is produced. To compensate for this effect, two elements are introduced - *wavefront sensor*, which measures the wavefront distortion introduced by the atmosphere, and *wavefront corrector*, which produces the phase function conjugated to the aberrated wavefront, thus correcting the distortion of an initial wavefront. The processing unit (computer) coordinates operation of these two elements (Fig. 1.3(b)). As the atmospheric distortions evolve over time, the system should perform several hundred measurements and corrections per second. In some systems, an additional tip-tilt mirror is used to reduce the large stroke requirements for the wavefront corrector. For compensation of aberrations produced by "thick" layers of highly aberrated media, multi-conjugate adaptive systems must be used. Volume aberrations are described satisfactorily by layered models [2], and several "wavefront sensor - wavefront corrector" pairs need to be used to compensate them.

In the past, until the 90s the area of applications was restricted to high-budget observatories and military projects on the delivery of high-energy laser beams from ground to space for missile defense and secure communications, due to the extremely high cost of AO systems. In the last decade, however, advances in sensors and electronic processing brought down the cost of adaptive optics, leading to many new applications in scientific, industrial and medical fields [3, 4]. The most important applications include retinal imaging in ophthalmology [5], confocal microscopy [6], ultra-short laser pulse shaping [7] and machine vision.

OKO Technologies not only produces affordable high-quality components for AO systems, but also provides integrated solutions based on "FrontSurfer" software, which allow for closed-loop control of a deformable mirror using the measurement data obtained from a (Shack-)Hartmann wavefront sensor. It can be integrated not only with the components produced by OKO Technologies but also with custom ones.

1.5 Structure of the catalogue

The introductory part gives a short overview of the field of application of our products and introduces basic concepts. In the following chapters the products are presented in detail.

Chapter 2 describes two deformable mirror technologies used by OKO Technologies, namely, MMDM and PDM, and makes comparison between them.

Chapter 3 contains technical information about standard models of deformable mirrors produced by OKO Technologies.

Chapter 4 describes electronic drivers for our deformable mirrors and their programming interfaces.

Chapter 5 describes basic principles and technical data of our liquid crystal adaptive lenses.

Chapter 6 presents “FrontSurfer” wavefront sensor systems produced by OKO Technologies. Sample measurement schemes using the Shack-Hartmann wavefront sensor for optical shop testing are described.

Chapter 7 contains recommendations on designing of an adaptive optical system using our components. It also describes the features of “FrontSurfer” software related to closed-loop wavefront control, presents adaptive optical systems offered by OKO Technologies and contains testing data of real MMDM and PDM systems.

Chapter 8 contains answers to frequently asked questions.

2

DEFORMABLE MIRRORS

OKO Technologies produces two types of deformable mirrors - Micromachined Membrane Deformable Mirrors (MMDM) and Piezoelectric Deformable Mirrors (PDM). They are discussed further in this chapter. First, we consider designs of these mirrors in general and discuss their principal differences. Then we introduce numerical models of MMDM and PDM and consider correction performances for these two mirror types. At the end of this chapter we present some results of experimental characterization of MMDM. Results of testing of MMDM and PDM in an adaptive optical system can be found in Chapter 7.

2.1 Differences between MMDM and PDM

MMDM in its essence is a membrane mirror. The membrane is fabricated using the technology of bulk micromachining. The membrane is very thin (0.5 to 10 μm thick) and can have diameters of up to 50 mm. The membrane is mounted over a two-dimensional array of electrodes. Any potential applied between the membrane and individual electrode, results in deformation of the membrane. Combinations of voltages applied to different electrodes can form very special shapes on the membrane surface.

Piezoelectric mirror is formed by a thin solid plate, made of glass, fuzed silica or silicon, depending on application. The plate is coated with appropriate coating and bonded to a two-dimensional array of piezoelectric actuators. Elongation of individual actuators cause global deformation of the reflective plate.

The MMDM membrane can be deflected only in the direction of the electrode structure because the electrostatic force can be only attractive. The deflected membrane can produce only concave optical shapes, if we take flat surface

as a reference. However, if we choose a slightly concave reference, then a bi-directional operation is possible. To achieve it, the membrane should be initially deflected towards the actuators and made perfectly spherical by adjusting the actuator voltages. From this state the membrane can be moved to both positive (from the electrode structure) and negative (towards the actuator structure) directions by controlling the actuators voltage (see Fig. 2.1).

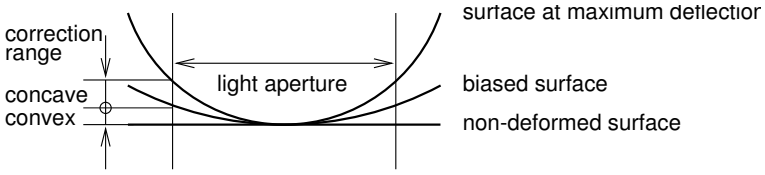

Figure 2.1: *Biased operation of MMDM.*

The membrane of MMDM is fixed at its edges. When a constant potential is applied to all actuators, the mirror will take a concave shape. If the membrane is round, the deformation will form a good approximation to a sphere. In general, the biased shape depends on the geometry of the membrane and the geometry of the actuators. Since the edges of MMDM membrane are fixed, the light aperture of MMDM is usually ~1.4 times smaller than the full membrane size.

MMDM is controlled by inexpensive electrostatic electrodes. It is possible to fabricate these electrode with very high density of small electrodes. However, small electrodes cause small deflections of the membrane. Therefore the maximum number of electrodes in a MMDM is limited by the amplitude of response of a single individual electrode.

There are two parameters that are important when the amplitude of MMDM response is described:

- maximum stroke when all actuators are at maximum (for a round mirror it corresponds to the sag of spherical surface);
- maximum difference between the neighbor actuators.

At present (April 2008) OKO Technologies produces 15 mm mirrors with 37 channels, 30 mm mirrors with 39, 59, and 79 channels, 40 mm mirrors with 59 and 79 channels, and 50 mm mirrors with 79 channels. All of them are optimized to achieve at least 600 to 1000 nm maximum deflection per actuator, with 1.8 mm minimum actuator pitch.

MMDMs feature zero hysteresis and can be used in feedforward control systems after preliminary calibration. Very low power consumption allows building of small and efficient power supplies for multichannel mirrors. We

have experience in building 40-channel MMDM controllers with total consumption not exceeding 1 W in active mode.

Unlike MMDM, the piezoelectric mirrors (PDM) have actuators that can push and pull the reflective plate. When they push, the plate is deformed and the neighbor actuators are also slightly deformed. The stroke per actuator is therefore defined not only by the force applied, but also by the stiffness of the actuator relative to the stiffness of the reflective plate. There are two parameters that are important when the amplitude of response is described:

- maximum stroke of a free actuator
- maximum difference between the neighbor actuators.

PDM deformable plate is bonded only to actuators and has a free edge. When all actuators move together, the plate is translated, without any deformation. The range of translation is equal to the maximum stroke of a free actuator.

At present (April 2008), OKO PDM can be fabricated with minimum pitch of about 4.3 mm, maximum free actuator stroke of 8 μm and, depending on the stiffness of the reflective plate, the inter-actuator stroke can reach 3 μm.

Piezoelectric mirrors demonstrate hysteresis of 7 to 15%. This property limits their applicability for feedforward control.

Since the amplitude of local response of a piezoelectric mirror depends only on the stiffness of the plate and the actuators, these mirrors can be scaled to very large numbers of control channels.

Piezoelectric mirrors are suitable for fast feedback-based correction of low and high-order aberrations with large amplitude.

2.2 Static models of DM deformation

2.2.1 Membrane mirror

The membrane model is applicable to simulation of the response of a MMDM when the thickness of the reflective substrate is so small that its cylindrical stiffness [8]

$$D = Eh^3/12(1-\nu) \tag{2.1}$$

can be neglected. Here E is the Young's modulus, h is the thickness of the substrate and ν is the Poisson ratio. We assume that the membrane is absolutely stretchable and preserves its shape due to its lateral tension. The shape of the stretched membrane depends mainly on the shape of its contour and on the amount of the surface tension. In the case of a relatively large membrane with $\sim$10 mm diameter and a thickness of only 0.5 μm, this model gives excellent approximation for the static mirror behavior. Let us consider the simplified scheme of the micro-fabricated adaptive mirror shown in Fig. 2.2.

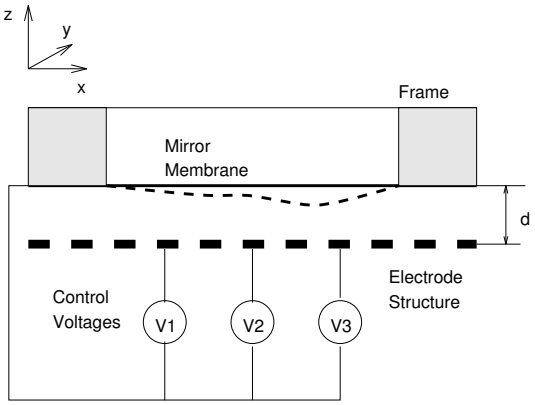

Figure 2.2: *Simplified scheme of a membrane mirror.*

Suppose the mirror surface is deformed by applying voltages $V_1 \dots V_N$ to the two-dimensional grid of N actuators positioned at a distance D under the membrane. Let the membrane, having a uniform thickness, be stretched by a uniform surface tension T [N/m]. In this model we shall also suppose that the distance d is much larger than the maximum membrane deflection, so that the electrostatic pressure P does not depend on the membrane deformation. A nonlinear case of large membrane deflections will be considered later.

The Z-component of the membrane deflection $S(x, y)$ in the linear case is described by the Poisson equation(2.2):

$$\Delta S(x, y) = P/T \tag{2.2}$$

where the electrostatic pressure P is given by:

$$P = \frac{\varepsilon\varepsilon_o V(x, y)^2}{d(x, y)^2} \tag{2.3}$$

Equations (2.2, 2.3) must be supplied with a set of boundary conditions, describing the shape of the membrane contour: $S_c = F(x, y)$.

Analytical solution of equations (2.2, 2.3) for arbitrary geometries of membrane contour and pressure distributions is complicated. For technical estimations the finite difference numerical model of the membrane adaptive mirror, allowing for arbitrary boundary conditions and pressure distributions, was developed.

To solve the Poisson equation numerically, the functions S and P are determined on a square grid with equal steps δ_{XY} in the X and Y directions. The grid knots are indexed as i and j for X and Y directions correspondingly. The

grid approximation of the Laplace operator has the form:

$$\Delta S \approx \frac{S_{i+1,j} + S_{i-1,j} + S_{i,j+1} + S_{i,j-1} - 4S_{i,j}}{\delta_{XY}^2}.$$

Using this form we can write a finite-differential version of the Poisson equation (2.2) as:

$$\frac{S_{i+1,j} + S_{i-1,j} + S_{i,j+1} + S_{i,j-1} - 4S_{i,j}}{\delta_{XY}^2} = \frac{P_{i,j}}{T}. \tag{2.4}$$

This system of linear equations (2.4) can be solved by a direct method of Gauss elimination. This leads to a very large matrix of coefficients, which is frequently not acceptable, because storage requirements for such a matrix in many cases exceed the memory possibilities of modern computers. The open form of the expression for the membrane deformation $S_{i,j}$ follows immediately from (2.4):

$$S_{i,j} = -\frac{1}{4}\left(\delta_{XY}^2 \frac{P_{i,j}}{T} - S_{i-1,j} - S_{i+1,j} - S_{i,j+1} - S_{i,j-1}\right) \tag{2.5}$$

The expression (2.5) can be used for solving the Poisson equation by iterations when the right-hand side of (2.4) $P_{i,j}/T$ is known and the boundary conditions $S_{i,j}$ are explicitly given. C-code for solving the problem for arbitrary actuator and membrane shapes is available free from OKO Technologies.

2.2.2 Continuous faceplate mirror

The continuous faceplate mirror model is applicable to simulation of the response of a PDM. The mechanical design of such a mirror is very simple in its essence: discrete actuators are fixed to a stable mirror base and bonded to a thin flexible mirror plate. The edge of the plate is left free. The geometry of the flexible plate is made circular for the majority of applications, but square and rectangular deformable mirrors are used for beam control in high-power lasers and for ultrafast pulse shaping.

Implementation of PDM is more complicated than the simple model described above. Stress-free assembly of the deformable plate with actuator stack, minimization of the coating stress, good initial figure, implementation of cooling system for a high-power operation — this is an incomplete list of problems. Nevertheless, a simple mechanical model of continuous faceplate deformable mirror is very useful for preliminary estimations of the amplitude and shape of the mirror influence functions and the correction performance.

Analysis that follows is based on a thin-plate model. Rigorous theory of thin plate bending can be found in [8].

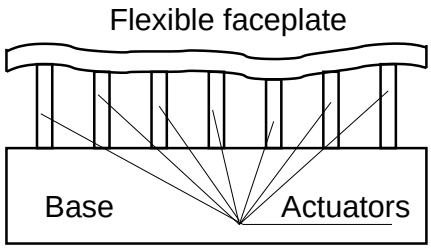

Figure 2.3: *Simplified scheme of a faceplate mirror.*

A small-deflection thin-plate model will be used to derive the expressions for deformable mirror response. In the framework of this model, the thickness of the plate is considered to be small in comparison with the plate size and the plate deformations are small in comparison to the plate thickness. These assumptions are satisfactory in many practical cases.

The deflection S of a thin plate is described by the biharmonic equation

$$\Delta\Delta S = \frac{P}{D} \tag{2.6}$$

where D is the cylindrical stiffness described by equation (2.1), and P is the load applied to the plate.

Let us consider a circular plate with a free edge. As shown in [9], its deformation is caused by a set of point-like forces P_i, which act in points ζ_i and can be presented as a superposition of functions, accurate to within the term $S_0 + S_1 r\cos\varphi + S_2 r\sin\varphi$. This term governs the translation and rotation of the plate as a whole:

$$S(z,\bar{z}) = \frac{1}{16\pi R}\sum_{i=1}^{N} P_i S(z,\bar{z},\zeta_i,\bar{\zeta}_i) + S_0 + S_1\mathrm{Re}\ z + S_2\mathrm{Im}\ z, \tag{2.7}$$

where

$$\begin{aligned} S(z,\bar{z},\zeta,\bar{\zeta}) &= (z-\zeta)(\bar{z}-\bar{\zeta})\left\{\ln(z-\zeta)+\ln(\bar{z}-\bar{\zeta})+\frac{1-\mu}{3+\mu}\right. \\ &\times \left.[\ln(1-z\bar{\zeta})+\ln(1-\bar{z}\zeta)]\right\}+\frac{(1-\mu)^2}{(1+\mu)(3+\mu)}z\bar{z}\zeta\bar{\zeta} \\ &+ \frac{8(1+\mu)}{(1-\mu)(3+\mu)}[(1-z\bar{\zeta})\ln(1-z\bar{\zeta})+k(z\bar{\zeta}) \\ &+ (1-\bar{z}\zeta)\ln(1-\bar{z}\zeta)+k(\bar{z}\zeta)], \end{aligned} \tag{2.8}$$

$z = r\cos\varphi + ir\sin\varphi$, $\zeta = \rho\cos\psi + i\rho\sin\psi$ are coordinates expressed in the complex-valued form, and k is the logarithmic integral

$$k(x) = \int_0^x \frac{\ln(1-\alpha)}{\alpha} d\alpha. \tag{2.9}$$

Equations (2.7)-(2.9) can be used for simulation of the influence functions of PDM and evaluation of its correction quality. For instance, to calculate the best approximation of an arbitrary wavefront $\phi(x, y)$ by a continuous faceplate mirror with a free edge and N actuators, it is necessary to find N unknown forces P_i and 3 coefficients S_0, S_1 and S_2. They can all be found from a system of $N+3$ linear equations. The first N equations are obtained by minimization of the *rms* error using the least-squares method; the 3 supplementary equations from statics represent conditions of mechanical equilibrium of the plate:

$$\begin{cases} \sum_{j=1}^{N} P_j \int\int_\Omega S(z,\bar{z},z_i,\bar{z}_i)S(z,\bar{z},z_j,\bar{z}_j)dxdy \\ +S_0 \int\int_\Omega S(z,\bar{z},z_i,\bar{z}_i)dxdy + S_1 \int\int_\Omega S(z,\bar{z},z_i,\bar{z}_i)xdxdy \\ +S_2 \int\int_\Omega S(z,\bar{z},z_i,\bar{z}_i)ydxdy \\ = \int\int_\Omega S(z,\bar{z},z_i,\bar{z}_i)\phi(x,y)dxdy, \qquad i = 1\ldots N, \\ \sum_{j=1}^{N} P_j = 0, \\ \sum_{j=1}^{N} P_j x_j = 0, \\ \sum_{j=1}^{N} P_j y_j = 0. \end{cases} \tag{2.10}$$

This system can be easily solved using standard Gauss elimination.

2.3 Evaluation of the correction performance

2.3.1 Approximation of Zernike polynomials by continuous deformable mirrors

The shape of a MMDMDM is described by the Poisson equation:

$$\Delta\varphi(x,y) = p(x,y)/T, \tag{2.11}$$

where p is the pressure caused by the actuators and T is the membrane tension. A similar equation (2.11) describes the shape of a bimorph mirror formed with two active layers, with the term p/T describing the distribution of bending moments applied to the plate [10] and the function φ satisfying to some additional boundary conditions.

The shape of a PDM, in the thin plate approximation is described by the biharmonic equation [8]:

$$\Delta^2\varphi(x,y) = p(x,y)/D, \tag{2.12}$$

where the source p describing the action of actuators satisfies the conditions of static equilibrum, D is the cylindrical stiffness and $\varphi(x,y)$ satisfies to some additional boundary conditions. Equation (2.12) assumes the plate have tip-tilt degrees of freedom in the points of attachment to the actuators.

To find the mirror controls p corresponding to the phase error $\varphi(x,y)$ we need to apply the differential operator Δ (Δ^2 for the continuous facesheet mirror) to the phase function φ.

It is a common practice to decompose aberrated wavefronts in series over the Zernike polynomials. Substituting $\varphi = Z_n^m$ where Z_n^m is a Zernike polynomial with the radial order n and azimutal order $\pm m$ as defined in [11], we find [12] that

$$\Delta\varphi(x,y) = 0, \tag{2.13}$$

for all Zernike polynomials Z_n^m with $n = |m|$ including piston, tip, tilt, astigmatism, trefoil, etc.; and

$$\Delta^2\varphi(x,y) = 0, \tag{2.14}$$

for all Zernike polynomials Z_n^m with $n = |m|$ and also with $n - 2 = |m|$, including piston, tip, tilt, defocus, astigmatism, trefoil, coma and some higher order aberrations.

This result can be explained by the fact that the equations (2.11, 2.12) describe the mirror shape in terms of actions p defined only within the correction aperture, while some modes can be exactly defined only by actuators positioned outside the correction aperture. These modes can not in principle be found as an exact solution of eq. (2.11) or (2.12) in terms of correction actions p inside the correction aperture.

Practical correction of any aberration satisfying to (2.13) for a membrane and bimorph mirror, or (2.14) for a thin-plate mirror, performed only by the actuators positioned within the aperture, results in a "bumpy" approximation to the desired shape. To obtain a high quality correction, a certain number

of actuators should be positioned outside of the mirror aperture so that the conditions (2.13, 2.14) are satisfied inside the aperture, while the external actuators produce the required correction. The number of these external actuators should be large enough to produce a sufficient number of independent modes. Considering all low-order Zernike polynomials up to the 4th order, we see that out of all 15 modes, 14 satisfy to the condition (2.14), and 9 satisfy to both (2.13) and (2.14). Counting very roughly that each actuator corrects one mode, we conclude that to correct the low-order terms described by (2.14), the continuous faceplate DM should have at least 14 actuators and a bimorph or a membrane DM should have at least 9 actuators placed outside its correction aperture.

Also, from very basic considerations, we can say that a continuous faceplate DM with a round aperture should have at least two rings of actuators positioned outside the correction area, to define the conditions on the contour of the correction area $\varphi|_S$ and $\frac{\partial\varphi}{\partial r}|_S$, where r is the radial coordinate, and S is the boundary of the correction area. Membrane mirrors should have at least one ring of actuators outside the correction aperture, as only the deflection $\varphi|_S$ should be defined.

For mirrors with large numbers of actuators, we need to count the number of Zernike polynomials satisfying to the conditions 2.14 and 2.13. Performing this easy task, we derive a general rule that defines the necessary number of actuators to be placed outside the correction aperture of a DM:

Any deformable mirror described by the Poisson equation requires at least two actuators to be placed outside the working aperture per period of the azimuthal aberration of the highest expected order.

Any deformable mirror described by the biharmonic equation, such as a continuous facesheet mirror with push-pull actuators, requires at least four actuators to be placed outside the working aperture per period of the azimuthal aberration of the highest expected order, and these actuators should not be positioned on a single circle.

2.3.2 Numerical simulation of the correction quality

Computer models described in section 2.2.1 and 2.2.2 were used for calculation of the influence functions of the 15-mm 37-channel MMDM ("OKO mirror"), 37-ch OKO PDM and 109-ch OKO PDM.

The *rms* correction for the Zernike polynomials up to the 8-th order is shown in Fig. 2.4 for three different values of the correction aperture $R = 0.8;\ 0.6;\ 0.4$ of a 37-ch MMDM. The case $R = 1$ is not considered due to the fixed edge. The graph clearly shows that the correction quality improves significantly with the decrease of R for all modes Z_n^m with $n = m$, which can be explained by the increase in the number of actuators positioned outside the aperture. Correction

of aberrations Z_7^1, Z_7^3 and Z_8^0 is strongly dependent on the number of internal actuators, resulting in optimal correction with $R = 0.8$ when the maximum number of actuators is positioned inside the correction aperture. All other modes require simultaneous correction with internal and external actuators, therefore the optimum correction is reached in the vicinity of $R = 0.6 \ldots 0.7$.

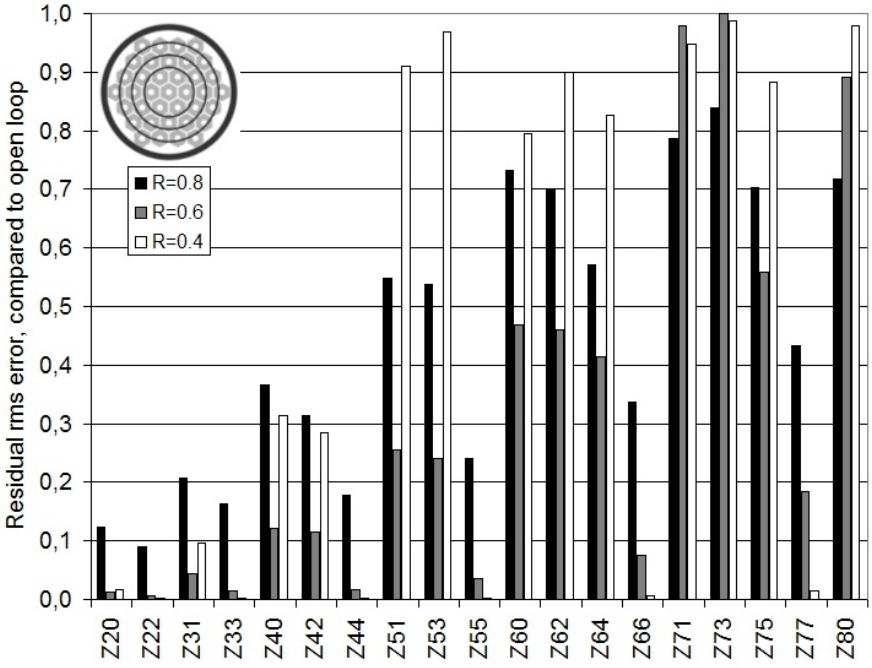

Figure 2.4: *Calculated quality of correction the Zernike modes Z_n^m up to $n = 8$ for the 15-mm MMDM controlled by 37 actuators, for different sizes of the correction aperture.*

Figure 2.5 (top) shows the residual *rms* correction error for a 37-ch DM for low order Zernike polynomials Z_n^m for three different values of the correction aperture $R = 1;\ 0.8;\ 0.65$. The correction quality of low-order aberrations is poor when the full aperture $R = 1$ is used and all actuators are positioned within the correction aperture. The quality improves significantly for smaller R practically for all low-order aberrations, as the number of actuators inside the correction aperture decreases, while the external actuators form the otherwise impossible correction modes. Polynomials Z_7^3 and Z_7^5 do not satisfy to (2.14), therefore the correction of these terms requires at least some actuators to be positioned within correction aperture. For these modes, the correction quality is better for the full aperture $R = 1$ and the error increases for smaller correction apertures such as $R = 0.8$ and $R = 0.65$.

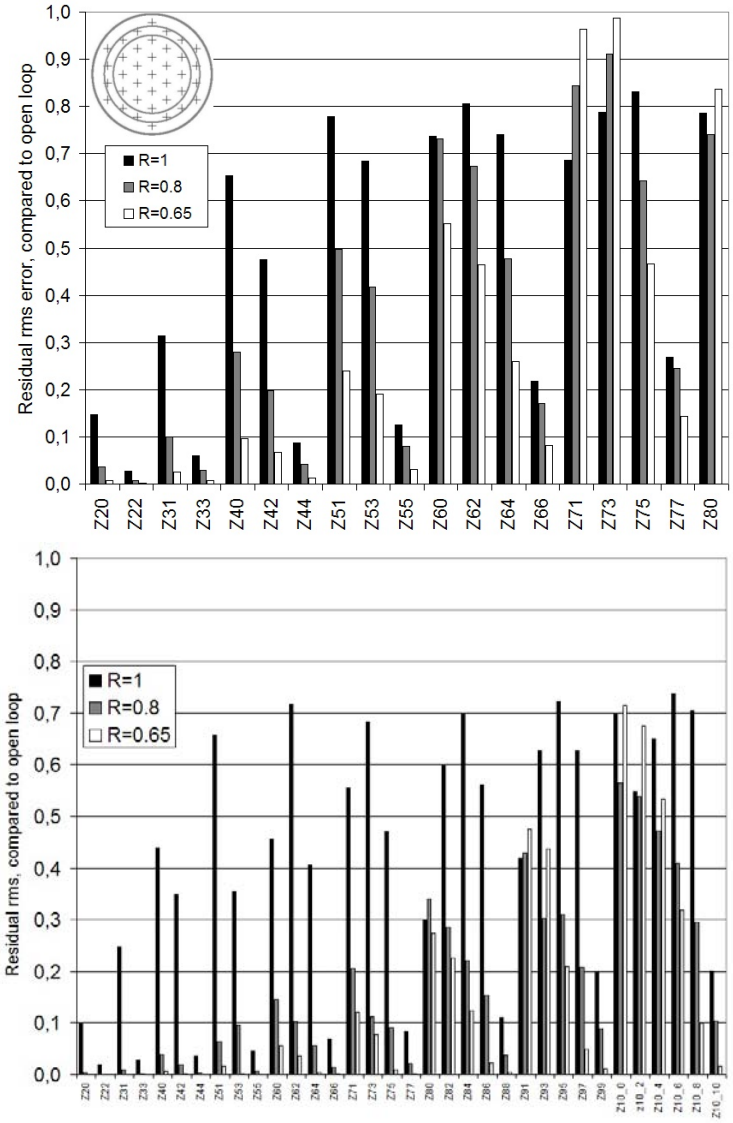

Figure 2.5: *Calculated quality of correction the Zernike modes Z_n^m up to $n = 8$ for a PDM controlled by 37 actuators (top) and for Zernike modes up to the 10-th order for a PDM controlled by 109 actuators, for different sizes of the correction aperture.*

The Fig. 2.5 (bottom) shows the correction quality calculated for a 109-ch PDM for Zernike terms up to the 10-th order. As in all previous cases, the correction reaches its optimum whan a significant number of actuators is positiones outside the correction aperture. The aperture of $R = 0.65 \dots 0.8$ is optimal for this mirror. For example, if the mirror diameter is 5cm, the optimal aperture would be in the range between 3.25 to 4 cm.

In practice, to achieve the optimal quality of correction, a MMDM should be used with correction apertures in the range $R = 0.6 \dots 0.7$ of the full membrane aperture, while a PDM should be used with working apertures in the range $R = 0.65 \dots 0.8$ of the full mirror aperture.

2.3.3 Comparison of the performance of different mirrors for the atmospheric correction

To evaluate optical performance of a wavefront corrector, we need to apply it to a whole class of optical fields. As the main practical application of adaptive optics for many years was high-resolution imaging through the turbulent atmosphere, we shall use the statistics of random wavefronts induced by atmospheric turbulence. The Kolmogorov model is the most frequently used for turbulence description because of its relative mathematical simplicity and good agreement with experiment [13].

Modal wavefront correction is usually described in terms of complete orthogonal sets of functions, such as Zernike polynomials or Karhunen-Loéve functions. The last one is a special set of functions, best fit for representation of random wavefronts with statistics described by the Kolmogorov theory. For these sets the *rms* wavefront aberrations were evaluated in [14] for the generalized case of modal correctors with Karhunen-Loéve basis.

The comparison study of different types of modal correctors was presented in [15]. Here we briefly describe the method used in this paper. Let the function $\phi(x, y, t)$ be a time-dependent turbulence-induced phase distribution across the aperture of a wavefront corrector. We can decompose this function over an orthogonal set of Zernike polynomials $Z_i(x, y)$:

$$\phi(x, y, t) = \sum_{i=0}^{\infty} \alpha_i(t) Z_i(x, y). \tag{2.15}$$

Here, the normalized Zernike polynomials with a unitary amplitude on a circle of unitary radius [11] are used.

Using cross-correlations of Zernike coefficients of turbulent phase with

Table 2.1: *Comparison of the optical performances of 37-channel piston, continuous faceplate and membrane mirrors with hexagonal structure of actuators.*

Mirror type	**Residual aberrations, %**	$(D_p/R_0)_{max}$	**Efficiency**
Piston	22.7	4.69	5
Membrane	9.68	10.9	22
Continuous faceplate, free edge	9.02	14.2	33

Kolmogorov statistics [16]

$$\langle a_i a_{i'} \rangle = \begin{cases} A, \ m = 0 \ \text{ and } m' = 0, \\ \sqrt{2}A, \ m = 0 \text{ and } m' \neq 0, \text{ or } m \neq 0 \text{ and } m' = 0, \\ 2A, \ m \neq 0 \text{ and } m' \neq 0, \end{cases} \tag{2.16}$$

$$A = 0.00386 \left(\frac{D_p}{r_0}\right)^{5/3} (n+1)(n'+1)\delta_{mm'}(-1)^{(n+n'-m-m')/2} \times \frac{\Gamma(14/3)\Gamma[(n+n'-5/3)/2]}{\Gamma[(n-n'+17/3)/2]\Gamma[(n'-n+17/3)/2]\Gamma[(n+n'+23/3)/2]},$$

and using the corrector's influence functions for approximation of Zernike polynomials, we can find *rms* error of correction for a given turbulence characteristic scale r_0

$$\sigma^2 = \sum_{i=0}^{\infty} \sum_{i'=0}^{\infty} \langle \Delta_i \Delta_{i'} \rangle_{\mathbf{r}} \cdot \langle \alpha_i \alpha_{i'} \rangle_t \,. \tag{2.17}$$

Here $\Delta_i(x, y)$ is the error of fitting of the i-th Zernike polynomial with the corrector's influence functions, and D_p is the diameter of the mirror's pupil.

Other common measures of corrector's performance are the approximate value of Strehl factor defined as $S = exp(-\sigma^2)$, where σ is given in radians, and the efficiency N_{KL} - an equivalent number of Karhunen-Loéve modes resulting in the same fitting error.

The results of comparison of optical performances of 37-channel piston, continuous faceplate and membrane mirrors are shown in Table 2.1. All the mirrors considered have the same hexagonal structure of actuators. Maximum values of the turbulence parameter D_p/r_0 in the third column correspond to the Strehl factor value equal to 0.5.

This method is quite useful for preliminary analysis and optimization of the mirror design. Among its limitations we can mention that it does not take into account limited stroke and dynamics of the mirror. With this consideration,

PDM is more advantageous; not only because it provides better fitting but also because of its faster response and larger stroke compared to MMDM.

2.4 Experimental characterization of MMDM

This section presents the results of investigation of MMDM under continuous laser load and in an optimization setup. Its temporal response and tip-tilt correction possibilities are also investigated. More technical details can be found in [17, 18].

2.4.1 MMDM under laser load

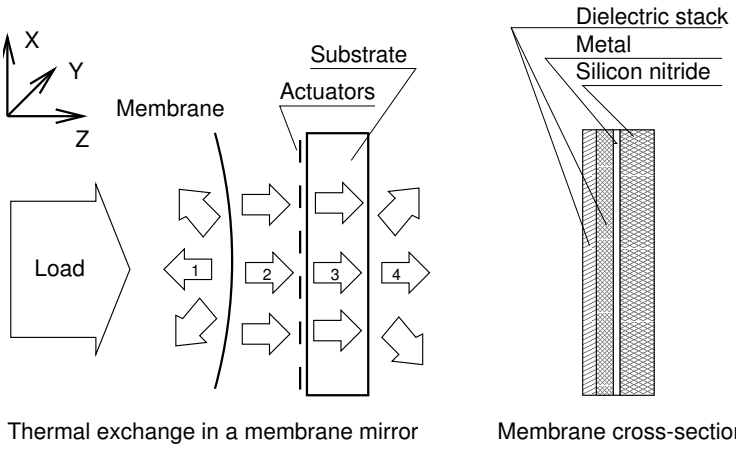

Figure 2.6: *A biased micromachined deformable mirror under laser load.*

Laser load causes change of the membrane temperature t, reducing the tension T due to the thermal expansion of the membrane material. Behavior of micromachined membrane deformable mirrors under continuous laser load has been investigated experimentally and theoretically in [17]. It was shown that load-induced variation of the membrane temperature and mechanical tension result in additional thermal deformation of the deformable mirror figure. Modeling the membrane tension and thermal deformation as functions of beam diameter, optical power and mirror design parameters, the authors found that the thermal resistance of the mirror substrate is critical for high-power operation. According to the estimations made, an optimally designed membrane mirror with 99.8% reflectivity can be safely loaded with up to 500 W of optical power in a 10 mm diameter beam. This model was compared with

experimental data obtained for micro-machined membrane deformable mirrors with five different types of reflective coatings loaded with up to 70 W beam with power density of up to 20 W/mm^2. Operation of a multilayer membrane mirror was demonstrated in a stable resonator of a diode-pumped YAG:Nd laser with output power of up to 4.5 W.

In [19] a 10 mm 19-channel MMDM coated with silver and a 12-layer dielectric stack was tested inside the resonator of a CV YAG laser with output power of 200 W. The optical load on the mirror reached 600 W in a 6 mm beam. The mirror operated continuously without any signs of degradation.

MMDMs can be used for CW laser applications with beam powers of up to 500 W with power density of the order of 2 kW/cm^2. The optimization of the package design can increase the loads, making the mirrors applicable for high-power CW applications. OKO mirrors for high-power applications satisfy the following requirements:

- High reflectivity is achieved by coating the membrane with a highly-reflective metal (silver) further enhanced by a multi-layer dielectric stack.
- Low thermal resistance of the gap between the membrane and the electrode structure.
- Low thermal resistance of the electrode structure and between the mirror substrate and the ambient, essential for heat evacuation.

2.4.2 Optimization-based operation

The experimental setup is shown in Fig. 2.7. This setup uses a pinhole (PH) as a source of ideal reference spherical wave. The reference spherical wave produced by the pinhole is returned to the pinhole after reflection from the biased adaptive mirror (AM). The response of the photodiode reaches its maximum when the AM has perfectly spherical shape. Interferometer formed by the beamsplitter (BS), AM and the reference mirror (RM) allows for real-time interferometric registration of the system behavior. The far-field (conjugated to the pinhole plane) intensity distribution is projected with a microlens (ML) onto the second CCD sensor to allow for real-time observation of the far-field intensity distribution.

The principle of operation is based on optimization of the adaptive mirror figure to maximize the amount of light, passed back through the pinhole to the feedback photodiode. From the geometrical point, the feedback signal is maximized when the mirror has perfectly spherical shape.

While working with MMDM, it is important to take into account that the mirror deflection is proportional to the square of applied voltage: $\Delta \sim V_a^2$. To

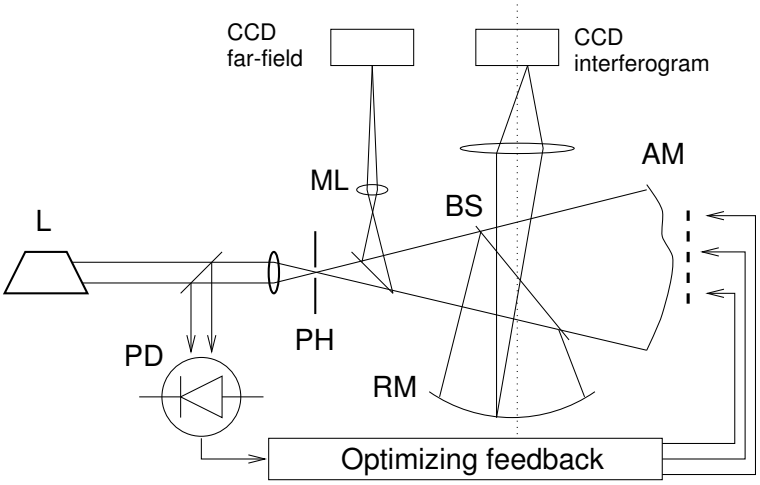

Figure 2.7: *Experimental setup used for calibration and characterization of MMDM.*

linearize the control, the voltages V_a applied to the mirror actuators should be proportional to the square root of the linear voltage V_c calculated by the control system: $V_a = V_c\sqrt{V_c/V_{max}}$. This conversion makes the mirror response proportional to V_c.

It was found that downhill simplex method, described for example in [20] provides reasonably fast and quite reliable convergence to the global optimum in the majority of situations. The time delay between the moment of setting the mirror voltages to the moment when the feedback value is measured was set to about 1.5 . . . 2 milliseconds. Average correction time for randomly introduced aberration in a 37-ch system, controlled by simplex optimization algorithm, was in the range 20 s to one minute, while the preliminary correction (feedback value reaches half of its maximum value) was typically achieved in a couple of seconds.

2.4.3 Tip-tilt correction

As the tip-tilt correction ability is of a special interest in many applications, special investigation on the tilt correction performance was conducted using 10-mm 19-channel MMDM. Micromachined adaptive mirrors have negligible hysteresis, permitting for quick and precise one-step program control of the surface shape. Scanning of the beam between image pixels was implemented with a speed of 500 pixels per second (see Fig. 2.8).

Figure 2.8: *Examples of a diffraction-limited focal spot scanning, demonstrating the tilt correction performance. These images were obtained by scanning 6-mm laser beam using 19-ch adaptive mirror having 1 cm clear aperture.*

2.5 Acceptable defects of deformable mirrors

Deformable mirrors fabricated by OKO Technologies are complex opto-electro-mechanical systems. In many cases we fabricate these mirrors on the customer's specification, which result in a unique product. It is practically impossible to deliver a custom-made DM which is absolutely free of any defects. In all cases we look for the best possible compromise.

This section gives an overview of mirror defects that we do tolerate.

2.5.1 Surface defects

Most of the mirrors delivered by OKO Technologies are free of surface defects. However, the process of fabrication of a DM is quite complicated, therefore sometimes we tolerate visible defects on the surface of a DM, if these defects do not impair the performance of the mirror.

Deformable mirrors are complex opto-electro-mechanical systems, they can have various defects in mechanics, electronics and optics, which are invisible to the human eye. Many of these defects can be real killers to the mirror performance, but since they are invisible, they are not a concern at the first inspection.

The situation is quite different with the surface defects. In vision systems, small surface defects practically do not influence the performance of the optics. They add slightly to the system scattering, but these effects are negligible compared to the harm caused by the phase distortions. We have experience with very badly scratched mirrors that perform perfectly in vision systems. In most cases surface defects are quite harmless. Unfortunately, at the first inspection, they take almost 100% of the customer's attention, simply because they are clearly visible.

Surface defects can be important in two cases: in AO systems with very low scattering and in high-power laser systems. In both cases we can deliver a mirror that is free of surface defects, or with some minor defects that do not impair the performance.

2.5.2 Scratches

Mirrors we deliver are free of major scratches. Some minor scratches may appear but the experience shows that these minor scratches appear most frequently in the imagination of the customer. Attempts to remove these minor scratches, does not matter real or imaginary, almost always result in real major scratches all over the mirror surface. Contact OKO Technologies if you have any doubt. We do not replace deformable mirrors scratched by the customers.

2.5.3 Temporal stability

Deformable mirrors can feature certain amount of temporal drift, caused by the relaxations of the internal strains in the mirror construction, glue shrinkage, actuator creep etc. These drifts do not exceed the maximum of 1μm *rms* surface error during the mirror guarantee period. As a rule, all major drifts happen just after the mirror is delivered, the drifts are expected but not guaranteed to be negligible in mirrors that are older than 1 year.

2.6 MrFit: DM simulation package

MrFit is a Windows program to simulate the static behavior of membrane and continuous facesheet DM. It calculates the voltages to be applied to the actuators, to achieve the best possible compensation of a specified aberration, defined as a combination of Zernike terms. The program shows - see for instance Fig. 2.9 and 2.10 - the surfaces of the wavefront, the best fit with a specified DM, and the approximation error. The output can be obtained as a grayscale plot, interferogram, or a 3D surface. The software can take into account the effects caused by the clipping of the actuator voltages, providing realistic output accounting for the limited stroke of the DM actuators.

The full commercial version of the program will simulate any circular membrane or a continuous facesheet DM, with any number and geometry of actuators.

A free version of the software is available from the OKO Technologies website. It simulates only the deformable mirrors produced by OKO Technologies.

Please contact OKO Technologies for any further information about the commercial and the free version of the software.

2.7 Publications based on OKO's mirrors

In addition to the testing results presented in this chapter, there are numerous publications containing useful technical information on our mirrors and their applications. An uncomplete list of these publications is given below.

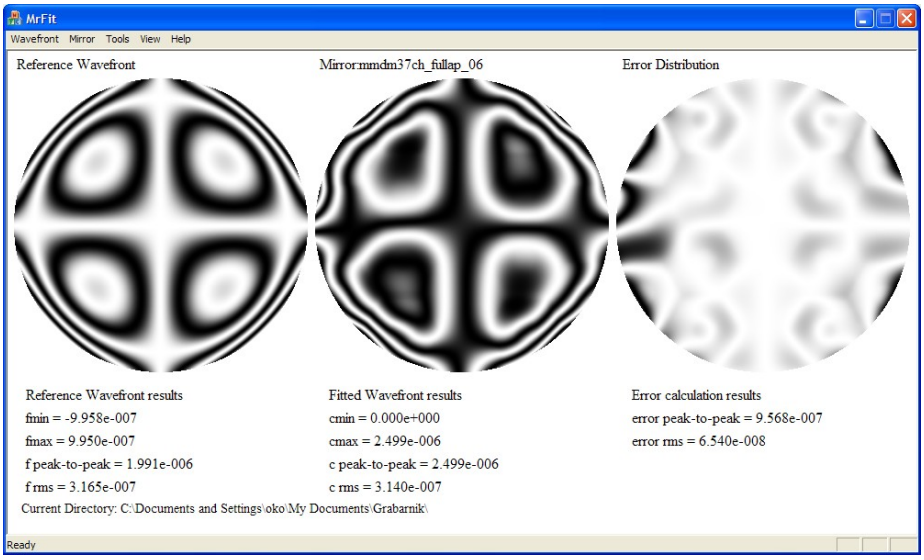

Figure 2.9: *MirrorFit working window with interferometric visualization.*

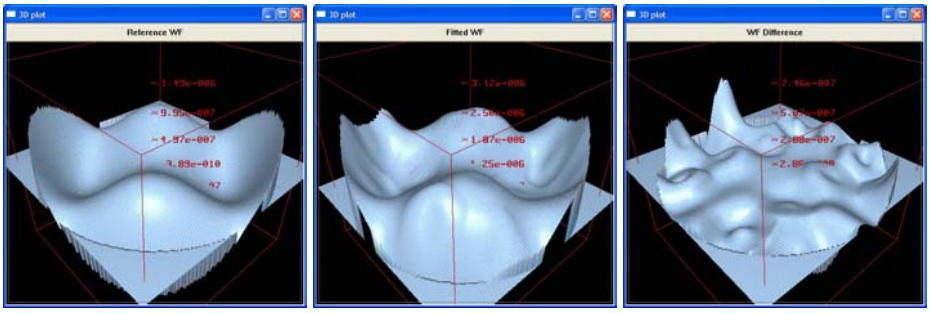

Figure 2.10: *3D plots of an aberration, the best fit obtained with a membrane DM, and the approximation error.*

- G. Vdovin, O. Soloviev, A. Samokhin, and M. Loktev, "Correction of low order aberrations using continuous deformable mirrors," Opt. Express **16**, 2859-2866 (2008)
- G. Vdovin, P. M. Sarro, Flexible mirror micromachined in silicon, Applied Optics **34**, 2968-2972 (1995)
- G. V. Vdovin, S. Middelhoek, P. M. Sarro, Technology and applications of micromachined silicon adaptive mirrors, Optical Engineering **36**, 1382-1390 (1997)
- F. Druon, G. Cheriaux, J. Faure, J. Nees, M. Nantel, A. Maksimchuk, G. Mourou, J. Chanteloup, and G. Vdovin, "Wave-front correction of femtosecond terawatt lasers by deformable mirrors," Opt. Lett. **23**, 1043-1045 (1998).
- H. Dyson, R. Sharples, N. Dipper, and G. Vdovin, "Cryogenic wavefront correction using membrane deformable mirrors," Opt. Express **8**, 17-26 (2001)
- E. Zeek, K. Maginnis, S. Backus, U. Russek, M. Murnane, G. Mourou, H. Kapteyn, G. Vdovin, Pulse compression by use of deformable mirrors, Optics Letters **24**, 493-495 (1999)
- L. Zhu, P.-C. Sun, D.-U. Bartsch, W. R. Freeman, Y. Fainman, Adaptive control of a micromachined continuous-membrane deformable mirror for aberration compensation, Applied Optics **38**, 168-176 (1999)
- L. Zhu, P.-C.Sun, Y. Fainman, Aberration-free dynamic focusing with a multichannel micromachined membrane deformable mirror, Applied Optics **38**, 5350-5354 (1999)
- L. Zhu, P.-C. Sun, D.-U. Bartsch, W. R. Freeman, Y. Fainman, Wave-front generation of Zernike polynomial modes with a micromachined membrane deformable mirror, Applied Optics **38**, 6019-6026 (1999)
- G. Vdovin, N. Kuegler, M. Schacht, Membrane deformable mirrors under CW laser load, Proceedings of SPIE **3762**, 58-66 (1999)
- C. Paterson, J. C. Dainty, Hybrid curvature and gradient wave-front sensor, Optics Letters **25**, 1687-1689 (2000)
- C. Paterson, I. Munro, J. C. Dainty, A low cost adaptive optics system using a membrane mirror, Optics Express **6**, 175-185 (2000)
- O. Albert, L. Sherman, G. Mourou, T. B. Norris, G. Vdovin, Smart microscope: an adaptive optics learning system for aberration correction in multiphoton confocal microscopy, Optics Letters **25**, 52-54 (2000)

- E. Zeek, R. Bartels, M. M. Murnane, H. C. Kapteyn, S. Backus, G. Vdovin, Adaptive pulse compression for transform-limited 15-fs high-energy pulse generation, Optics Letters **25**, 587-589 (2000)
- R. Bartels, S. Backus, E. Zeek, L. Misoguti, G. Vdovin, I. P. Christov, M. M. Murnane, H. C. Kapteyn, Shaped-pulse optimization of coherent emission of high-harmonic soft X-rays, Nature **406**, 164-166 (2000)
- E. J. Fernández, I. Iglesias, P. Artal, Closed-loop adaptive optics in the human eye, Optics Letters **26**, 746-748 (2001)
- M. R. Armstrong, P. Plachta, E. A. Ponomarev, R. J. D. Miller, Versatile 7-fs optical parametric pulse generation and compression by use of adaptive optics, Optics Letters **26**, 1152-1154 (2001)
- G. Vdovin, V. Kiyko, Intracavity control of a 200-W continuous-wave Nd:YAG laser by a micromachined deformable mirror, Optics Letters **26**, 798-800 (2001)
- R. K. Tyson, B. W. Frazier, Microelectromechanical system programmable aberration generator for adaptive optics, Applied Optics **40**, 2063-2067 (2001)
- W. Lubeigt, G. Valentine, J. Girkin, E. Bente, D. Burns, Active transverse mode control and optimisation of an all-solid-state laser using an intracavity adaptive-optic mirror, Optics Express **10**, 550-555 (2002)
- S. C. McQuaide, E. J. Seibel, R. Burstein, T. A. Furness III, Three-dimensional virtual retinal display system using a deformable membrane mirror, SID 02 Digest **50.4** (2002)
- J. Garduño-Mejía, A. H. Greenaway, D. T. Reid, Designer femtosecond pulses using adaptive optics, Optics Express **11**, 2030-2040 (2003)
- E. Theofanidou, L. Wilson, W. J. Hossack, J. Arlt, Spherical aberration correction for optical tweezers, Optics Communications **236**, 145150 (2004)
- E. Dalimier, C. Dainty, Comparative analysis of deformable mirrors for ocular adaptive optics, Optics Express **13**, 4275-4285 (2005)
- R. El-Agmy, H. Bulte, A. H. Greenaway, D. T. Reid, Adaptive beam profile control using a simulated annealing algorithm, Optics Express **13**, 6085-6091 (2005)

- A. J. Wright, B. A. Patterson, S. P. Poland, J. M. Girkin, G. M. Gibson, M. J. Padgett, Dynamic closed-loop system for focus tracking using a spatial light modulator and a deformable membrane mirror, Optics Express **14**, 222-228 (2006)
- S. R. Chamot, C. Dainty, S. Esposito, Adaptive optics for ophthalmic applications using a pyramid wavefront sensor, Optics Express **14**, 518-526 (2006)
- A. Naumov, M. Loktev, I. Guralnik, and G. Vdovin, "Liquid-crystal adaptive lenses with modal control," Opt. Lett. **23**, 992-994 (1998)

3

DEFORMABLE MIRRORS, TECHNICAL DATA

3.1 15mm 37-channel MMDM ("OKO mirror")

15 mm 37-channel MMDM was introduced in 1997 and has been the most popular deformable mirror ever made.

The mirror, shown in Fig. 3.1, consists of a silicon chip mounted over a PCB holder. The chip contains silicon nitride (composite) membrane, which is coated to form a mirror. The PCB contains the control electrode structure, spacer and connector. It also serves as the mirror package. The shape of the reflective membrane is controlled by voltages applied to the control electrodes with the membrane grounded.

The device can be used for fast dynamic correction of low-order optical aberrations such as defocus, astigmatism, coma, etc. in lasers, telescopes, ophthalmic devices, displays and imaging optics.

The scheme of the assembled mirror and the principle of control are illustrated in Fig. 3.2

3.1.1 Technical data

See Table 3.1 for typical technical parameters of the mirror.

Small surface defects are possible. They do not influence the quality of the mirror.

Figure 3.1: *Typical view of a 37-channel micromachined deformable mirror with and without package. Please note that these mirrors can be fabricated with different package designs, so the mirror you have may look differently.*

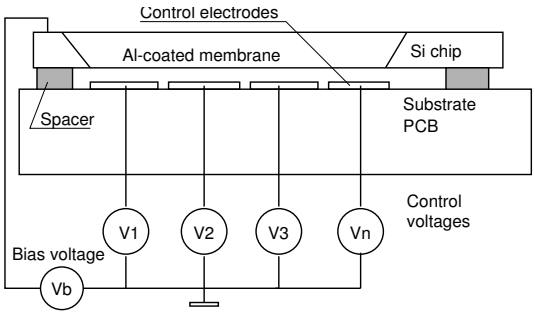

Figure 3.2: *Schematic section of the micromachined adaptive mirror.*

3.1.2 Actuator structure

The membrane is mounted over the printed actuator structure shown in Fig. 3.4. The center-to-center distance between actuators is 1.8mm. The whole actuator structure is located within 12mm circle under the mirror membrane.

The first (close to the mirror) cable connector controls central 19 actuators of the hexagonal structure and provides connection to the ground. The second connector controls 18 peripheral electrodes (two pins are not connected). In principle the mirror can be used with only one control board (19-channel variant) - ground the actuators 20...37 for reliable mirror operation.

19 amplifiers of the driver board connected to the first connector are used to drive the mirror actuators. The membrane is grounded (right jumper on the driver board in the upper position, no left jumper). The membrane can be

Table 3.1: *Technical parameters of 15mm 37-channel MMD mirror.*

Parameter	Value
Aperture shape	approximately circular
Mirror coating	Metal or Metal + dielectric
Aperture dimensions	15mm diameter
Number of electrodes	37 (19) (see Fig. 3.4)
Control voltages V_c	0 . . . 150 to 300 V, dependent on the mirror
Initial RMS deviation from plane	less than 0.45 μm
Main initial aberration	1.5 fringes at 630nm
Maximum deflection of the mirror center	10 μm
Package dimensions	see Fig. 3.3
Weight	140 g

connected to the amplifier number 20 (bias) by setting both jumpers on the amplifier board to the lower position - **this is not recommended**.

3.1.3 Optical quality

Typical interferograms of the mirror are shown in Fig. 3.5.

3.1.4 Specific remarks

When operated with 19 channels, use shorting link for the second connector to prevent charging of floating electrodes.

See also general remarks on page 69.

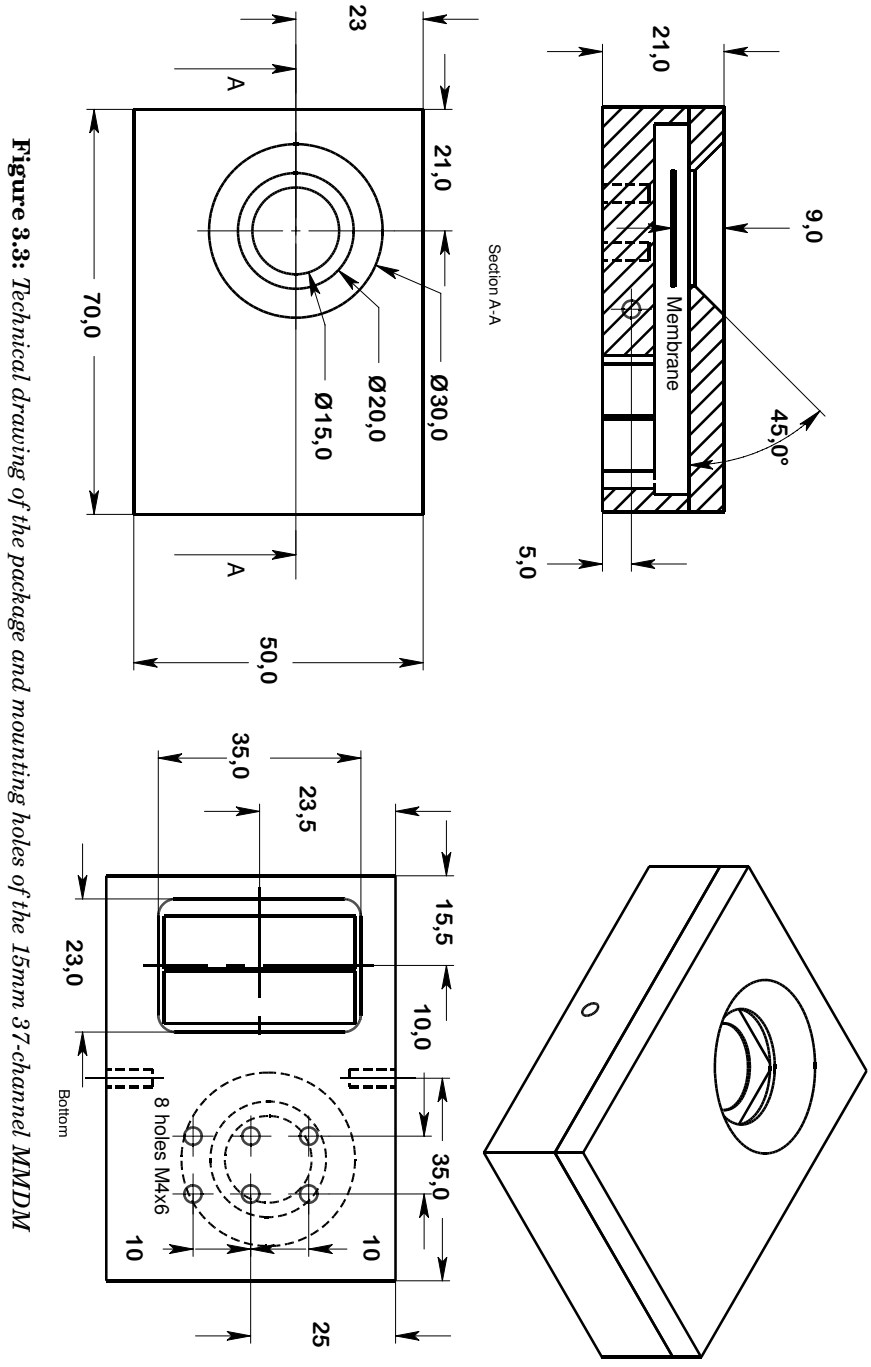

Figure 3.3: *Technical drawing of the package and mounting holes of the 15mm 37-channel MMDM*

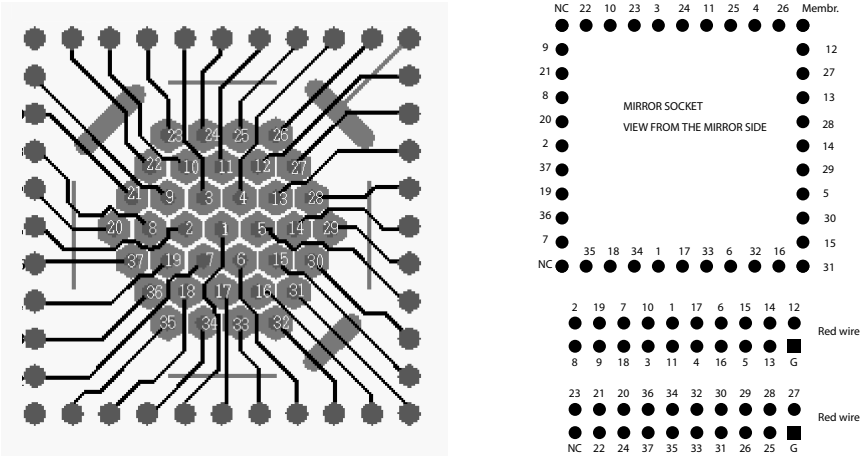

Figure 3.4: *The PCB actuator structure and the pinout (actuator numbers) of PGA connector, shown from the top (mirror surface) view. The cables should be connected from the back side with red-colored wire oriented to the “Ground” pin. See “Red wire” mark in the figure.*

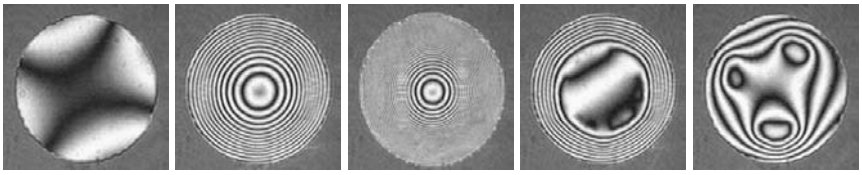

Figure 3.5: *Test of the mirror: zero voltage applied, control byte 180 applied to all actuators, control byte 255 applied to all actuators, control byte 255 applied to actuators 20 to 37, non-zero bytes applied to some actuators (left to right)*

3.2 30mm 39/59/79-channel MMDM

The mirror, shown in Fig. 3.6, consists of a silicon chip mounted over concentric electrostatic electrode structure. The chip contains multilayer silicon nitride membrane, which is coated to form the mirror. The PCB contains the control electrode structure, spacer and connectors. The initial shape of the reflective membrane can be adjusted using 8 adjustment micrometric screws on the back side of the mirror mount.

The device can be used for fast dynamic correction of low-order optical aberrations such as defocus, astigmatism, coma, etc. in lasers, telescopes, ophthalmic devices, displays and imaging optics.ed for fast dynamic correction of optical aberrations.

The scheme of the assembled mirror and the principle of biased control are illustrated in Fig. 3.2 on page 32

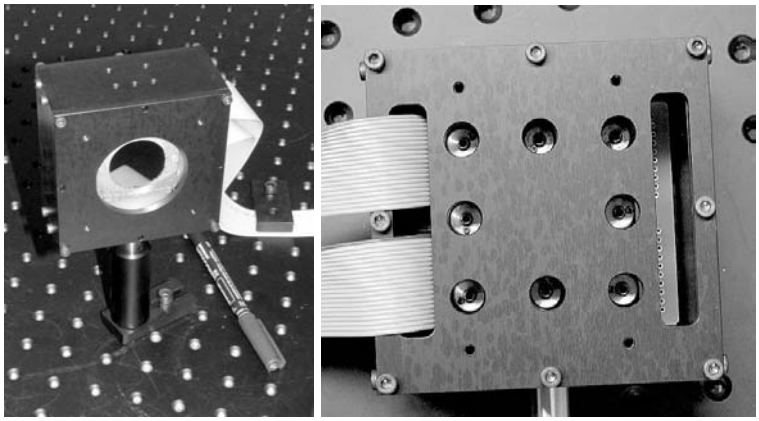

Figure 3.6: *Front and back view of the mirror.*

3.2.1 Technical data

See Table 3.2 for typical technical parameters of the mirror.

A number of surface and coating defects with total area not exceeding 2mm^2 can be present on the mirror surface. These defects do not influence the quality of the mirror.

3.2.2 Actuator structure

The membrane is mounted over the printed actuator structure (20mm in diameter for 39ch mirror and 30mm in diameter for 59- and 79-channel mirror)

Table 3.2: *Technical parameters of 30mm 39 / 59-channel MMD mirror.*

Parameter	Value
Aperture shape	approximately circular
Aperture dimensions	30mm diameter
Number of electrodes	39/59/79 (see Fig. 3.7-3.8)
Control voltages V_c	0 . . . 150 to 300 V, dependent on the mirror
Initial RMS deviation from reference sphere	less than 0.9μm
Main initial aberration	astigmatism
Maximum deflection of the mirror center	9μm
Surface defects	up to 2 coating defects
Package dimensions	see Fig. 3.9
Weight	≈500 g

shown in Fig. 3.7.

3.2.3 Optical quality

The mirror was tested interferometrically before shipping. The interferometric patterns are shown in Fig. 3.10.

3.2.4 Specific remarks

See also general remarks on page 69.

Mirror realignment

In the first days of operation, the mirror figure can drift due to relaxation of internal stresses. The mirror can be re-aligned.

OKO Technologies is not responsible for the result of alignment procedure and provides no warranty!

To align:

1. remove the cable bracket and put the cable aside (do not disconnect). Connect the mirror to the control board.
2. put the mirror into interferometer and fix it solidly.
3. Using 0.9mm hex key release the screw latches (see Fig. 3.6).
4. Set all actuator voltages to zero and align the mirror to observe zero interferometric pattern.
5. By slight clockwise turns of alignment screws adjust the mirror figure. Do not turn the screws more than 10 degrees of arc counterclockwise! By doing

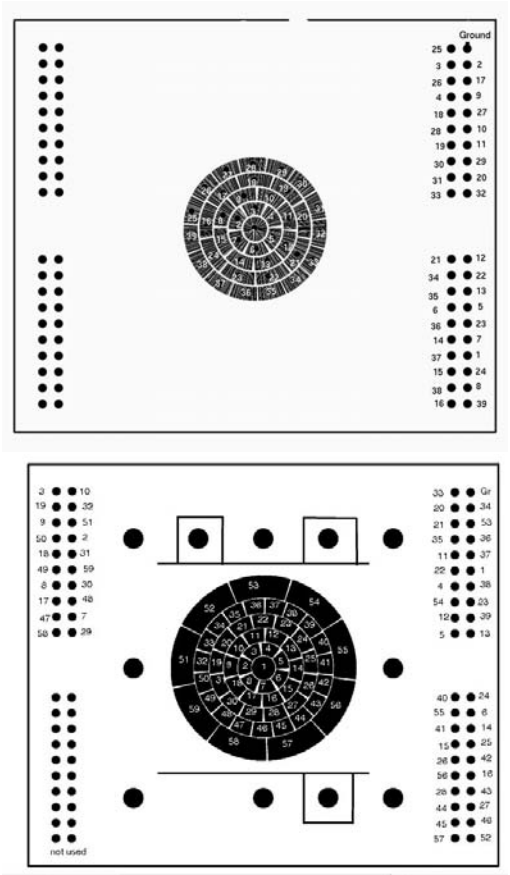

Figure 3.7: *The PCB actuator structure and pinout, top (mirror surface) view.*

that you may land the membrane onto the actuator structure and destroy the mirror. Use hex key with a very long handle to improve the sensitivity of alignment. In general you will need extremely gentle movement (about one degree of arc) of the screws. Be careful - the screws can be quite tight.

6. Apply maximum voltage to all actuators and check whether the deformation is symmetrical with respect to the mirror center. If not - realign the membrane to make it parallel to the actuator structure.
7. Repeat 5...6 until satisfaction is reached.
8. Fix the screw latches.

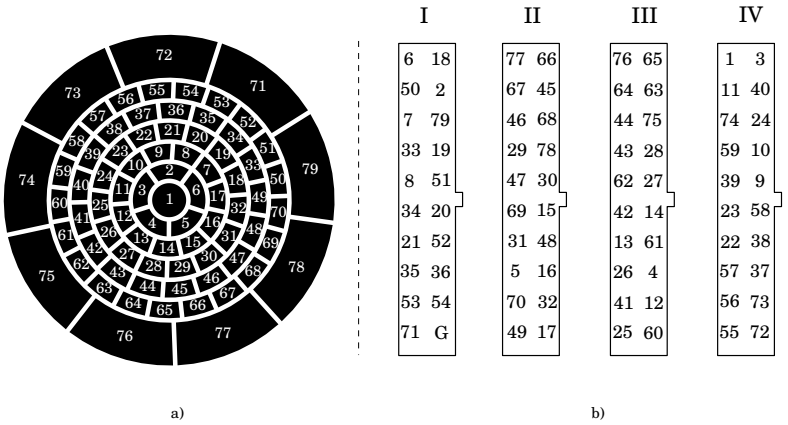

Figure 3.8: *a) The geometry of 79-channel 30mm mirror actuators and its correspondence to b) the mirror connectors pinout.*

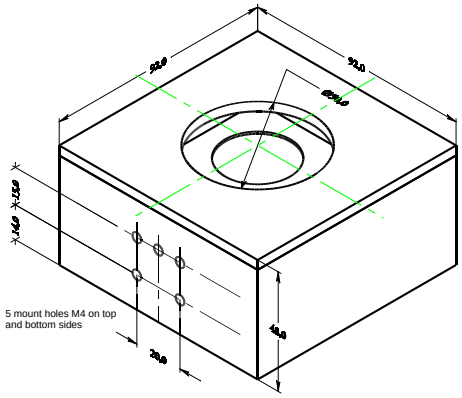

Figure 3.9: *Technical drawing of the package and mounting holes of the 30mm 39/59/79-channel MMDM*

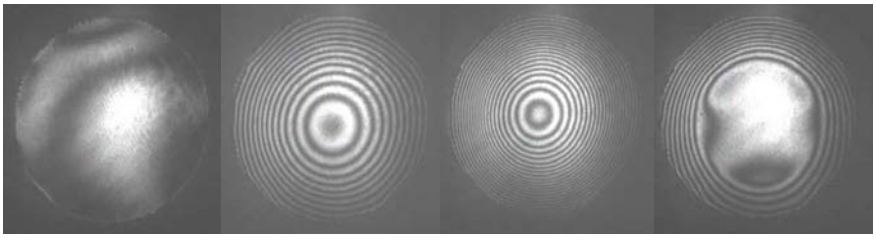

Figure 3.10: *The initial optical figure of the 39ch adaptive mirror, response to control byte 180 applied to all actuators (top row), control byte 255 applied to all actuators and to edge alignment actuators. Maximum deflection of the order of 25 fringes with all actuators on at maximum voltage.*

3.3 40mm 59/79-channel MMDM

The mirror consists of a silicon chip mounted over concentric electrostatic electrode structure. The chip contains multilayer silicon nitride membrane, which is coated with a special coating to form the mirror. The PCB contains the control electrode structure, spacer and connector. The initial shape of the reflective membrane can be adjusted using 8 adjustment micrometric screws on the back side of the mirror mount.

The device can be used for fast dynamic correction of optical aberrations.

The scheme of the assembled mirror is illustrated in Fig. 3.2 on page 32.

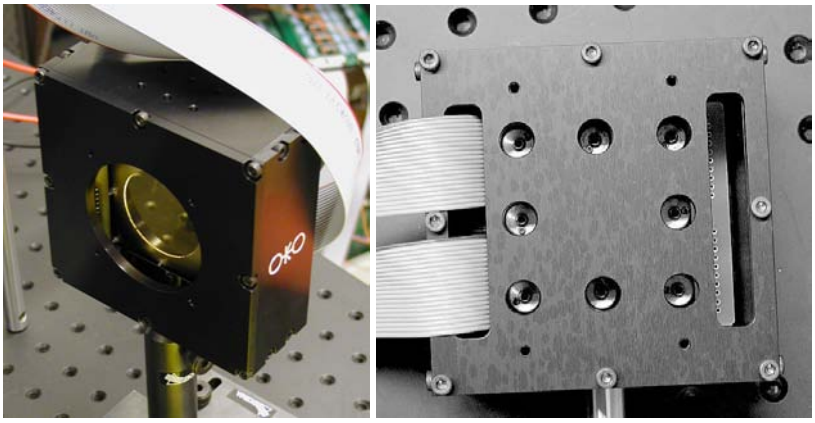

Figure 3.11: *Front and back view of the mirror. Back view of a 30-mm mirror is shown, other modification have similar features. The 40-mm mirror does not have any adjustment holes in the back cover. The cover should be removed for mirror alignment.*

3.3.1 Technical data

See Table 3.3 for typical technical parameters of the mirror.

Small surface defects are possible. They do not influence the quality of the mirror.

3.3.2 Actuator structure

The membrane is mounted over the printed actuator structure (40mm in diameter for a 59ch mirror) shown in Fig. 3.12.

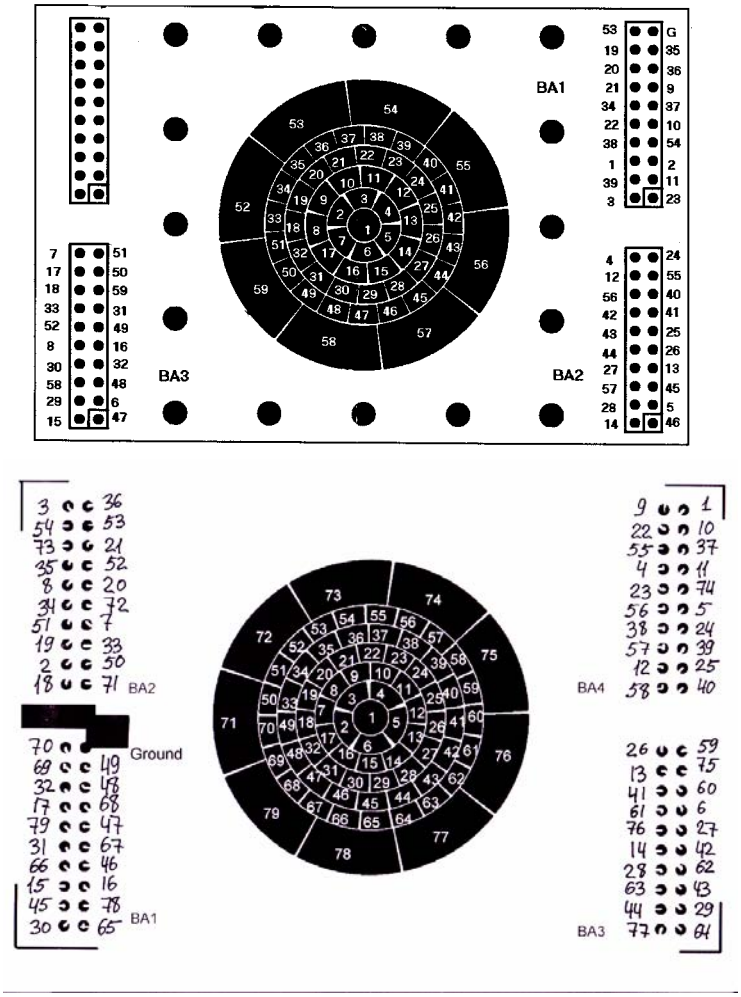

Figure 3.12: *The PCB actuator structure and pinout for 59- and 79-channel MMDMs, top (mirror surface) view.*

Table 3.3: *Technical parameters of 40mm 59 / 79-channel MMD mirror.*

Parameter	Value
Aperture shape	approximately circular
Aperture dimensions	40mm diameter
Number of electrodes	59 or 79 (see Fig. 3.12)
Control voltages V_c	0 . . . 150 to 300 V, dependent on the mirror
Initial RMS deviation from reference sphere	less than 0.9μm
Main initial aberration	coma
Maximum deflection of the mirror center	15μm
Reflectivity	better than 89% in visible
Surface defects	up to 2 coating defects
Package dimensions	see Fig. 3.13
Weight	≈600 g

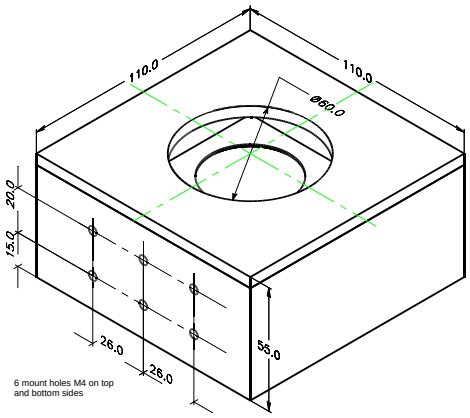

Figure 3.13: *Technical drawing of the package and mounting holes of the 40mm 59 / 79-channel MMDM*

3.3.3 Optical quality

Typical interferometric patterns of the mirror are shown in Fig. 3.14.

3.3.4 Specific remarks

See also general remarks on page 69.

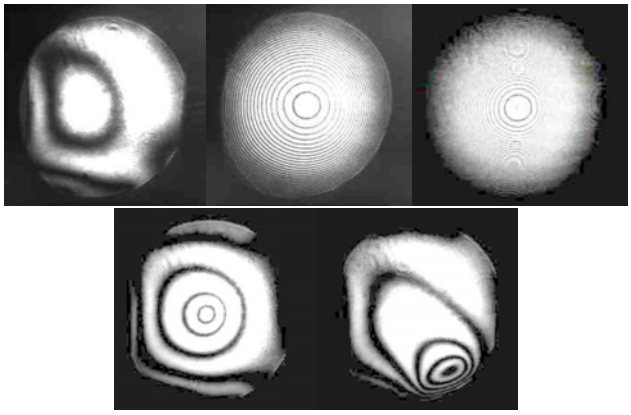

Figure 3.14: *The initial optical figure of the 59ch adaptive mirror, response to control byte 180 applied to all actuators (top row), control byte 255 applied to all actuators, to the central actuator and to the edge actuator. Maximum deflection of the order of 40 fringes with all actuators on at maximum voltage.*

3.4 11×39mm 19/38-channel linear MMDM

Silicon micromachined mirrors are fabricated by OKO Technologies using the technology of silicon bulk micromachining.

In the temporal domain, the device can be used to control the duration and the temporal shape of ultrafast pulses in femtosecond lasers and amplifiers. In the spatial domain, the device can be used as a normal deformable mirror to control the phase of extended in one dimension laser beams.

The mirror, shown in Fig. 3.15, consists of a silicon chip mounted over a PCB holder. The chip contains thin micromachined membrane, which is coated to form the mirror. The chip is mounted over 6 micrometric (see Fig. 3.15(b)) screws to adjust the mirror figure and the mirror-to-actuator distance.

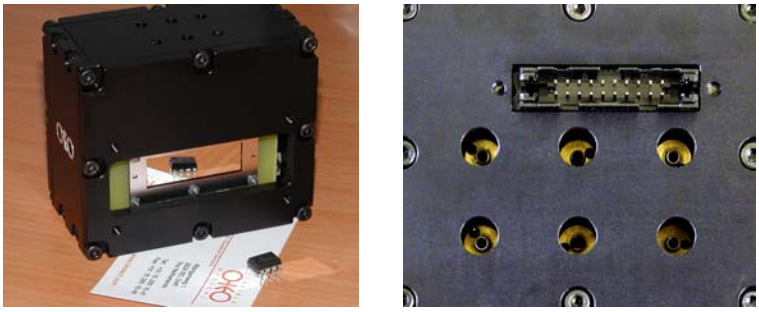

(a) **(b)**

Figure 3.15: *(a) Typical view of a linear 19-channel micromachined deformable mirror and (b) adjustment micrometric screws on the back side of the mirror. Please note that these mirrors can be fabricated with different package designs, so the mirror you have may look differently.*

The printed circuit board substrate contains the control electrode structure and connectors. It also serves as the mirror package.

The scheme of the assembled mirror and the principle of biased control are illustrated in Fig. 3.2 on page 32

3.4.1 Technical data

See Table 3.4 for technical parameters of the mirror before shipping.

Small surface defects are possible. They do not influence the quality of the mirror.

Table 3.4: *Technical parameters of 19 / 38 linear MMD mirror.*

Parameter	Value
Aperture shape	rectangle 11x39mm
Number of electrodes	19 or 38
Control voltages V_c	0 . . . 150 to 300 V, dependent on the mirror
Mirror coating	Metal or Metal + dielectric
Initial RMS deviation from plane/cylinder	less than 1μm
from plane/cylinder	
Main initial aberration	defocus/cylinder/adjustable
Maximum deflection of the mirror center	10μm (30 fringes)
Maximum optical load	not available
Package dimensions	see Fig. 3.16
Weight	≈500 g

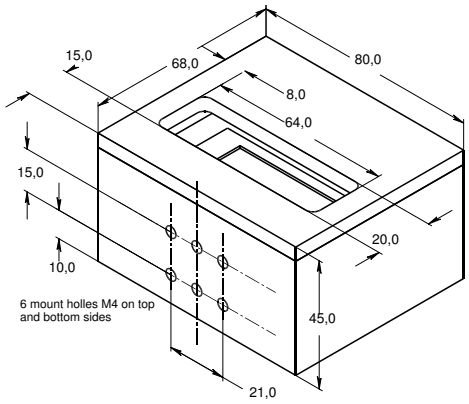

Figure 3.16: *Technical drawing of the package and mounting holes of the linear MMDM*

3.4.2 Actuator structure

The membrane is mounted over the printed actuator structure. On Fig. 3.17 addresses, with reference to the base address of PCI board are shown in large font, corresponding actuator numbers - in small font. The array of actuator addresses from one side of the 19-ch mirror to another – see Fig. 3.17(a):

```
7 4 5 2 3 0 1 14 15 13 12 11 10 9 8 23 22 21 20
```

In the case of a 38-ch mirror the actuators have the following addresses – see Fig. 3.17(b):

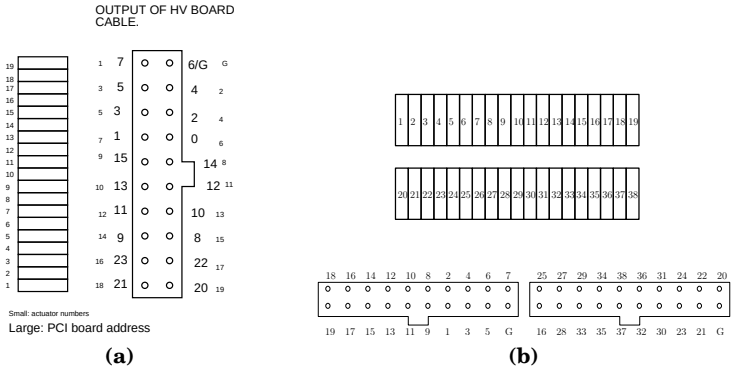

Figure 3.17: *Actuator connections for (a) 19- and (b) 38-ch mirrors.*

```
top row:    20 21 22 23 8 9 10 11 12 13 14 15 7 5 4 3 2 1 0

bottom row: 13 12 15 10 11 8 14 1 0 9 22 23 20 21 3 2 5 4 7
```

3.4.3 Optical quality

Typical interferometric patterns of the mirror are shown in Fig. 3.18.

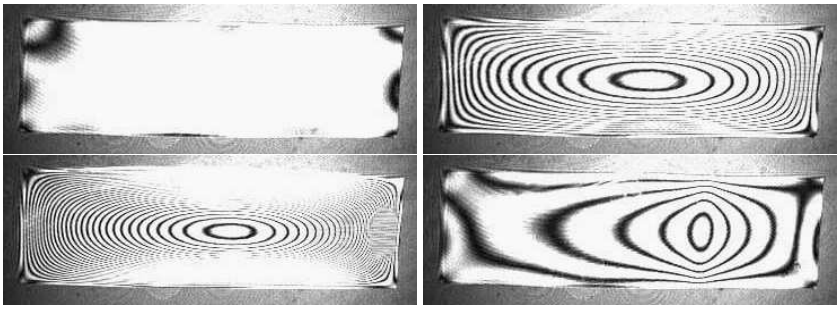

Figure 3.18: *The response to control byte 0, 180, 255 applied to all electrodes and 255 to a single electrode (left to right, top to bottom).*

3.4.4 Specific remarks

See also general remarks on page 69.

3.5 30mm 19-channel PDM

The mirror, shown in Fig. 3.19, consists of 19 piezoelectric column actuators bonded to the base holder. Reflective plate is bonded to the top of the actuator structure and coated to form the mirror. The shape of the faceplate is controlled by the voltages applied to the actuators.

The device can be used for fast dynamic correction of low-order optical aberrations such as defocus, astigmatism, coma, etc, in lasers, telescopes, ophthalmology, displays and general imaging optics.

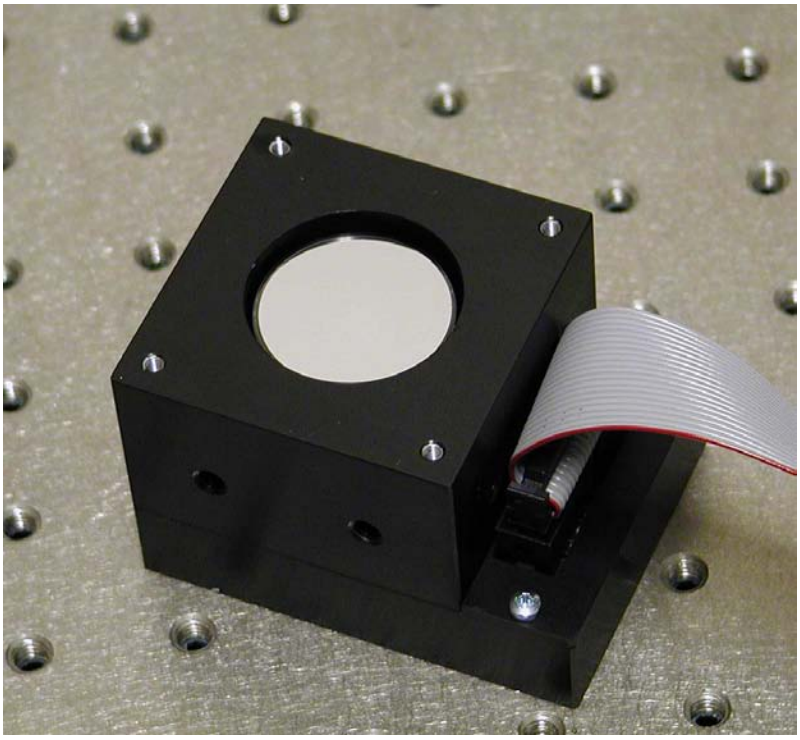

Figure 3.19: *Typical view of a 19-ch piezoelectric deformable mirror. Please note that these mirrors can be fabricated with different package designs, so the mirror you have may look differently.*

3.5.1 Technical data

See Table 3.6 for typical technical parameters of the mirror.

The mirror can be supplied with initially slightly curved spherical surface.

Table 3.5: *Technical parameters of 30mm 19-channel PD mirror.*

Parameter	Value
Aperture shape	circular 30 mm in diameter
Mirror coating	Metal or Metal + dielectric
Actuator voltages	$0 + 400$V (with respect to the ground electrode)
Number of electrodes	19 (see Fig. 3.21)
Actuator capacitance C_a	5 nF
Main initial aberration	sphere
Initial RMS deviation from reference sphere	less than 1μm
Maximum stroke	8μm at $+400V$
Actuator pitch	7 mm
Package dimensions	see Fig. 3.20
Weight	320 g

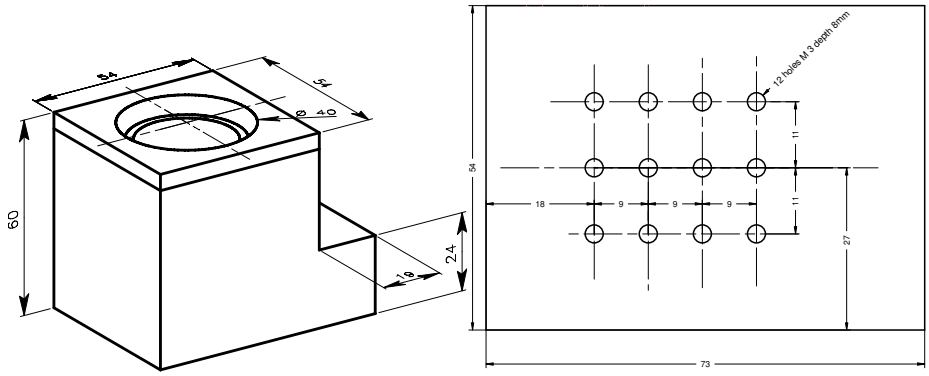

Figure 3.20: *Technical drawing of the package and mounting holes of the 30mm 19-channel PDM*

This sphericity is caused by the stress in the mirror coating. It does not influence the parameters of the mirror, but should be taken into account when the mirror is incorporated into the optical setup.

Due to hysteresis of actuators, the initial aberration may change during the mirror usage and deviate more from the reference sphere. This deviation is a superposition of actuator response functions and is irrelevant in active setups with closed-loop control, though it may slightly reduce the correction range.

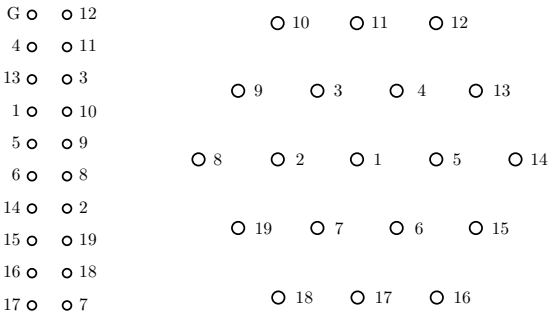

Figure 3.21: *The connector pinout and the geometry of mirror actuators for the 19-ch mirror (view from the back side of the mirror).*

3.5.2 Optical quality

Typical interferograms of the mirror are shown in Fig. 3.22.

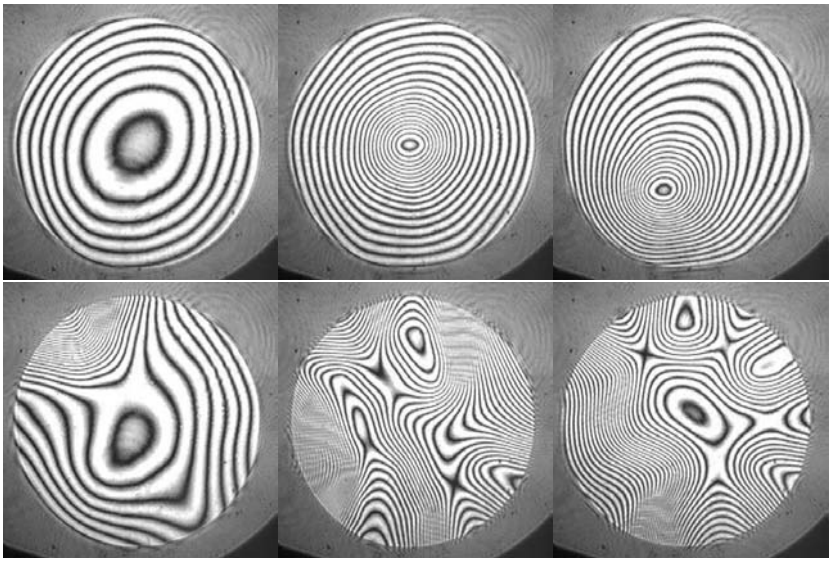

Figure 3.22: *Test of the mirror: zero voltage applied, 300V applied to the central, internal and edge actuators, random voltages to all actuators.*

3.5.3 Specific remarks

See also general remarks on page 69.

3.6 30mm 37-channel PDM

The mirror, shown in Fig. 3.23, consists of 37 piezoelectric column actuators bonded to the base holder. Reflective plate is bonded to the top of the actuator structure and coated to form the mirror. The shape of the faceplate is controlled by the voltages applied to the actuators.

The device can be used for fast dynamic correction of low-order optical aberrations such as defocus, astigmatism, coma, etc, in lasers, telescopes, ophthalmology, displays and general imaging optics.

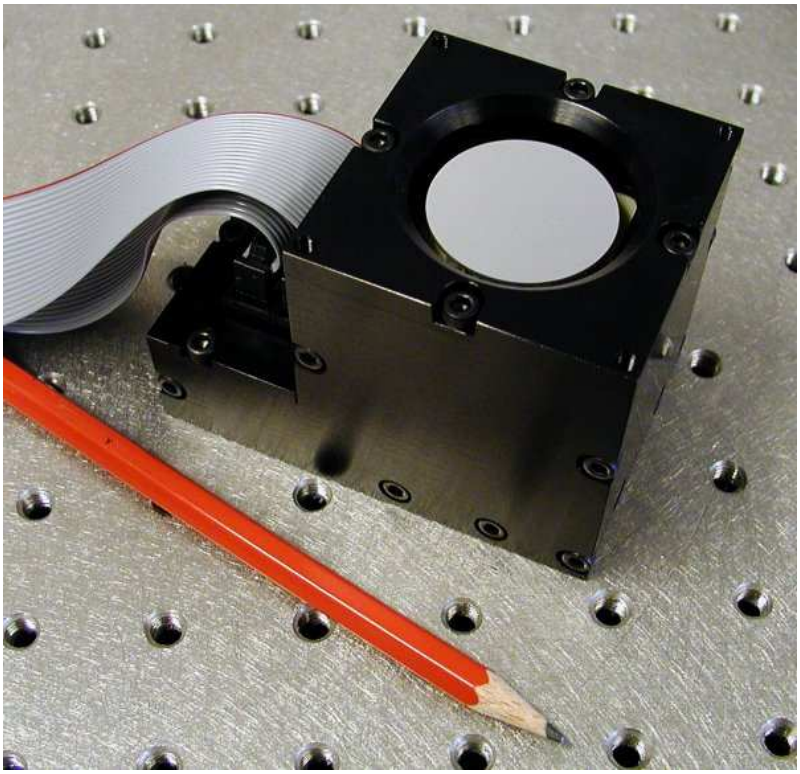

Figure 3.23: *Typical view of a 37-ch piezoelectric deformable mirror. Please note that these mirrors can be fabricated with different package designs, so the mirror you have may look differently.*

3.6.1 Technical data

See Table 3.6 for typical technical parameters of the mirror.

Table 3.6: *Technical parameters of the mirror.*

Parameter	Value
Aperture shape	circular 30 mm in diameter
Mirror coating	Metal or Metal + dielectric
Actuator voltages	$0 + 400$V (with respect to the ground electrode)
Number of electrodes	37 (see Fig. 3.25)
Actuator capacitance C_a	5 nF
Main initial aberration	sphere
Initial RMS deviation from reference sphere	less than 1μm
Maximum stroke	8μm at $+400V$
Actuator pitch	4.3 mm
Package dimensions	see Fig. 3.24
Weight	370 g

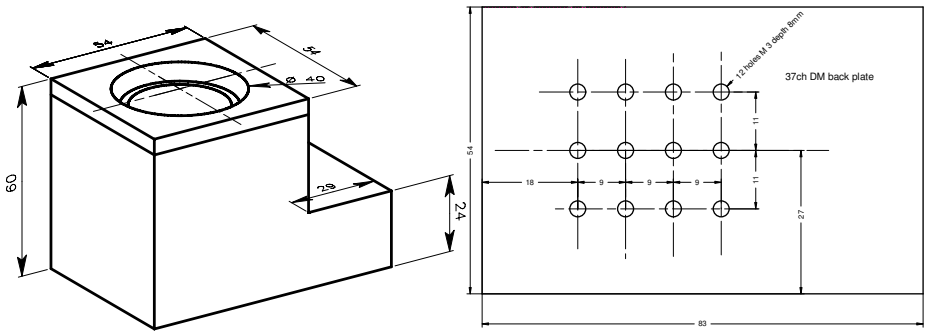

Figure 3.24: *Technical drawing of the package and mounting holes of the 30mm 37-channel PDM*

The mirror can be supplied with initially slightly curved spherical surface. This sphericity is caused by the stress in the mirror coating. It does not influence the parameters of the mirror, but should be taken into account when the mirror is incorporated into the optical setup.

Due to hysteresis of actuators, the initial aberration may change during the mirror usage and deviate more from the reference sphere. This deviation is a superposition of actuator response functions and is irrelevant in active setups with closed-loop control, though it may slightly reduce the correction range.

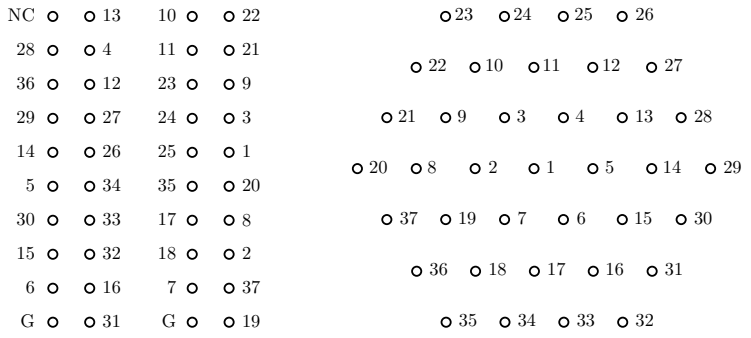

Figure 3.25: *The connector pinout and the geometry of mirror actuators for the 37-ch mirror (view from the back side of the mirror).*

3.6.2 Optical quality

Typical interferograms of the mirror obtained before shipping are shown in Fig. 3.26.

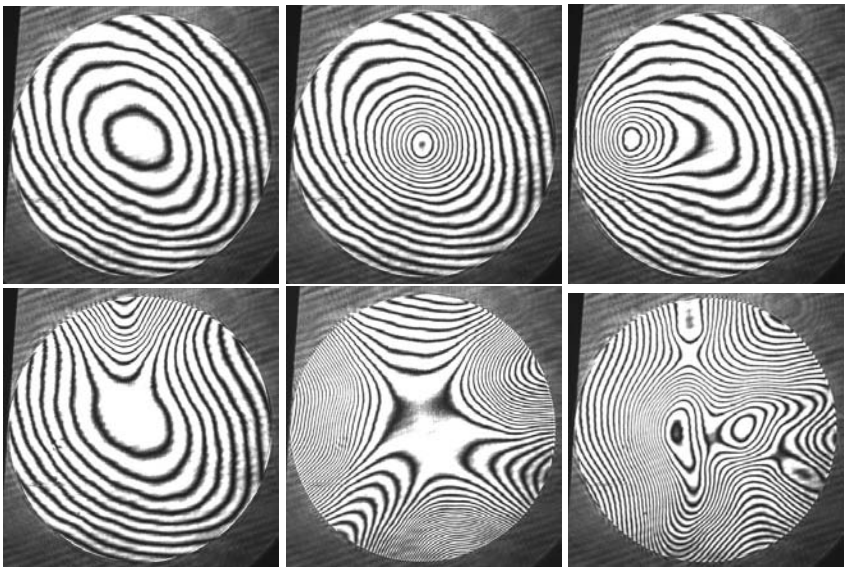

Figure 3.26: *Test of the mirror: zero voltage applied, 300V applied to the central, internal and edge actuators, random voltages to all actuators.*

Typical interferograms of actively flattened mirror are shown in Fig. 3.27 (see Chapter 7 on page 117 for details).

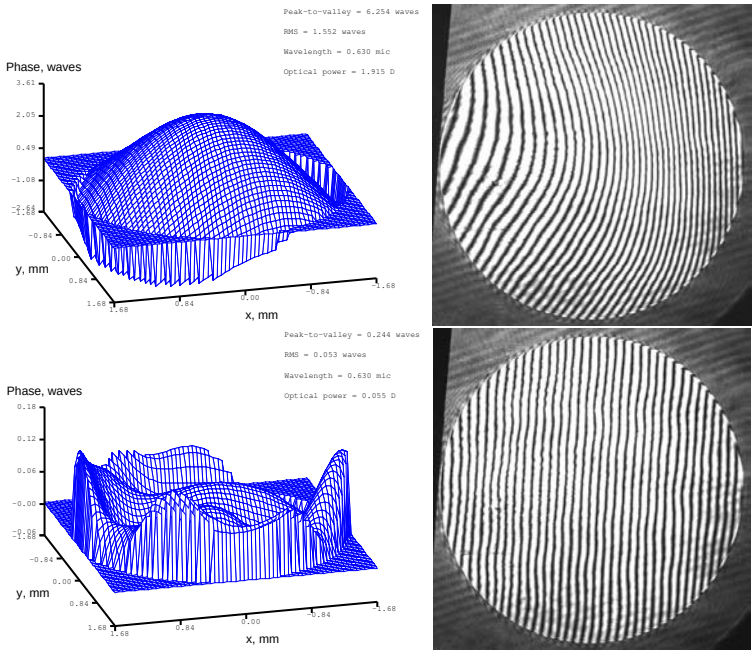

Figure 3.27: *Initial shape of the mirror, which was produced by setting all mirror values to zero, and shape of the mirror after active flattening.*

3.6.3 Specific remarks

See also general remarks on page 69.

3.7 50mm 37-channel PDM

The mirror, shown in Fig. 3.28, consists of 37 piezoelectric column actuators bonded to the base holder. Reflective plate is bonded to the top of the actuator structure and coated to form the mirror. The shape of the faceplate is controlled by the voltages applied to the actuators.

The device can be used for fast dynamic correction of low-order optical aberrations such as defocus, astigmatism, coma, etc, in lasers, telescopes, ophthalmology, displays and general imaging optics.

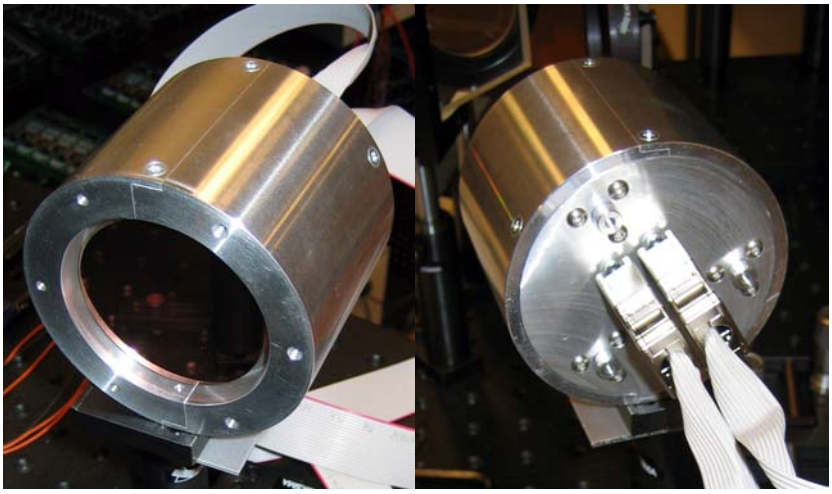

Figure 3.28: *Typical front and back views of a 37-ch piezoelectric deformable mirror. Please note that these mirrors can be fabricated with different package designs, so the mirror you have may look differently.*

3.7.1 Technical data

See Table 3.7 for typical technical parameters of the mirror.

The mirror can be supplied with initially slightly curved spherical surface. This sphericity is caused by the stress in the mirror coating. It does not influence the parameters of the mirror, but should be taken into account when the mirror is incorporated into the optical setup.

Due to hysteresis of actuators, the initial aberration may change during the mirror usage and deviate more from the reference sphere. This deviation is a superposition of actuator response functions and is irrelevant in active setups with closed-loop control, though it may slightly reduce the correction range.

Table 3.7: *Technical parameters of the mirror.*

Parameter	Value
Aperture shape	circular 50mm in diameter
Mirror coating	Metal or Metal + dielectric
Actuator voltages	$0 + 400$V (with respect to the ground electrode)
Number of electrodes	37 (see Fig. 3.30)
Actuator capacitance C_a	~ 15nF
Main initial aberration	sphere or astigmatism
Initial RMS deviation from reference sphere	less than 1μm
Maximum stroke	8μm at $+400V$
Actuator pitch	7mm
Package dimensions	see Fig. 3.29
Weight	≈600 g

3.7.2 Optical quality

Typical interferograms of the mirror are shown in Fig. 3.31. **NB!** The interferograms were registered at wavelength $\lambda = 530$nm in interferometer with total aperture less than 50mm.

3.7.3 Specific remarks

See also general remarks on page 69.

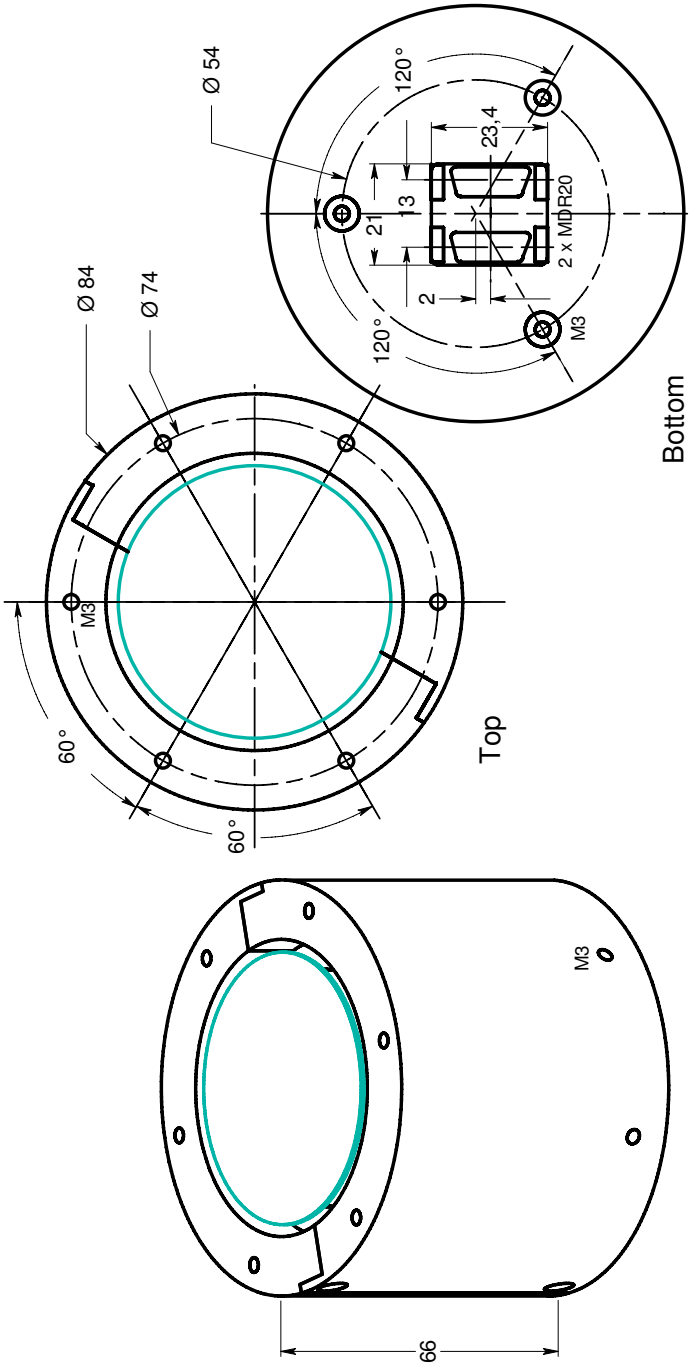

Figure 3.29: *Technical drawing of the package and mounting holes of the 50mm 37-channel PDM*

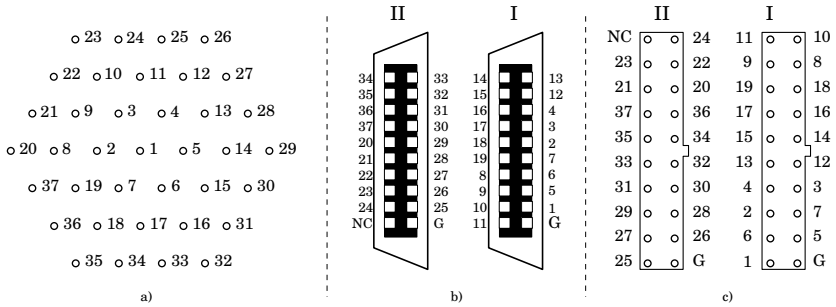

Figure 3.30: *a) The geometry of mirror actuators and its correspondence to b) the mirror connectors pinout and c) the high-voltage amplifier pinout.*

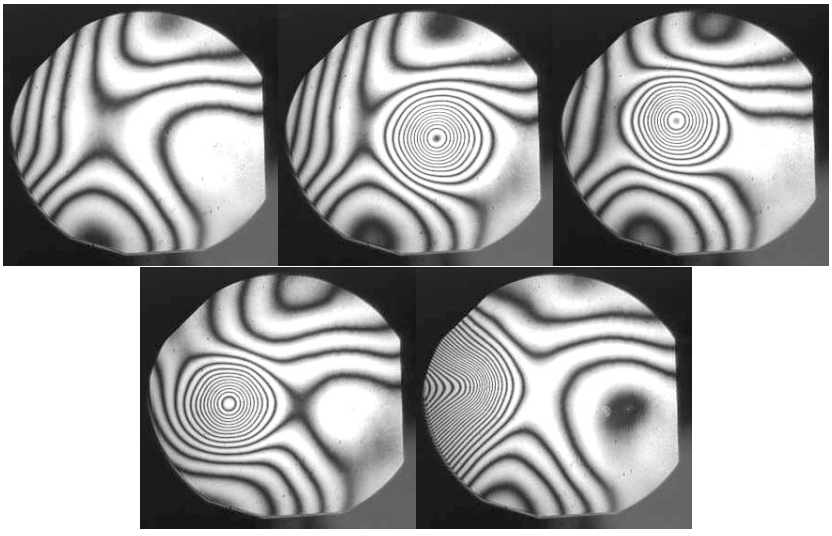

Figure 3.31: *Test of the mirror: zero voltage applied, 300V applied to the central, internals and edge actuators.*

3.8 50mm 37/79/109-channel PDM

The mirror, shown in Fig. 3.32, consists of 37, 79 or 109 piezoelectric column actuators bonded to the base holder. Reflective plate is bonded to the top of the actuator structure and coated to form the mirror. The shape of the faceplate is controlled by the voltages applied to the actuators.

The 37/79/109-ch 50 mm piezoelectric OKO mirror is suitable for fast dynamic correction of large high-order optical aberrations such as defocus, astigmatism, coma, etc, in lasers, telescopes, ophthalmology, displays and general imaging optics.

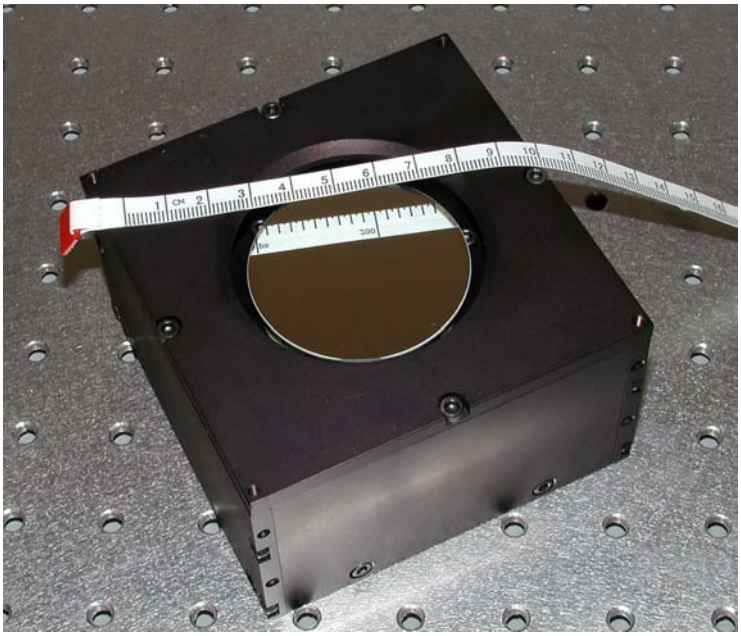

Figure 3.32: *Typical front view of a 37/79/109-ch piezoelectric deformable mirror. Please note that these mirrors can be fabricated with different package designs, so the mirror you have may look differently.*

3.8.1 Technical data

See Table 3.8 for typical technical parameters of the mirror.

The mirror can be supplied with initially slightly curved spherical surface. This sphericity is caused by the stress in the mirror coating. It does not influence the parameters of the mirror, but should be taken into account when the mirror is incorporated into the optical setup.

Table 3.8: *Technical parameters of the mirror.*

Parameter	Value
Aperture shape	circular 50mm in diameter
Mirror coating	Metal or Metal + dielectric
Actuator voltages	$0 + 400$V (with respect to the ground electrode)
Number of electrodes	37/79/109 (see Fig. 3.34 - 3.36)
Actuator capacitance C_a	$\sim$ 5nF
Main initial aberration	sphere
Initial RMS deviation from reference sphere	less than 2μm
Maximum stroke	8μm at $+400V$
Actuator pitch	$6.83, 4.72, 4.3$mm
Package dimensions	see Fig. 3.33
Weight	650 g

Due to hysteresis of actuators, the initial aberration may change during the mirror usage and deviate more from the reference sphere. This deviation is a superposition of actuator response functions and is irrelevant in active setups with closed-loop control, though it may slightly reduce the correction range.

3.8.2 Optical quality

Typical interferograms of the mirror are shown in Fig. 3.37.

3.8.3 Specific remarks

See also general remarks on page 69.

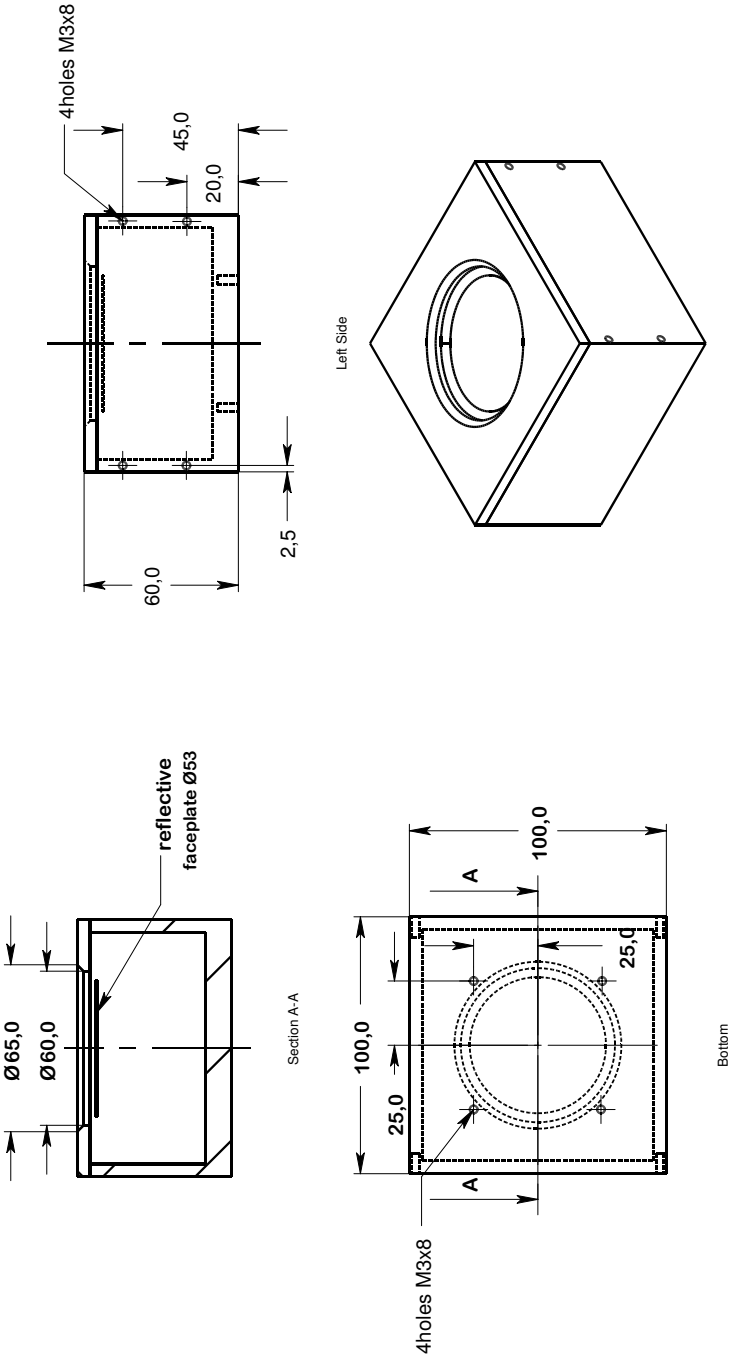

Figure 3.33: *Technical drawing of the package and mounting holes of the 50mm 109-channel PDM*

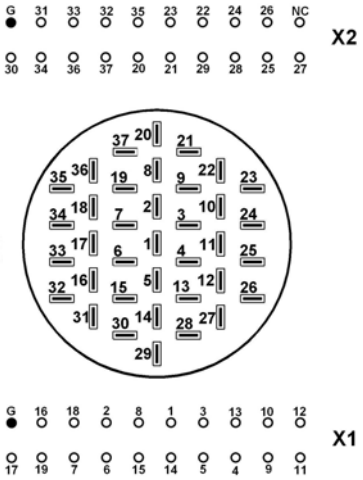

Figure 3.34: *The geometry of the 37-ch mirror actuators and its correspondence to the mirror connectors pinout (view from the mirror side).*

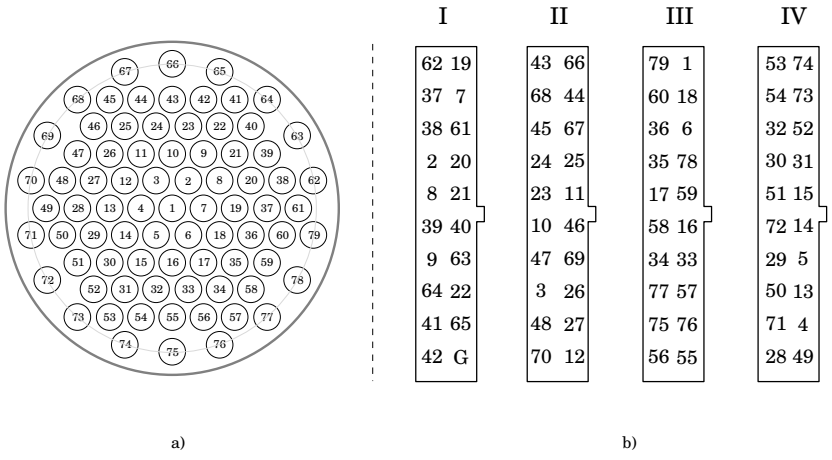

Figure 3.35: *The geometry of the 79-ch mirror actuators and its correspondence to the mirror connectors pinout (view from the mirror side).*

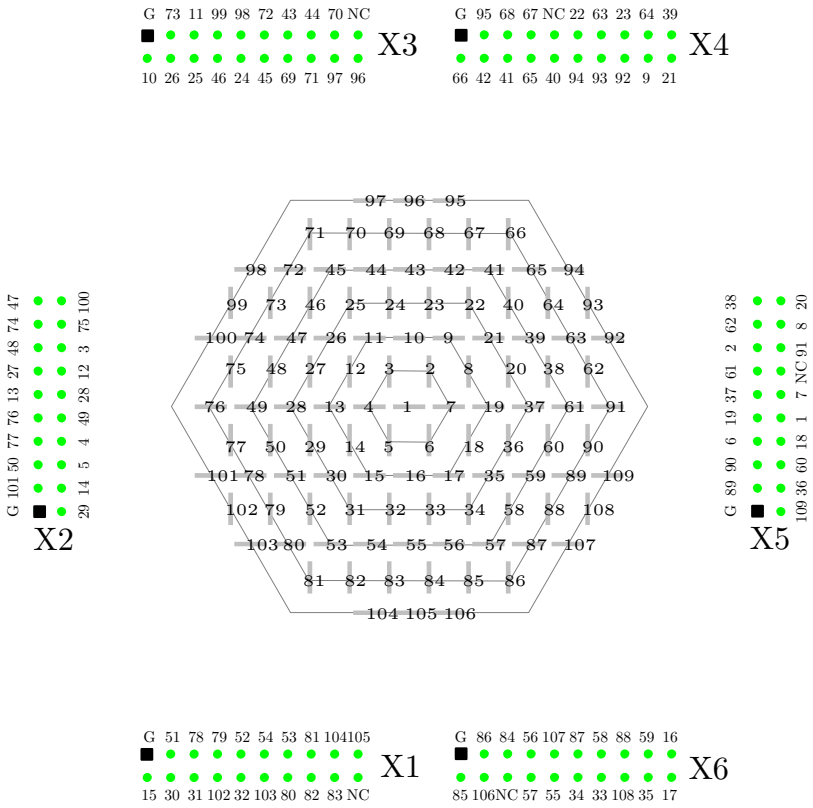

Figure 3.36: *The geometry of the 109-ch mirror actuators and its correspondence to the mirror connectors pinout (view from the mirror side)*

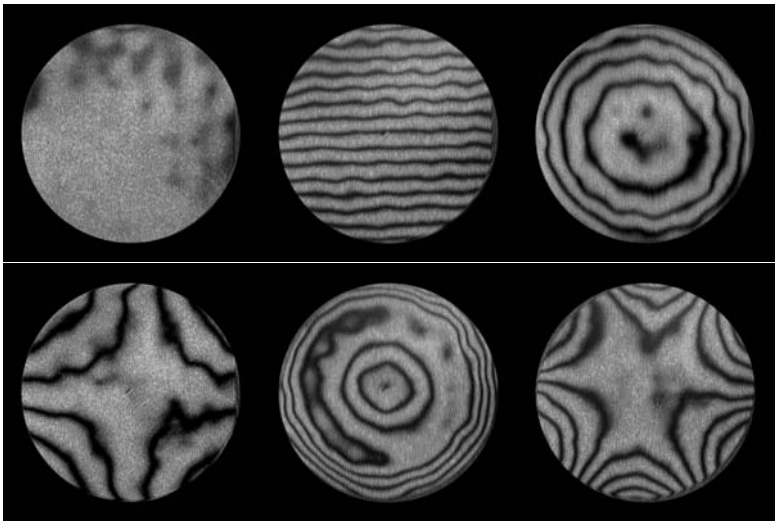

Figure 3.37: *Test of the 109-ch mirror: mirror flattening (initial aberration corrected), shown with and without tilt introduced, defocus, astigmatism, spherical aberration and trefoil generated.*

3.9 11×55mm 20-channel linear PDM

The mirror, shown in Fig. 3.38, consists of 20 piezoelectric column actuators bonded to the base holder. Reflective plate is bonded to the top of the actuator structure and coated to form the mirror. The shape of the faceplate is controlled by the voltages applied to the actuators.

In the temporal domain, the device can be used to control the duration and the temporal shape of ultrafast pulses in femtosecond lasers and amplifiers. In the spatial domain, the device can be used as a normal deformable mirror to control the phase of extended in one dimension laser beams.

Figure 3.38: *Typical view of a 20-ch linear piezoelectric deformable mirror. Please note that these mirrors can be fabricated with different package designs, so the mirror you have may look differently.*

3.9.1 Technical data

See Table 3.9 for typical technical parameters of the mirror.

The mirror can be supplied with initially slightly curved spherical surface. This sphericity is caused by the stress in the mirror coating. It does not influence the parameters of the mirror, but should be taken into account when the mirror is incorporated into the optical setup.

Due to hysteresis of actuators, the initial aberration may change during the mirror usage and deviate more from the reference sphere. This deviation is a

Table 3.9: *Technical parameters of the mirror.*

Parameter	Value
Aperture shape	rectangular 10×50 mm^2
Mirror coating	Metal or Metal + dielectric
Actuator voltages	$0 + 400$V (with respect to the ground electrode)
Number of electrodes	20 (see Fig. 3.40)
Actuator capacitance C_a	6 nF
Main initial aberration	sphere
Initial RMS deviation from reference sphere	less than 1 μm
Maximum stroke	8μm at $+400V$
Actuator pitch	5 mm
Package dimensions	see Fig. 3.39
Weight	300 g

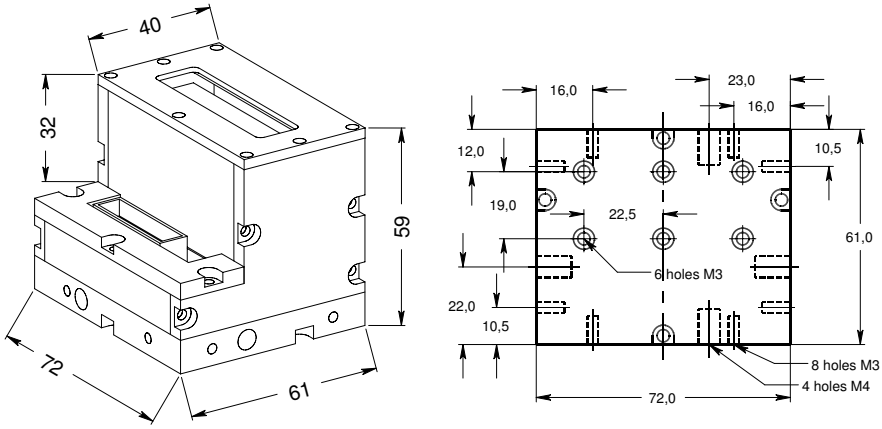

Figure 3.39: *Technical drawing of the package and mounting holes of the 30mm 37-channel PDM*

superposition of actuator response functions and is irrelevant in active setups with closed-loop control, though it may slightly reduce the correction range.

3.9.2 Optical quality

Typical interferograms of the mirror are shown in Fig. 3.41. A result of the active flattening using FrontSurfer wavefront sensor is shown in Fig. 3.43; the initial shape is shown in Fig. 3.42. The interferograms are shown for the

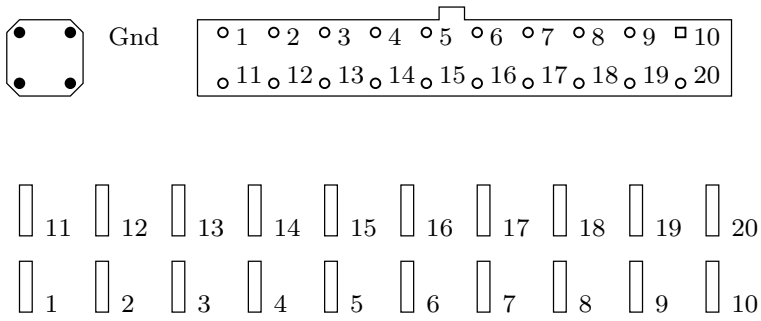

Figure 3.40: *The connector pinout and the geometry of mirror actuators for the 20-ch linear piezoelectric mirror (view from the front side).*

wavelength of λ = 633 nm.

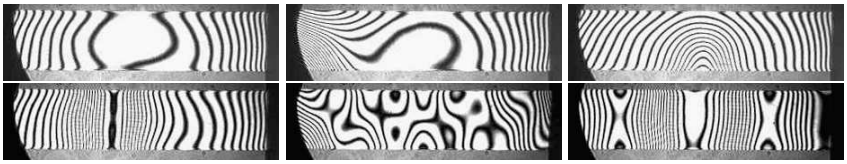

Figure 3.41: *Test of the mirror. Top row, left to right: zero voltage applied, maximum voltage applied to the 1st actuator, maximum voltage applied to the bottom center actuator; bottom row: non-zero bytes applied to some actuators.*

3.9.3 Specific remarks

Connection to the control electronics

For a 20-channel mirror, you need a USB unit with a ground connector on its back panel (Fig. 4.8 on page 79). This USB unit is configured to provide 20-channel output in the signal corrector and a separate ground connector. Do not change the jumper setting of the USB unit.

See also general remarks on page 69.

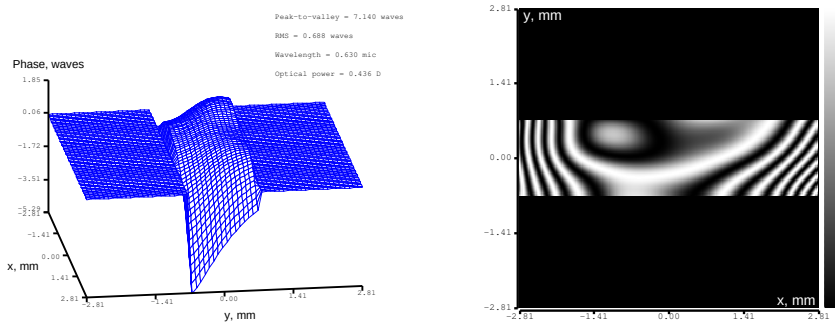

Figure 3.42: *Initial shape of the mirror; tested using FrontSurfer wavefront sensor.*

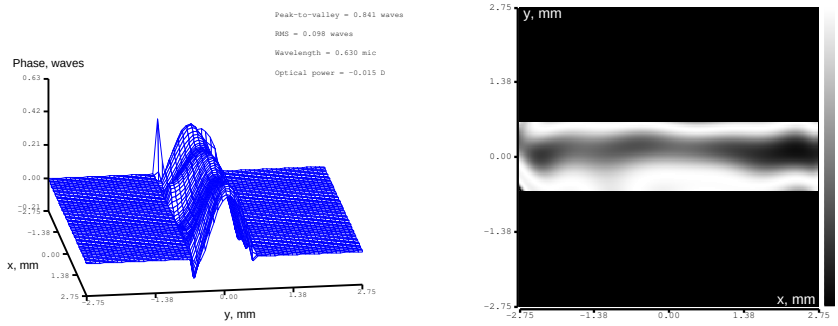

Figure 3.43: *The mirror shape after active flattening; tested using FrontSurfer wavefront sensor.*

3.10 General remarks

The maximum voltage for the mirror should never exceed the specified maximum control voltage.

For OEM version. **Use high-quality stabilized filtered high-voltage supply.** Some high-voltage supplies generate short high-voltage spikes at the output, these deviations can destroy the mirror, driver electronics and even the control computer. Do not turn on V_high directly to its maximum value. Set V_high to 100V before switching the system off. Switch the system on with V_high not higher than 120V. Increase V_high to its working value after switching on the digital boards and setting the control voltages to zero. Supply voltage for the amplifier boards should never exceed the specified V_high.

The jumpers on the amplifier board or in the amplifier unit, in the DAC USB control unit are preset before shipping; this configuration should not be changed. **The system and jumper configuration were tested before shipping.**

Do not touch or clean the mirror. We are not responsible for any damage to the mirror due to a cleaning attempt. If you need to clean the mirror, please contact us; we can clean it for you.

3.10.1 First run of the system

- **Read this document through before performing any practical steps**. Follow the instructions exactly, if it's written `connect the board`, `connect the mirror` — **first** connect the board and **then** connect the mirror.
- All following operations refer to:
  - either *DAC-40-USB unit* connected to a computer running Windows - we used XP SP2 for final tests
  - or *digital boards* installed in a computer running Linux - we used RH 7.2 for final tests.
- *For DAC-40-USB unit.* Connect the DAC USB unit to the computer USB port. Install the software (refer to the DAC USB unit guide). Jumpers of the USB unit are already preset to the correct position (every connector provides 19-channel output and ground). Run the example programs supplied with the CD to test the DAC USB unit functionality.
- Switch the computer off. Connect band cables to the connector(s) in the mirror holder. Connect the amplifier unit to the DAC USB unit. At this stage the system is fully assembled but the adaptive mirror is not used yet. Switch on the amplifier unit. Test the output voltages in the mirror

socket. These voltages must be in the range 0...2V. Turn the computer on. At this stage the voltages in mirror socket may have values between 0V and 213 V. Run the test programs. Control all channels. Switch off the amplifier unit and computer.

- *For digital boards.* Insert digital boards into computer slots. Install the software (refer to the PCI board guide) and determine the base address (look at /proc/pci for PROTO 3 boards). Connect the bandcables to the digital boards. Switch the computer on. Run the example programs supplied with the CD to test the board functionality.

- *For OEM version.* Switch the computer off. Connect band cables to the connectors in the mirror holder. Connect the amplifier boards to mirror driver boards. Connect the driver boards to low and high voltage power supplies. At this stage the system is fully assembled but the adaptive mirror is not used yet. Switch on the power supplies in the order: +15V, -15V, +V_high. Do not use V_high higher than 120V for the first test. The current (positive supply to ground) should not exceed 0.125A for one board (zero output of all 20 amplifiers) and 0.25A for two boards (40 amplifiers). The high voltage current should not exceed 0.05A for V_high=150V for two boards. Test the output voltages in the mirror socket. These voltages must be in the range 0...1V. Turn the computer on. While turned on, the boards are initialized to random output voltages. At this stage the voltages in mirror socket may have values between 0V and V_high. Run the test programs. Control all channels. Switch off power supplies and computer (in the order V_high, +15V, -15V, computer).

- For mirrors shipped separately from the PCB holder, position the marked corner of the mirror to the mark on the mirror holder and insert (gently) the mirror into the socket. Place the mirror into interferometer or a setup with a wavefront sensor. Fix the cables to the optical table. You may also test the mirror by reflecting a good collimated beam from the mirror surface and observing the near field intensity distribution. **Clamp the mirror holder, do not clamp the mirror**, clamping the mirror will cause extra deformation of the socket and the the mirror package. At this stage you do not have to feed any supply voltages to the control boards but the power supplies must be grounded appropriately.

- Control the initial mirror figure (astigmatic up to 1 fringes P-V).

- Switch on all supply voltages (*For OEM version* in the order +15V, -15V, V_high. Do not use V_high higher than 100V at this stage.)

- Switch on the computer. After the system is loaded, the mirror figure represents strongly distorted concave surface. Use test programs to

control the mirror figure. Peripheral actuators (channels 20 to 37) are less sensitive.

- You may start to use the mirror if all channels work. Use “am_set” and “rotate” as templates to write your own control programs.

4

DRIVERS AND SOFTWARE

4.1 High-voltage amplifier units

High-voltage amplifier unit is specially designed to control the deformable mirrors.

Each unit contains:

- 1 or 2 HV amplifier board(s);
- high-voltage power supply;
- low-voltage power supply.

The high-voltage power supply can be tuned to the desired maximum voltage in the range 100. . . 400 V.

The high-voltage control-amplifier unit simplifies significantly the setup and use of AO systems in respect with OEM configuration. Every unit shipped with any OKO adaptive mirror is pre-configured for this specific mirror eliminating the need of any further configuration by user.

To use the unit, you must connect it to the mirror, to a DAC USB unit (or PCI boards) and to the wall outlet (85 to 250V AC, 50 to 60 Hz). Connect the mirror with a supplied flat ribbon cables to the 20-pin connectors on the front side, and the driver boards or the USB unit to the 26-pin connectors. When using two or more HV units, connect them together using the ground sockets on the back panels.

For 20-channel linear PDM Connect the ground pin of the mirror with the ground connector of the amplifier unit located on the back panel (Fig. 4.2) using the supplied cable and to the ground connector of the USB unit (or to the metal case of the PC, if PCI board is used to drive the mirror). See Fig. 4.2 for the reference.

Figure 4.1: *40- and 20-channel high-voltage amplifier units.*

4.2 A4MEMS

A4MEMS is 4-channel high-voltage amplifier specially designed as a quick low-cost solution for prototyping of multichannel high-voltage MEMS circuits. Each of its 4 independent amplifiers with gain of 51 is capable of driving

Figure 4.2: *Front and back panels of 40 channel high-voltage amplifier unit.*

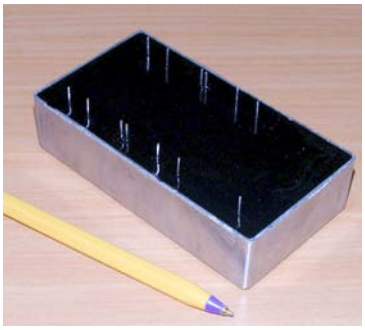

Figure 4.3: *Typical view of 4-channel high-voltage DC amplifier A4MEMS*

capacitive loads up to 10 nF in the frequency range of DC to 250 Hz. 1 nF loads can be driven in the frequency range of up to 1 kHz, with full 300 V amplitude. A4MEMS is usable for driving a wide variety of electrostatic and piezoelectric actuators.

A4MEMS measures 110 x 60 x 30mm. It provides $0 \ldots 300$ V output in 4 independent channels. Voltage ranges up to $0 \ldots 400$ V are available on special order. The unit does not require any external high voltage supply and can be powered from any 16 V 200 mA laboratory supply (lower voltages can be used to trim the maximum output voltage). See Table 4.1 for the technical parameters.

A4MEMS features a complete short circuit protection – the unit can continuously operate with all 4 outputs connected to the ground, regardless of the state of its inputs. Several units can be combined for quick prototyping of multi-channel high-voltage drivers in telecom applications and adaptive optics. The device have single common ground for all inputs, outputs, and the power supply. The case of the device is grounded.

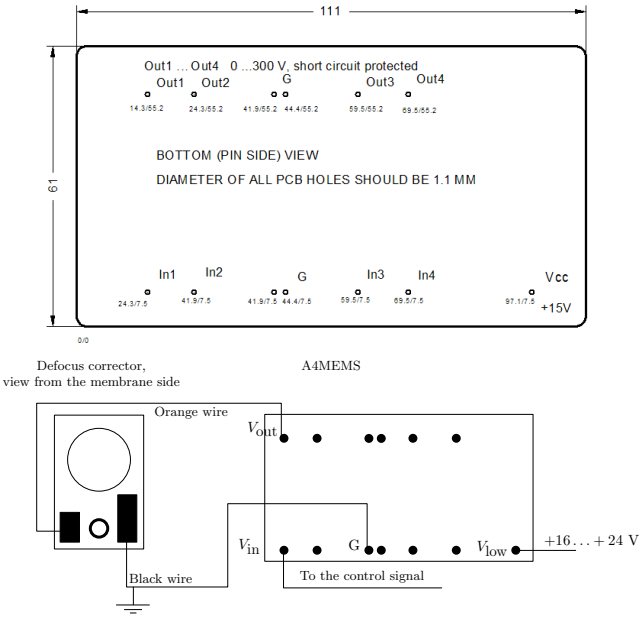

Figure 4.4: *Pin-out and an example of connection scheme for the defocus corrector and A4MEMS.*

Figure 4.5: *DAC-40-USB driver module.*

4.3 40-channel USB driver module

Digital-to-analog converter unit “DAC-40-USB” (see Figure 4.5) is intended to provide multi-channel voltage output controlled from a personal computer via a USB port. Its primary purpose is to drive deformable mirrors produced by OKO Technologies.

Technical data are shown in Table 4.2 on the facing page.

Table 4.1: *Technical parameters*

Parameter	Value
Number of channels	4
DC Gain	≈ 51
Output impedance	330 kΩ
Short circuit protection	yes
Frequency range at 1 nF load	0...1 kHz
Input voltage	0...12 V
Low voltage power supply	14...24 V
Output voltage	0.5 ...300 V
Maximum capacitive load	30 nF
Power dissipation	3.4 W
Size	$110 \times 60 \times 30$ mm^3
Weight	330g

Table 4.2: *40-channel DAC USB unit*

Parameter	Value
Analog outputs	40
Output range	0...5.5 V
Output resolution	12 bits (4096 levels)
Output mode	synchronous for all channels
Range of adjustment of the maximum control voltage	2.5...5.5 V
Ohmic load, each channel	$\geq$ 100 kΩ
Load capacitance, each channel	$\leq$ 500 pF
Power	provided via the USB port

4.3.1 General design

"DAC-40-USB" is designed as a PCB with two double-row angle connectors BH-20R (male) and a B-type USB connector; it is mounted in a compact housing. Pins of the output connectors are labeled according to the numbering order of the output channels. The maximum output voltage value can be adjusted (all channels simultaneously) by a variable resistor, whose slot is sunk in a hole on the front side of the unit (Figure 4.6). To provide access to the PCB, one should disconnect upper and lower decks of the housing by simultaneous depression of their side surfaces. To close the housing, the decks must be pushed vertically one to another till latched.

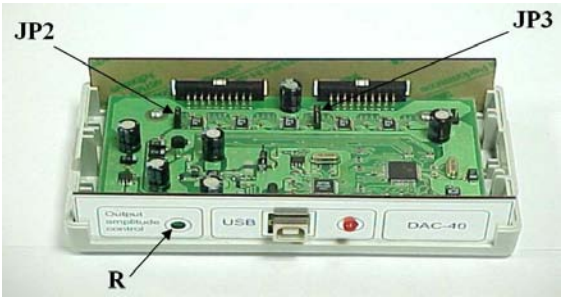

Figure 4.6: *DAC-40-USB; view from the output connectors' side*

Table 4.3: *Jumpers settings and output connectors commutation*

JP2	Pin 1 of X3
1–2	Channel #1 output
2–3	Ground

JP3	Pin 1 of X4
1–2	Channel #21 output
2–3	Ground

4.3.2 Jumper settings for version 1.0

Jumpers JP2 and JP3 are mounted on the PCB (Figure 4.7). By connecting contacts 2 and 3 of jumpers JP2 and JP3 pin #1 of connector X3 (channel 1) and/or pin #1 of X4 (channel 21), correspondingly, can be connected to the ground (see Table 4.3). It should be kept in mind that when pin #1 of X3 (pin #1 of X4) is connected to the ground, the 1st (or 21st, correspondingly) channel of the DAC is disconnected from the connector.

For a 20-channel mirror, you need a USB unit with a ground connector on its back panel (Fig. 4.8). This USB unit is configured to provide 20-channel output in the signal corrector and a separate ground connector. Do not change the jumper setting of the USB unit.

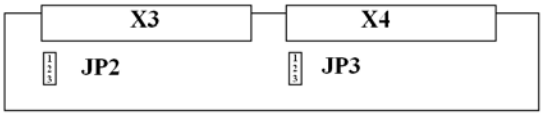

Figure 4.7: *PCB layout and numbering of jumpers' contacts*

Figure 4.8: *Back panel of the USB control unit with a ground connector.*

4.3.3 Jumper settings for version 2.0

Jumpers X3 and X4 are mounted on the PCB (Fig. 4.9). By connecting contacts 2 and 3 of jumpers X3 and X4 pin #1 of connector X5 (channel 1) and/or pin #1 of X6 (channel 21), correspondingly, can be connected to the ground (see Table 4.4 on the next page). It should be kept in mind that when pin #1 of X3 (pin #1 of X4) is connected to the ground, the 1st (or 21st, correspondingly) channel of the DAC is disconnected from the connector.

Jumpers X7 and X8 allow swapping pins 1 and 2 of the output connectors X5 and X6 (see Table 2 for details).

Jumper X9 can be set to connect the outer case of the USB connector X2 to ground.

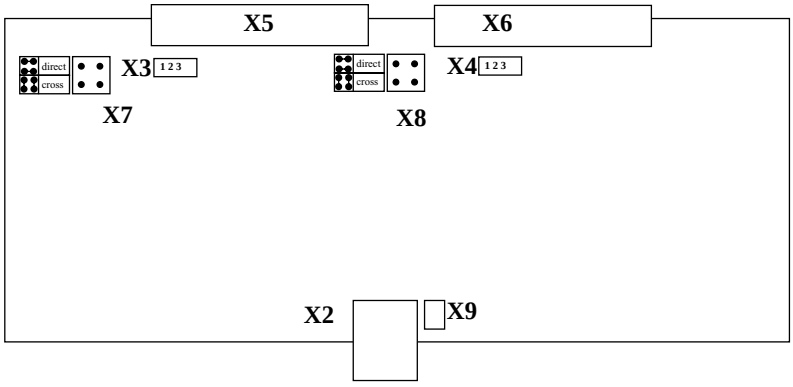

Figure 4.9: *PCB layout and numbering of jumpers contacts for V.2.0*

Table 4.4: *Jumper settings and output connectors commutation for version 2.0*

X7	X3	Pin1 of X5	Pin2 of X5
direct	1–2	Channel #1 output	Channel #2 output
	2–3	Ground	Channel #2 output
cross	1–2	Channel #2 output	Channel #1 output
	2–3	Channel #2 output	Ground

X8	X4	Pin1 of X6	Pin2 of X6
direct	1–2	Channel #21 output	Channel #22 output
	2–3	Ground	Channel #22 output
cross	1–2	Channel #22 output	Channel #21 output
	2–3	Channel #22 output	Ground

4.3.4 Getting started

Before using the unit, it is necessary to check settings of jumpers or appropriately configure those according to specifications of connected device(s) as described above.

To put the unit into operation following steps must be done.

- Plug connecting cables into the output connectors of the unit.
- Connect the unit to the USB port of your PC using the USB cable. The LED lit on the USB port face in 2–2.5 seconds indicates normal operation of the unit.
- Install FDTI Direct Driver for Windows 98/2000/ME/XP from the folder **/Drivers** of the supplied software CD. Updated drivers can be downloaded from http://www.ftdichip.com.
- Run **TEST_DAC40.EXE**, move the pointer of the output voltage into U_{max} position, then adjust the output voltage to the required value by rotation of the spindle of the variable resistor R. The level of the output voltage must be measured by a voltmeter connected to one of the output pins with respect to the grounded pin.

4.3.5 Programming interface

Data transfer between PC and DAC via USB bus is managed by the interface chip FT245BM. To provide necessary speed of data transfer between PC and DAC it is necessary to use FDTI Direct Driver. The corresponding program interface is implemented in the library **FTD2XX.DLL**.

To provide access to the DAC, the following functions of **FTD2XX.DLL** are implemented:

- **FT_ListDevices** - allows to detect the number of connected devices, their serial numbers and specifications;
- **FT_Open** - opens of the device for data transfer;
- **FT_Write** - send a packet of control data from the PC to the device;
- **FT_Close** - closes the device.

Specifications of these functions are given in the programmer's manual of the library FTD2XX (available from www.ftdichip.com).

To facilitate programming of the unit, one may use the function **MakePacket**. It transforms an array consisting of 40 two-byte words, each of them coding an output voltage at the corresponding channel, into the data packet, which can be transferred via USB. Text of the function and an example of its usage are given below.

```
#include "ftd2xx.h"

void    MakePacket(WORD *buf,BYTE *packet);
// Function of data package for DAC formation

void dac_setup(void)
// Sample:  To set voltages with level codes 0,100,200...4000
//          at the DAC outputs  1,2,3,..., 40
{
WORD   buf[40];                 // Buffer of DAC channels
BYTE   packet[130];             // DAC data package
FT_HANDLE  DAC;                 // DAC descriptor

FT_STATUS fs = FT_Open(0,&DAC);
// Open a device with system # 0(1,2,etc)
if(fs==FT_OK)               // If the device is opened successfully
{
unsigned long BR;
for(int i=0;i<40;i++)   // Fill up the buffer of channels with
buf[i]=i*100;           // codes of voltage levels
MakePacket(buf,packet); // Transform buffer of the channels
                        // into data package
FT_Write(DAC,packet,130,&BR); // Transfer data package into the DAC
```

```
FT_Close(DAC);                  // Close the device
}
else                          {// Error handling...}
} // End dac_setup()

//---------------------------------------------------------------------
static BYTE DAC_CHANEL_TABLE[40]= // Table of DAC channels
    {
/*DAC-> 0   1   2   3   4    |
        ---------------------+  OUTPUT    */
        7, 15, 23, 31, 39, //|  A
        6, 14, 22, 30, 38, //|  B
        5, 13, 21, 29, 37, //|  C
        4, 12, 20, 28, 36, //|  D
        3, 11, 19, 27, 35, //|  E
        2, 10, 18, 26, 34, //|  F
        1,  9, 17, 25, 33, //|  G
        0,  8, 16, 24, 32  //|  H
    };
//---------------------------------------------------------------------
void MakePacket(WORD *buf,BYTE *packet)
/*          Form a data packet from the buffer of channels:
      buf - an input array consisting of forty 16-digit words, which
            code voltage levels of the outputs ##1-40
   packet - the resulting 129-byte output array to be transferred
            into the unit via USB bus
*/
{
 BYTE *p=packet+1;
 for(int i=0,s=0;i<8;i++,s+=5)
    {
    // Form address parts of control words for five DAC chips
    *(p++)=0;
    *(p++)=(i&4)?0x1f:0;
    *(p++)=(i&2)?0x1f:0;
    *(p++)=(i&1)?0x1f:0;

    // form control codes from the array of voltages according
    // to the table
    for(int j=0,mask=0x800;j<12;j++,mask>>=1)
        *(p++)=
            ((buf[DAC_CHANEL_TABLE[s+0]]&mask)?0x01:0) |
            ((buf[DAC_CHANEL_TABLE[s+1]]&mask)?0x02:0) |
            ((buf[DAC_CHANEL_TABLE[s+2]]&mask)?0x04:0) |
            ((buf[DAC_CHANEL_TABLE[s+3]]&mask)?0x08:0) |
            ((buf[DAC_CHANEL_TABLE[s+4]]&mask)?0x10:0) ;
    }
  packet[0]   = 0xff; // non-zero starting byte
}
```

When connecting two or more DACs “DAC-40-USB” to the computer it is necessary to define their system numbers by means of **FT_ListDevices** function. An example of usage of function **FT_ListDevices** is given below. For

synchronous control of the units one may use the function **MakePacket**. It is implied that before this all devices “DAC-40-USB” are opened by means of the function **FT_Open**, with preliminary defined system numbers of these modules.

This sample code shows how to get the number of devices currently connected

```
FT_STATUS ftStatus;
DWORD numDevs;

ftStatus = FT_ListDevices(&numDevs,NULL,FT_LIST_NUMBER_ONLY);
if (ftStatus == FT_OK) {
    // FT_ListDevices OK, number of devices
    // connected is in numDevs
}
else {
    // FT_ListDevices failed
}
```

This sample shows how to get the serial number of the first device found. Note that indexes are zero-based. If more than one device is connected, incrementing **devIndex** will get the serial number of each connected device in turn.

```
FT_STATUS ftStatus;
DWORD devIndex = 0;
char Buffer[16];

ftStatus = FT_ListDevices((PVOID)devIndex,Buffer,
              FT_LIST_BY_INDEX|FT_OPEN_BY_SERIAL_NUMBER);
if (FT_SUCCESS(ftStatus)) {
    // FT_ListDevices OK, serial number is in Buffer
}
else {
    // FT_ListDevices failed
}
```

This sample shows how to get the product descriptions of all the devices currently connected.

```
FT_STATUS ftStatus;
char *BufPtrs[3];       // pointer to array of 3 pointers
char Buffer1[64];       // buffer for the product description
                        // of first device found
char Buffer2[64];       // buffer for the product description
                        // of second device
DWORD numDevs;          // initialize the array of pointers

BufPtrs[0] = Buffer1;
BufPtrs[1] = Buffer2;
BufPtrs[2] = NULL;      // last entry should be NULL
```

Table 4.5: *Technical parameters of HV amplifier boards*

Parameter	Value for boards marked as		
	1997	**2004**	**2005**
Number of channels	20*	20*	20*
DC gain	59	35	79
Output impedance, kΩ	270	50	5
Short circuit protection	yes	no	no
Input voltage, V	0...12	0...12	0...12
Low voltage DC power supply, V	±12	±12	12
High voltage Dc power supply, V_high, V	0... 400	0... 400	0... 400
Maximum capacitive load, nF	0.6	10	20
Power dissipation, W	6	1.5	3
Size, mm^2	100×150	100×160	100×160

```
ftStatus = FT_ListDevices(BufPtrs,&numDevs,
            FT_LIST_ALL|FT_OPEN_BY_DESCRIPTION);
if (FT_SUCCESS(ftStatus)) {
// FT_ListDevices OK, product descriptions are in Buffer1 and
// Buffer2, and numDevs contains the number of devices connected
}
else {
// FT_ListDevices failed
}
```

4.4 *OEM Parts:* high-voltage 20-ch DC amplifier boards

In case of OEM version of the system, the mirror is controlled by one or several high-voltage amplifier boards (see Fig. 4.10). Each board contains 20 non-inverting DC amplifiers with gain 35, 59, or 79 depending on the board type (see Table 4.5, and should be connected to a high-voltage power supply and to a stabilized ±15V DC supply. Connect the ground, +15V and -15V to the pins marked G,+ and –. Connect positive high-voltage stabilized DC supply to the pin marked V_high, connect negative high voltage terminal to the ground (see Fig. 4.11). **The high voltage supply should not exceed the value specified in the technical passport!** Use the flat ribbon cable supplied to connect the driver board to the mirror socket.

*19 channels can be used with one extra grounded channel #1 (see jumper configuration)

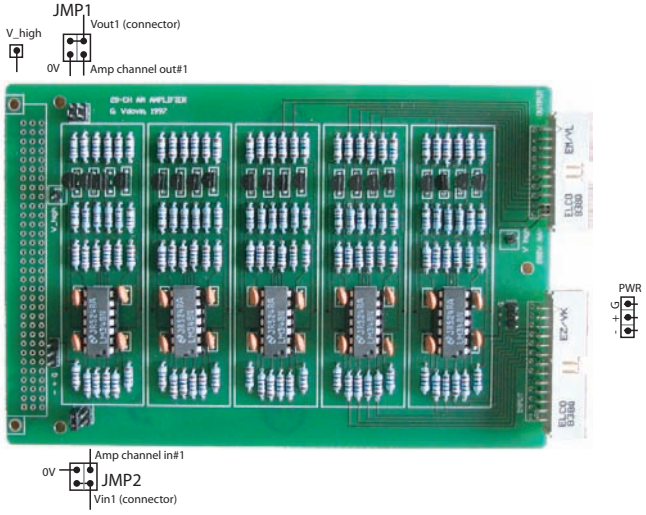

(a) 1997

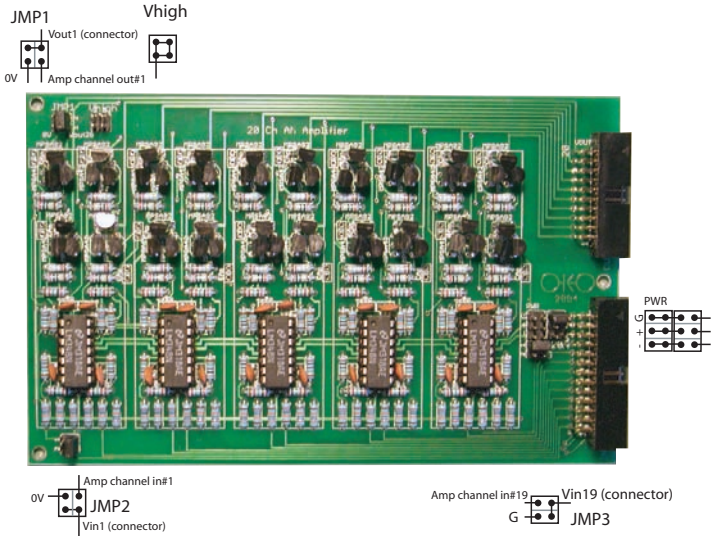

(b) 2004

Figure 4.10: *Three types of high-voltage 20-channel DC amplifier boards, to be distinguished by the design's year.*

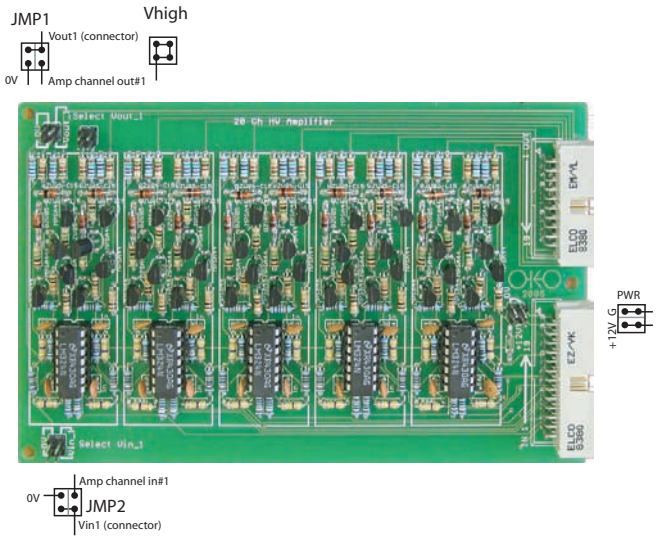

(c) 2005

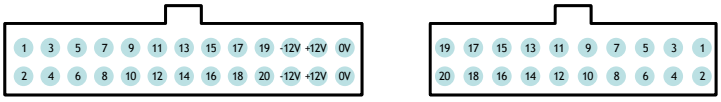

(d) *Pinout of In- and Out-connectors*

JMP1 - Vout1 configuration (set to 0V to have ground as the output);

JMP2 - Vin1 configuration (set to GND to ignore input voltage);

JMP3 - Vin19 configuration (set to G to ignore input voltage);

V_high - high voltage supply;

PWR - low voltage supply (12V); for board marked **2004**: use jumpers to connect the voltage supply with the corresponding input connectors pins

(e) *Configuration of jumpers and pins*

Figure 4.10: *Three types of high-voltage 20-channel DC amplifier boards, to be distinguished by the design's year.*

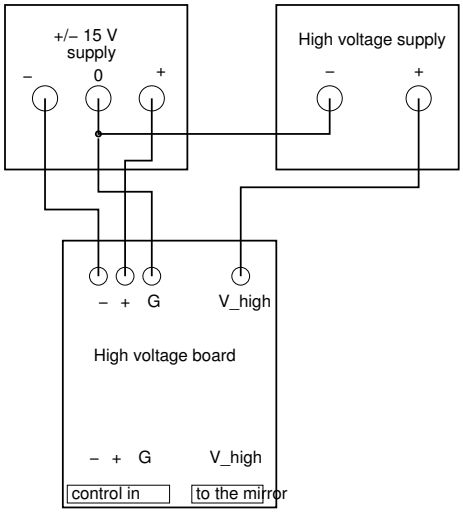

Figure 4.11: *Power supply wiring for OEM version of the system. Position of the connectors can be different; refer to the board manual and/or marking on the board.*

4.5 *OEM Parts:* 24-channel PCI DAC board

OKO digital PCI boards provide 8-bit voltage control for 24 output channels. The output voltage range can be trimmed continuously in the range 2.5. . . 10 V for all channels. Setting time per channel is about 1 microsecond, each channel is controlled by a separate DAC. Several boards can be used simultaneously with a single PC. These boards are applicable to a range of environments when a simultaneous independent control of a large number of analog output channels is required.

Figure 4.12: *24-channel 8-bit PCI DAC board.*

The pinout of the board and the pinouts of the board cable and the cable coming from the high voltage board are shown in Fig. 4.13. The board connector pinout is given for the board make connector. The cable pinouts are given for the cable female connectors viewed from the front side.

4.5.1 Programming interface

The output voltage of the channel N [N=0...23] of the 24-channel DAC board is controlled by sending control byte V [0...255] to the output port BA+N*4, where BA is the base address of the board. The most simple way to do it is to use direct access to the output ports corresponding to the control channels of the digital boards. In a Linux program written in C (GCC compiler), addressing to I/O ports is implemented using “write_port” function, and in Windows using “DlPortWritePortUchar” function of “DlPortIO” library (Scientific Software Tools, Inc.), which is freely available. The installer of DlPortIO (`port95nt.exe`) and programming example

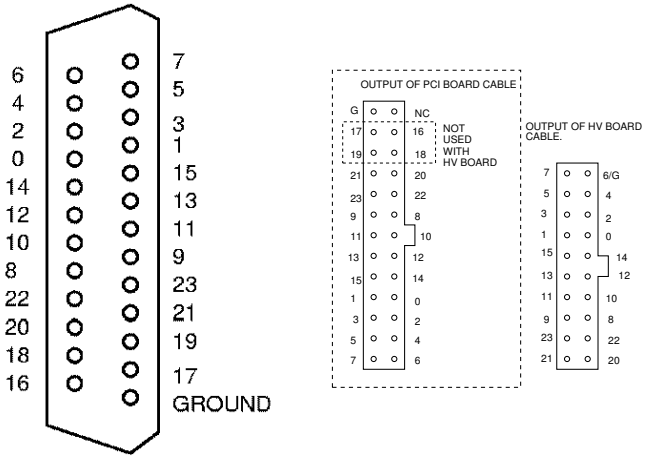

Figure 4.13: *Pinouts of the digital board and cables. The numbers correspond to the addresses of the pin with respect to the base address of the board.*

(`am_set_pci.cpp`) are supplied on a CD enclosed with the boards (directory `\Drivers\PortDriver\deformable_mirror`).

To obtain the base I/O address of the board, go to "Control Panel → System → Hardware → Device manager". The boards are listed in the section "Multifunction adapters". Double-click on the device named "PROTO-3/PCI" and check the section "Resources" for its base I/O address.

Alternatively, it is possible to use Windows driver and its programming interface supplied by Kolter Electronics. It allows to use plug-and-play features of the boards. Please refer to the separate technical passport of the PCI DAC board (`oko_pci.pdf`) for detailed installation guide and programming example.

NB! In some systems running under Windows XP SP2, hardware resource problem can occur, and Widows cannot allocate base address for OKO PCI boards. Please *disable* Plug-and-Play functionality of the PC BIOS in this case.

4.5.2 LabView driver

This section describes how to install and use LabVIEW driver for OKO PCI controller card.

Driver installation

This LabVIEW driver needs `port95nt.exe` both on Windows 95/98/Me and NT/2000/XP versions. If this driver is not installed (or if you are not sure)

please run `port95nt.exe` from
`\Demos\windows_drivers\deformable_mirror`
directory of the OKO drivers CD.

To install the LabVIEW OKO PCI controller unzip the `OkoLabVIEW.zip` with relative paths into the LabVIEW folder tree
(e.g. `C:\Program Files\NationalInstruments\LabVIEW 7.0\`).
This creates the following file subtree:

```
.\
  examples\
           OKO\
                Example_SequencePoke.vi
                Example_Triangle_test.vi
  help\
       OKOLib.chm
  user.lib\
           OKO\
               OkoPciLibrary.llb
               dir.mnu
```

Then (re)start LabVIEW. The OKO sub-palette (Fig. 4.14) should appear in the "UserLib" subpalette of the Functions Palette.

(a) **(b)** *Edit this VI!*

Figure 4.14: *OKO PCI Controller palette*

To complete the installation, you should know base addresses of all cards installed in your system. Locate the function AddressByNumber in the palette, open it for edit, and fill in the base addresses(see Fig 4.15). Right click on entered values an choose "Data Operations ▶ Make Current Value Default". Save the VI.

Functions reference

The OKO driver subpalette contains three functions:

ArrayToCard "High-level" function; allows to write array of 24 numbers to one of the installed in the system cards, addressing by this card's number.

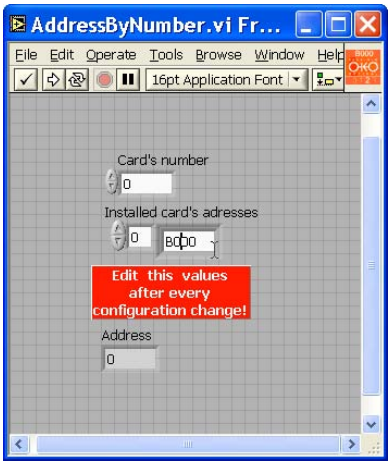

Figure 4.15: *Edit values of the Installed card's addresses control and save them as default*

AddressByNumber Auxiliary function; converts the card number to its memory address. You should edit and save this VI every time you changed the configuration of your system.

WriteToChannel "Low-level" function; writes 8-bit value to one of the channel of one of the installed in the system cards, addressing by this card's base address.

Additional help for the functions is shown in the context help menu.

Examples

There are two example VI's supplied with the driver. They can help you to test driver's installation and to understand better provided functions.

Example_Triangle_test.vi This example generates sawtooth signals on two channels with inverse shapes. You can monitor those signals using oscilloscope.

Example_SequencePoke.vi This example VI first initialises the card by setting all its channels to the midvalue and then it sequentially sets every channel to its maximum value and back to the middle level.

The examples are available from the `OKO` subfolder of the LabVIEW examples. You can browse for them as for usual LabVIEW examples (Fig.4.16).

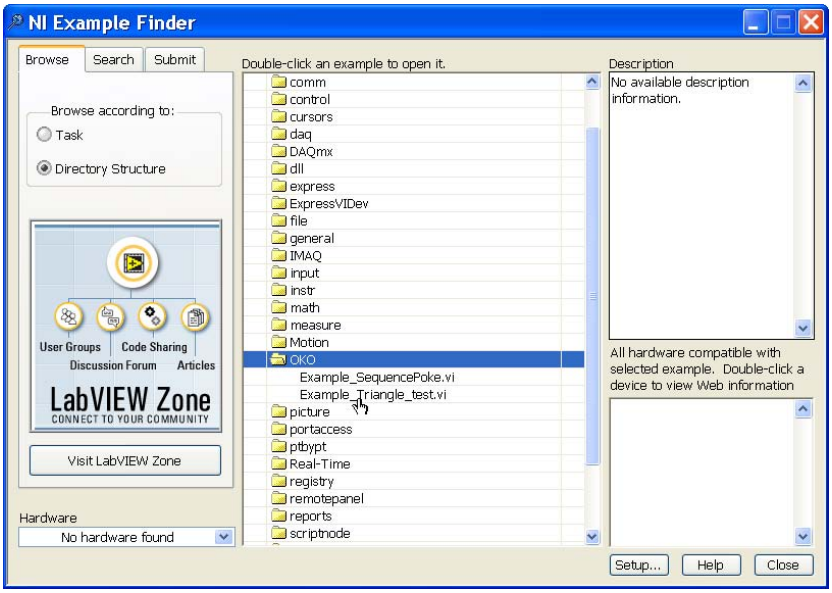

Figure 4.16: *Installed examples*

5

LIQUID CRYSTAL ADAPTIVE LENSES

Correction of low-order aberrations (defocus and astigmatism) is a vital problem in astronomical applications, human vision correction and technical vision systems, bar codes, CD and DVD-ROM readers, and others. Adaptive optics systems for such applications should contain either mechanically driven optics or a lens (spherical or cylindrical) with variable focal distance. Since LC-based phase modulators have attracted increased attention due to their transparency, low control voltages and low cost, adaptive liquid crystal (LC) lenses have been proposed as a favorable alternative for adaptive optical elements based on deformable mirrors.

Two configurations of adaptive LC lenses are available from OKO Technologies, namely, a cylindrical and a spherical one.

5.1 Principles of operation

The design of the LC lens is shown in Figure 5.1. Electrically controlled birefringence (ECB) in nematic liquid crystal with planar alignment is used for phase modulation. By introduction of a highly resistive coating with contacts at the periphery (one annular contact for spherical lens and two linear contacts for cylindrical lens), one can achieve a quasi-parabolic phase profile generated in a liquid crystal layer in response to AC voltages applied to the contacts [21]. Variation of amplitude and frequency of the AC voltages affects the focusing properties of the lens; thus, it can be used for control of the focal distance in the range from infinity to a certain minimum limit, F_{min}.

The minimum focus distance, F_{min}, can be estimated from the value of

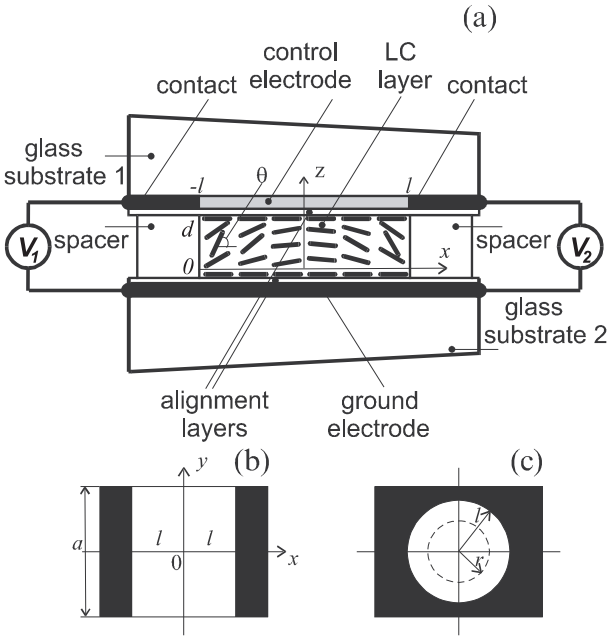

Figure 5.1: *General schematic for a LC lens (a) and the contacts layout for cylindrical (b) and spherical (c) lenses.*

the optical anisotropy of the LC, Δn, LC layer thickness, d, and the aperture diameter, D,

$$F_{min} = \frac{D^2}{8d\Delta n}. \tag{5.1}$$

For instance, for a LC lens with a 5 mm aperture and 25 μm-thick layer of commercially available LC mixture with $\Delta n = 0.28$), F_{min} is equal to 44.6 cm.

The lens can be controlled manually by a function generator with sine or square waves. Roughly, the optical power increases with frequency and decreases with voltage. The lens can be calibrated in order to minimize the spherical aberration and set the correspondence between the focal distance and the parameters of control voltage [22]. For focal distances close to F_{min} the spherical aberration is mainly due to strong non-linear dependency of generated phase delay on voltage and cannot be compensated completely; however, for focal distances $\geq 2F_{min}$ it can be compensated efficiently.

Besides, the spherical LC lens can be calibrated to generate a certain spherical aberration additionally to the control of defocus [23]. When the LC lens is to be integrated into an optical system to provide accommodation, this property can be used for compensation of static spherical aberration of the system.

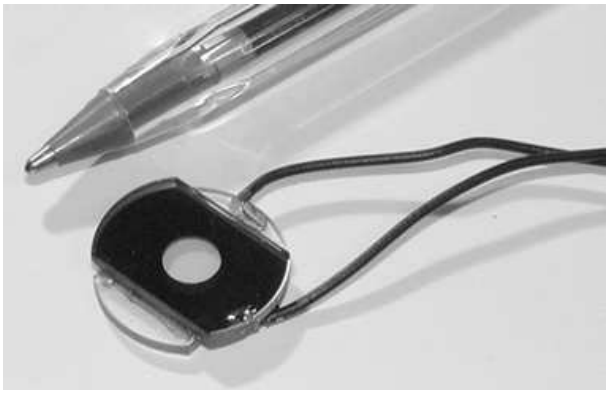

Figure 5.2: *Spherical adaptive LC lens.*

The cylindrical LC lens can be calibrated to operate as a wedge with controllable deflection angle.

Due to the electro-optic effect used, the adaptive LC lens affects only one polarization component of light, which is parallel to the initial planar alignment of the LC layer. Combination of two LC lenses operating on two different polarization components of light can be used to make a polarization-independent device.

5.2 Technical data

We have a limited stock of cylindrical and spherical LC lenses (shown in Figure 5.2) with the configurations as follows.

Configuration	1	2	3	4
LC thickness (d), μm	40	50	50	50
Aperture diameter (D), mm	5	5	7.5	5
External diameter, mm	10	10	12	12
F_{min}, cm	27.9	22.3	50.2	22.3
Type	spherical	spherical	spherical	cylindrical

Characteristics of these lenses are given in the table below.

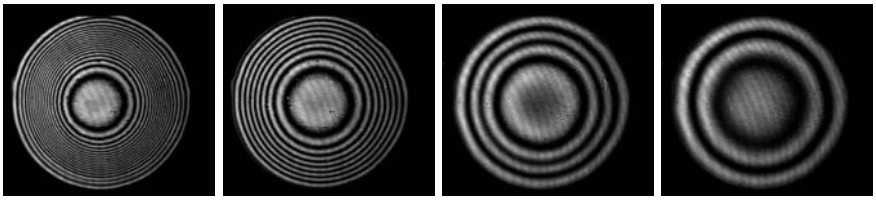

Figure 5.3: *Interference fringe patterns of a spherical LC lens (configuration 2) for focal distances 25 cm, 50 cm, 1 and 2 m (left to right).*

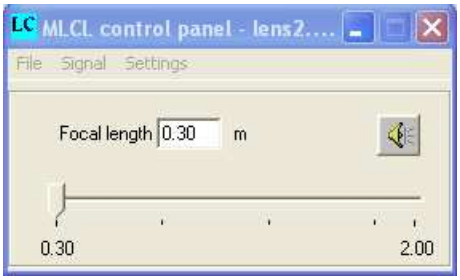

Figure 5.4: *Interface of the "MLCL control panel" program*

Parameter	Value
Wavelength region	0.44...2 μm
Transmittance (without antireflection coatings)	about 70 %
Range of voltages	below 10 V, typically 3...5 V
Range of frequencies	1...50 kHz
Geometry	cylindrical or spherical
Switching speed (for $d = 25$ μm and $D = 5$ mm)	780 ms from 1 to 2 m focal distance, 860 ms from 2 to 1 m

Interferometric fringe patterns of a calibrated lens with $F_{min} = 22.3$ cm (configuration 2) are shown in Figure 5.3 for four different focal distances.

A series of LC lenses with customized parameters can be manufactured by request. However, delivery cannot be guaranteed for arbitrary specifications and arbitrary amount; it should be discussed for each particular case. Aperture diameter can be varied from 2 to 70 mm, LC thickness from 5 to 50 μm, and antireflection coatings can be made to increase the transmittance. The switching time is roughly proportional to the square of the LC layer thickness and decreases for higher voltages.

The lens can be supplied with an ISA interface card, which operates as a controllable square wave generator. The focal distance of a calibrated lens can be controlled from a program called “MLCL control panel”. We also offer a console program, which allows driving the lens from the command line and is supplied with source code. It is also possible to supply a calibrated lens without a control unit, but with a table of calibration data for a function generator.

6

WAVEFRONT SENSOR SYSTEMS

This chapter describes the wavefront analysis and control system "FrontSurfer", based on Hartmann (Hartmann-Shack) measurement principle. The system can be used for:

- Optical shop testing of transmissive and reflective optics: lenses, mirrors, lens assemblies, collimators, etc.;
- Real-time display of low-order aberrations (tip/tilt, defocus, coma, astigmatism) in so-called "Alignment mode".
- Real-time control and compensation of wavefront aberrations in combination with OKO Technologies deformable mirror system.

"FrontSurfer" includes:

- "FrontSurfer" software that runs under W95/98/2000/NT/XP. Linux is not supported for the latest versions of "FrontSurfer", but the Linux version can be supplied by request with a complete system including computer;
- measurement head, including a 1/2" monochromatic CCD or CMOS camera with computer interface and a high-precision Hartmann mask or a lenslet array in a C-mount. The measurement head consisting of UI-2210M camera and C-mounted microlens array is shown in Figure 6.1.

The system reconstructs two-dimensional wavefront profiles with *rms* sensitivity of better than $\lambda/100$. The system can be used for measurements in visible (using either monochromatic or white light) and infrared.

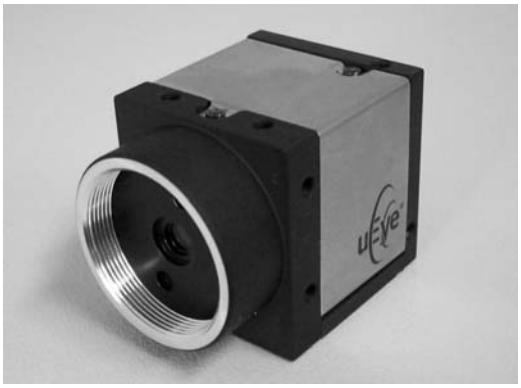

Figure 6.1: *Shack-Hartmann wavefront sensor, measurement head*

A special configuration was developed for volume control of the quality of microlens arrays. The system automatically measures the low-order aberrations of each microlens. As a result, the distribution of low-order aberrations, pitch irregularities and other defects can be plotted over the whole array area. Arrays of up to 30x40 microlenses were measured. The processing time for one array of 1200 microlens did not exceed 10 hours. This configuration is available by request and includes a stepper motor.

6.1 "FrontSurfer" software

"FrontSurfer" is available in two configurations: with and without support for deformable mirrors and adaptive optics feedback.

6.1.1 Basic features

All versions of "FrontSurfer" have the following features:

- Reconstructs the optical wavefront from Hartmann and Shack-Hartmann sensor data.
- Produces wavefront plot, synthetic interferogram, far field intensity and reports on Zernike terms (see Figure 6.2). All measurement data and results can be saved with one mouse click.
- Processes spot patterns obtained with hexagonal, orthogonal or random Hartmann masks and microlens arrays with arbitrary number of apertures.

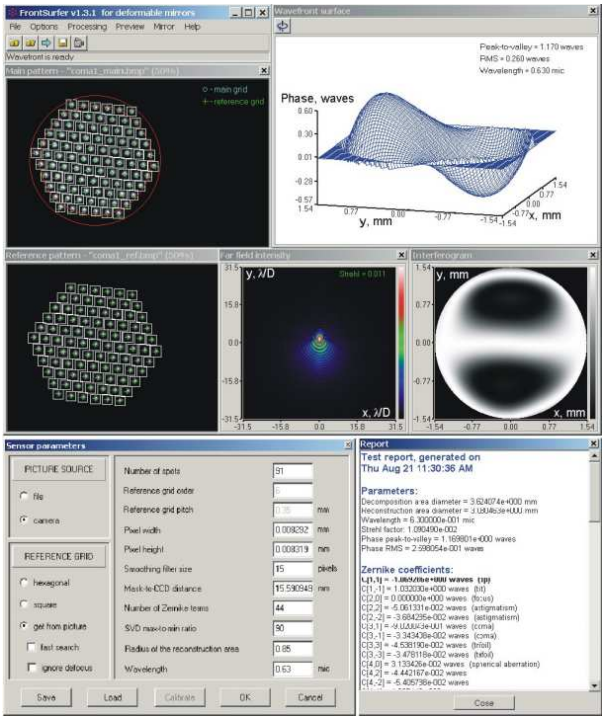

Figure 6.2: *“FrontSurfer” interface*

- Operates with and without reference pattern: in the last case the parameters of the Hartmann mask or microlens array are used as a reference.
- In the reference mode, allows manually defining the area of interest (aperture), which could be circular, elliptic, square or rectangular with an optional circular obscuration in the center.
- In the alignment mode, real time bar graph display of tip, tilt, defocus, coma and astigmatism; polar display of tilt, coma, astigmatism and position of the intensity maximum (see Figure 6.3).
- Allows to extract any aberration expressed in Zernike polynomials or eliminate any Zernike terms.
- Can be interfaced to any camera by developing a custom video plugin according to our specification.

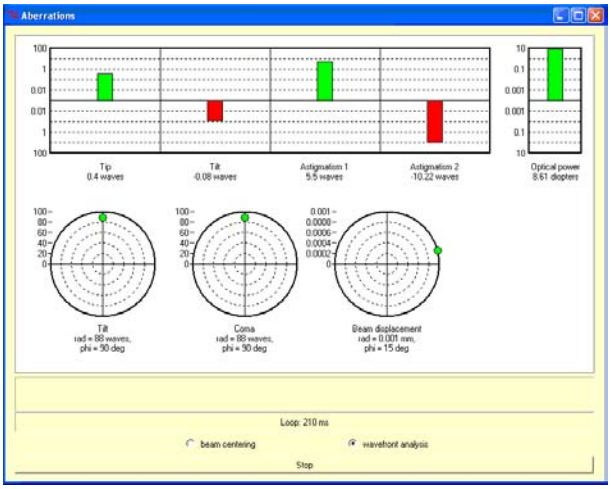

Figure 6.3: *"Aberrations" window in the alignment mode*

6.1.2 Features of the version for deformable mirrors

The "FrontSurfer" version for deformable mirrors has the following features:

- Manual control of voltages supplied to the mirror.
- Closed-loop correction in real time. Average correction rate is 25 Hz and higher for the wavefront sensor based on UI-2210M CCD camera and 50 Hz for Basler A602f CMOS camera.
- Singular value decomposition (SVD) algorithm with user-defined number of modes for stable feedback.
- Can generate a given aberration in addition to the reference. The aberration is defined as a combination of Zernike polynomials and can be manually controlled during the closed-loop correction using arrow keys of the computer keyboard.
- Supports all types of MMDM and PDM produced by OKO Technologies.
- Can be configured for a custom-made mirror interfaced to OKO's PCI boards and USB driver modules.
- Can be interfaced to a custom mirror driver by developing a mirror plugin according to our specification.

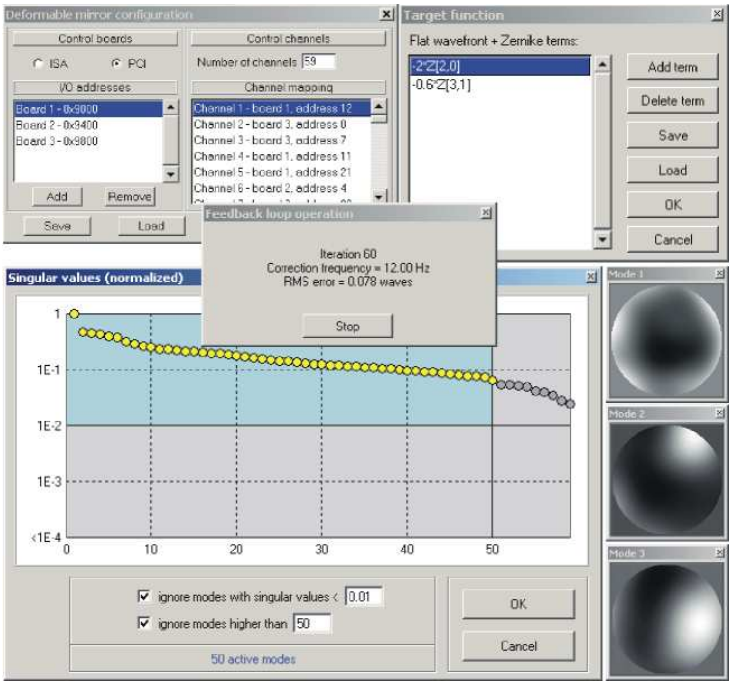

Figure 6.4: *“FrontSurfer”, interface of the version for deformable mirrors*

6.2 “FrontSurfer” hardware

6.2.1 Typical wavefront sensor configuration

Characteristics of three typical configurations of FrontSurfer wavefront sensor are given in Table 6.1. However, the system can be reconfigured according to the customer’s requirements by choosing a different camera, Hartmann mask or microlens array. The options currently available are given below.

6.2.2 CCD and CMOS cameras

Our “standard” options are as follows:

- 1/2-inch CCD camera UI-2210M from IDS Imaging, Germany. It has 640x480 pixels, USB 2.0 interface, maximum frame rate 75 fps at full resolution and higher with partial scanning. Provides the average speed of feedback loop operation with FrontSurfer about 25 iterations per second and higher, depending on the computer.

Table 6.1: *Characteristics of three typical FrontSurfer Shack-Hartmann wavefront sensor configurations*

Parameter	Config. 1	Config. 2	Config. 3
Camera model	UI-2210M	Basler A601f/A602f	UI-2210M
Camera type	digital CCD	digital CMOS	digital CCD
Camera interface	USB 2.0	Firewire	USB 2.0
Array geometry	hexagonal	orthogonal	orthogonal
Array pitch	300 μm	200 μm	150 μm
Array focal distance	$\sim$18 mm	7 mm	10 mm
Clear aperture	3.9 mm	$\leq$4.5 mm	$\leq$4.5 mm
Subapertures	127	$\leq$400	$\leq$700
Maximum tilt, fast mode	0.008 rad	0.014 rad	0.007 rad
Maximum tilt, slow mode	0.066 rad	N/A	N/A
Repeatability, RMS	$\lambda/300^{*}$	$\lambda/150^{*}$	$\lambda/150^{*}$
Repeatability, P-V	$\lambda/60^{*}$	$\lambda/20^{*}$	$\lambda/20^{*}$
Acquisition rate	$\geq$75 fps	60/$\geq$100 fps	$\geq$75 fps
Processing rate, fast mode	25 fps**	15/30 fps**	10 fps**
Processing rate, slow mode	1 fps**	N/A	N/A
Recommended Zernike terms	$\leq$44	$\leq$150	$\leq$300
Wavelength	400...900 nm	400...1000 nm	400...900 nm
Absolute mode	Yes	No	No
Reference mode	Yes	Yes	Yes

* For λ=0.633 μm

** For low-order aberration analysis on a PC with AMD Athlon XP1800+ processor and 256 MB RAM

- 1/2-inch CMOS camera A601f from Basler, Germany. It has 656x491 pixels, Firewire interface, maximum frame rate 60 fps. Provides the average speed of feedback loop operation with FrontSurfer about 22 iterations per second.

- 1/2-inch CMOS camera A602f from Basler, Germany. It has 656x491 pixels, Firewire interface, maximum frame rate 100 fps at the maximum resolution and higher for reduced one. Provides the average speed of feedback loop operation with FrontSurfer up to 50 iterations per second.

Using the custom video plugin interface, any camera can be interfaced to FrontSurfer. The plugin can be developed either by OKO Technologies (if requested) or by a customer himself according to our specification.

6.2.3 Microlens arrays

OKO Technologies produces high-quality replicated microlens arrays specially for the use with FrontSurfer wavefront sensors. As one of the standard options, we offer a hexagonal array of 127 microlenses with a focal distance about 18 mm and a pitch of 300 μm, mounted in a C-mount.

Besides, OKO Technologies offers a range of microlens arrays fabricated in glass and fused silica with small numerical aperture and 99% optical fill factor. Microstructures provide for optimum spectral efficiency (UV to far infrared) and for the best mechanical and thermal stability. These arrays work with very high optical loads. To provide a cost-efficient solution, all listed arrays can be replicated in series in plastic. Microlens arrays with orthogonal and hexagonal arrangements are listed in Table 6.2 and Table 6.3, respectively. Recommended options to be used with 1/2-inch cameras are as follows:

- APO-Q-P192-F3.17, provides ~400 subapertures over a 4.5 mm circular area;
- APO-Q-P200-F7.0, ~400 subapertures over 4.5 mm;
- APO-Q-P150-F10, ~700 subapertures over 4.5 mm;
- APO-Q-P150-F3.5, ~700 subapertures over 4.5 mm.

Table 6.2: *Positive orthogonal microlens arrays*

Product type	**Material**	**Pitch, μm**	**Radius, mm**	**Focal distance,** mm	**Maximum size**
APO-Q-P2200-F209 (633)	Fused silica	2200	95,52	209	30x30 lenses (70x70mm)
APO-GB-P1500-F24.3 (633)	BK-7	1500	12,5	24,3	6x6 lenses (10x10mm)
APO-GB-P1500-F39.3 (633)	BK-7	1500	20,4	39	6x6 lenses (10x10mm)
APO-Q-P1100-F105 (633)	Fused silica	1100	48.0	105	55x55 lenses (62x62mm)
APO-Q-P1100-F209 (633)	Fused silica	1100	95,52	209	55x55 lenses (62x62mm)
APO-Q-P1061-F158 (633)	Fused silica	1061	72,4	158	55x55 lenses (62x62mm)
APO-Q-P1000-F40 (633)	Fused silica	1000	18.0	40	60x60 lenses (61x61mm)
APO-Q-P1000-F4,64 (633)	Fused silica	1000	2,12	4,64	60x60 lenses (61x61mm)
APO-Q-P500-F19,7 (633)	Fused silica	500	9	19,7	100x100 lenses (50x50mm)
APO-Q-P500-F8,31 (633)	Fused silica	500	3,8	8,31	100x100 lenses (50x50mm)
APO-Q-P300-F40 (633)	Fused silica	300	18.0	40	200x200 lenses (61x61mm)
APO-Q-P300-F118 (633)	Fused silica	300	54	118	200x200 lenses (61x61mm)

Table 6.2: *Positive orthogonal microlens arrays, continued*

Product type	Material	Pitch, μm	Radius, mm	Focal distance, mm	Maximum size
APO-Q-P300-F2 (633)	Fused silica	300	0,94	2,0	200x200 lenses (61x61mm)
APO-Q-P384-F5.75 (633)	Fused silica	384	2 627	5,75	5x5 lenses (2,5x2,5mm)
APO-Q-P222-F1,86 (633)	Fused silica	222	0,85	1,86	200x200 lenses (45x45mm)
APO-Q-P222-F0,93 (633)	Fused silica	222	0,43	0,93	200x200 lenses (45x45mm)
APO-Q-P192-F5.75 (633)	Fused silica	192	2 627	5,75	9x9 lenses (2x2mm)
APO-Q-P192-F3.17 (633)	Fused silica	192	1,45	3,17	200x200 lenses (45x45mm)
APO-Q-P200-F7.0 (633)	Fused silica	200	3,2	7.0	300x300 lenses (61x61mm)
APO-Q-P200-F40 (633)	Fused silica	200	18,2	40	300x300 lenses (61x61mm)
APO-Q-P150-F10 (633)	Fused silica	150	4,57	10	400x400 lenses (61x61mm)
APO-Q-P150-F3.5 (633)	Fused silica	150	1,6	3,5	400x400 lenses (61x61mm)
APO-Q-P148-F1,24 (633)	Fused silica	148	0,6	1,24	400x400 lenses (61x61mm)
APO-Q-P100-F0,217 (532)	Fused silica	100	0,1	0,217	500x500 lenses (51x51mm)
APO-GT-P100-F0,143 (633)	StiH-53	100	0,12	0,143	500x500 lenses (51x51mm)
APO-P(GB)-P250-F0,57 (633)	BK-7/NOA-61	250	0,32	0,57	25x25mm
APO-P(GB)-P200-F1,25 (633)	BK-7/NOA-61	200	0,7	1,25	40x40mm
APO-P(GB)-P200-F6,4 (633)	BK-7/NOA-61	200	3,32	6,4	25x25mm
APO-P(GB)-P300-F1,7 (633)	BK-7/NOA-61	300	0,94	1,7	25x25mm
APO-P(GB)-P300-F107 (633)	BK-7/NOA-61	300	60	107	25x25mm

6.2.4 Hartmann masks

OKO Technologies offers calibrated Hartmann masks with orthogonal and hexagonal geometries. Masks are fabricated in glass and fused silica and coated with patterned aluminum (glass masks) or chromium (fused silica masks). Since the holes are positioned with very high precision and aberration of the mask is negligible, these masks can be used for absolute wavefront sensing, without calibration on a reference light beam. Available configurations are listed in Table 6.4.

Table 6.3: *Positive hexagonal microlens arrays*

Product type	**Material**	**Pitch,** μm	**Radius,** mm	**Focal distance,** mm	**Maximum size**
APH-GT-P1300-F5.2 (633)	StiH-53	1300	4,3	5,2	20x20 lenses (26x26mm)
APH-GT-P1300-F3,26 (633)	StiH-53	1300	2,74	3,26	20x20 lenses (26x26mm)
APH-Q-P1000-F36,7 (633)	Fused silica	1000	16,8	36,7	60x60 lenses (61x61mm)
APH-Q-P480-F10,91 (633)	Fused silica	480	5	10,9	100x100 lenses (51x51mm)
APH-Q-P250-F2 (633)	Fused silica	250	1	2	240x240 lenses (60x60mm)
APH-P(GB)-P250-F0,57 (633)	BK-7/NOA-61	250	0,32	0,57	145x145mm
APH-P(GB)-P30-F0,042 (633)	BK-7/NOA-61	30	0,024	0,042	50x50mm

6.2.5 How to choose a proper microlens array or Hartmann mask

Choice of a proper microlens array or Hartmann mask for your application should be a trade-off between the range of aberrations to be measured and the precision to be achieved. We would suggest the following criteria of choice.

1. The array should have sufficient sampling for the aberrations to be measured. If the aberrations can be described by N Zernike terms, we would recommend using at least $2N \ldots 3N$ subapertures. Your relay optical scheme should rescale the beam in such a way that it will cover the desired number of sub-apertures.

2. Microlens arrays are more efficient in terms of collecting light energy, providing smaller and brighter spots, which is especially important for low-light applications. However, Hartmann masks can be manufactured with higher precision and can provide better results in the absolute wavefront measurement mode (see page 108).

3. The wavefront tilt (i.e., direction of the rays with respect to the optical axis) should not exceed half pitch of the microlens array divided by its focal distance. It will ensure that the spots will not overlap with each other, and the software can determine the correspondence between the measured pattern and the reference one.

4. The Strehl ratio of net aberrations over the area of each sub-aperture should be sufficiently high; from practical point of view, it should exceed 0.2. It will ensure that the spots’ blur due to aberrations will not prevent them from detection by FrontSurfer.

Table 6.4: *Hartmann masks; size of each mask is* 10×10 *mm*

Material	Geometry	Aperture	Subapertures		
		size, mm	number	type	diameter, μm
Glass	Orthogonal	7	64	Circular	200
Glass	Orthogonal	7	64	Circular	300
Glass	Orthogonal	7	64	Circular	450
Glass	Orthogonal	7	64	Square	200
Glass	Orthogonal	7	64	Square	300
Glass	Orthogonal	7	64	Square	450
Glass	Orthogonal	3.5	36	Circular	200
Glass	Orthogonal	3.5	36	Circular	300
Glass	Orthogonal	3.5	49	Circular	200
Glass	Orthogonal	3.5	49	Circular	300
Glass	Orthogonal	3.5	64	Circular	200
Glass	Orthogonal	3.5	64	Circular	300
Glass	Orthogonal	3.5	81	Circular	200
Glass	Hexagonal	3.5	37	Circular	300
Fused silica	Hexagonal	3.5	37	Circular	200
Fused silica	Hexagonal	3.5	61	Circular	200
Fused silica	Hexagonal	3.5	91	Circular	200
Fused silica	Hexagonal	3.5	127	Circular	100
Fused silica	Hexagonal	3.5	169	Circular	100

5. The sensitivity of the wavefront sensor improves proportionally to to the focal distance of the microlens array (or, in case of a Hartmann sensor, to the distance between the mask and image sensor).

6.3 Wavefront measurement with “FrontSurfer”

The principle of (Shack-)Hartmann test is shortly explained in Section 1.2.2. Here we describe how “FrontSurfer” processes the measurement data to reconstruct the wavefront and give some hints on how to achieve better results.

6.3.1 Choice of the measurement mode

“FrontSurfer” can operate with and without a reference pattern. In the latter case, the geometric parameters of the Hartmann mask or microlens array are used as a reference, which allows for absolute wavefront sensing. A complete hexagonal or orthogonal structure of spots (see Figure 6.5) is desirable for this mode, although the program can tolerate up to 5 % missing spots. In the

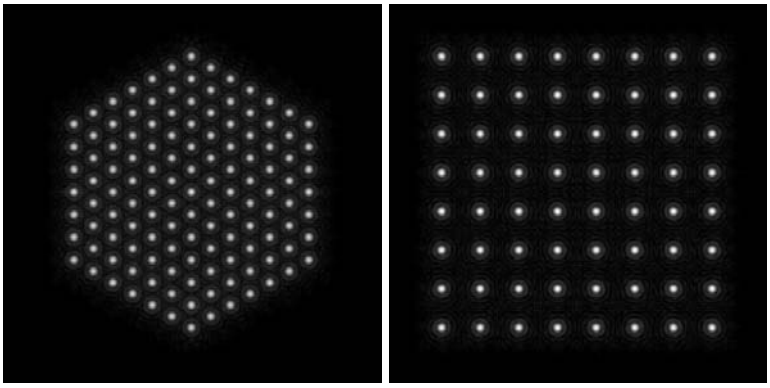

Figure 6.5: *Complete hexagonal (left) and orthogonal (right) spot patterns.*

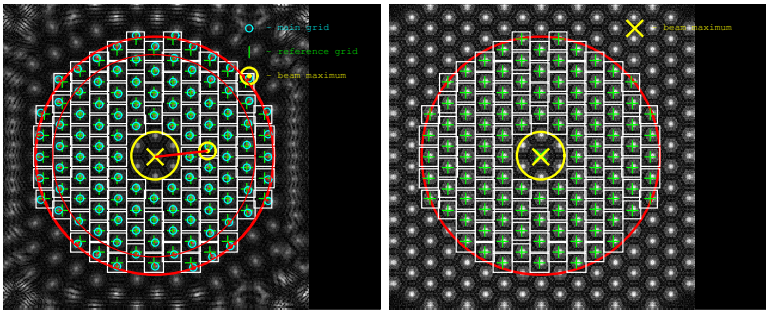

Figure 6.6: *Main (left) and reference (right) Hartmann spot patterns in the reference mode with manually defined aperture and central obscuration.*

reference mode, the pattern can be neither complete nor regular; one can even use an array with random positioning of sub-apertures.

The choice between the *absolute measurement* and *reference* modes depends on the application. If the wavefront sensor is used for alignment of an optical system (i.e., collimation or astigmatism removal) then the absolute measurement mode would be more useful. If it is used in an optical testing scheme similar to those described in Section 6.4 then the reference mode is preferable, as it allows to neglect aberrations of the relay optics.

The reference mode allows the user to define area of interest (aperture) in the reference pattern manually. This feature is very useful for sensors with a large mask (or lenslet array), whose sub-apertures fill the whole area of the image sensor. The user can choice between circular, elliptic, square and rectangular aperture. Example hartmanngrams with manually defined circular aperture and central obscuration are shown in Figure 6.6.

6.3.2 Hartmanngram capture

"FrontSurfer" provides interfacing to video capture devices using external plugins. It makes possible to customize "FrontSurfer" for using with almost any camera and any frame grabber. At the moment, the following plugins are included with FrontSurfer.

- Picasso PCI-2SQM framegrabber from Arvoo.
- DFG/LC1 framegrabber from Imaging Source.
- A601f and A602f CMOS digital camera from Basler; may be suitable for some other models of Basler but not tested yet.
- Firefly digital camera from Point Grey Research.
- UI-2210M and UI-2410M CCD digital cameras from IDS Imaging; may be suitable for some other models of IDS but not tested yet.

Besides, "FrontSurfer" has embedded support of "Video for Windows" interface, which allows to work with any TV tuner device using this interface. However, the alignment mode and the close-loop operation mode are not supported for "Video for Windows".

In the absolute measurement mode we deal with only one intensity pattern; we refer to it as the *main pattern* as it contains information about the wavefront to be reconstructed. In the reference mode, we also use the second intensity pattern, which contains information about geometry of the Hartmann mask (lenslet array) and aberrations of the relay optics. We refer to it as the *reference pattern*.

6.3.3 How to obtain a good hartmanngram

Each sub-aperture of the Hartmann mask (lenslet array) produces a light spot on the CCD or CMOS image sensor matrix; thus, the reconstruction software should deal with an intensity distribution consisting of a set of spots. For correct processing it is important to minimize the background noise and prevent saturation of spots. Although it may be possible to locate spots in presence of noise and saturation, these factors may affect the precision and repeatability of the results. Examples of a good and bad intensity patterns are shown in Figure 6.7

It is also important to minimize the variation of intensity between the spots. This variation may be caused by the structure of the illuminating beam, interference with parasitic beams reflected from the components of the optical system, bad optical conjugation between the sensor and the object under test, birefringence of the object and too strong aberrations. Example

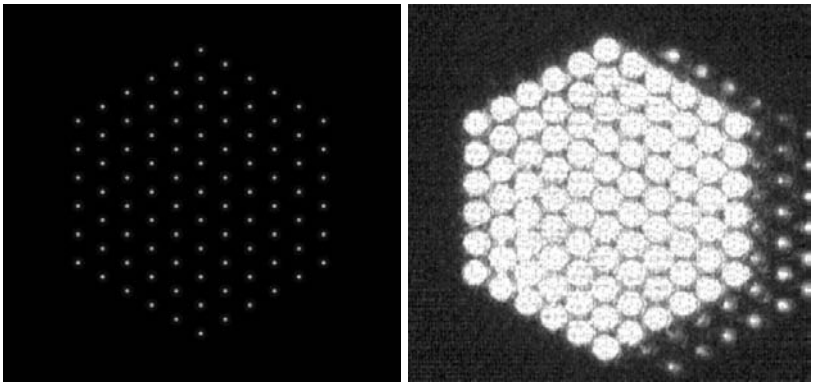

Figure 6.7: *Intensity patterns from the Shack-Hartmann sensor; a good quality one (left), one with noise and saturation (right).*

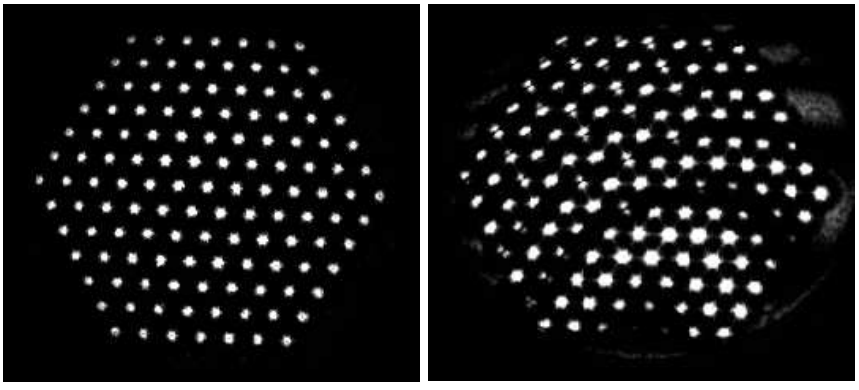

Figure 6.8: *Intensity patterns with inhomogeneous intensity; acceptable (left) and unacceptable quality (right).*

hartmanngrams with acceptable and unacceptable intensity variation are shown in Figure 6.8.

6.3.4 How "FrontSurfer" works

At the first stage of processing, "FrontSurfer" applies a smoothing filter to the intensity pattern in order to minimize the influence of the intensity noise. Then it tries to locate centroids of the brightest spots in the smoothed intensity distribution. Not more than a given number of spots with the intensity higher than a specified threshold value is being located. The window size of the smoothing filter, the maximum number of spots to be located and the intensity threshold (with respect to the maximum intensity) can be adjusted by the user.

Centroids of spots of the main pattern form the so-called *main grid*, and ones of the reference pattern form the *reference grid*. In the absolute measurement mode, "FrontSurfer" generates the reference grid as an ideal hexagonal or orthogonal grid with a specified pitch and dimension. "FrontSurfer" optimizes the position and rotation angle of the ideal grid to provide the closest correspondence between the nodes of the two grids.

At the next stage "FrontSurfer" calculates local tilts of the wavefront. This is implemented by finding a correspondence between coordinates of centroids of two grids – the main and reference ones – and calculating displacement of each spot due to aberrations. The minimum permitted displacement can be specified by the user. If no correspondence is found for a certain spot, or its displacement exceeds the specified limit, the spot is discarded. For calculation of the tilts, "FrontSurfer" uses the pixel dimensions and the distance between the Hartmann mask (lenslet array) and the CCD (CMOS) matrix. These parameters can be either set by the user manually or obtained by calibrating the sensor.

Wavefront reconstruction is performed based on the reference grid and the array of the corresponding local tilts. "FrontSurfer" uses *modal reconstruction*, which means that the required wavefront is represented by a series expansion over a system of linearly independent basis functions, and the coefficients of expansion are calculated in terms of this basis. The reconstructed wavefront is then defined continuously throughout the whole aperture of the sensor.

The reconstruction is divided in several stages:

1. **Calculation of the basis responses**. As the basic functions, "FrontSurfer" uses sets of tilts, which correspond to aberrations represented by Zernike polynomials. The number of Zernike terms can be adjusted by the user. As the reconstruction error tends to grow with the number of terms over a certain limit [24], for each mask there is an optimum number of terms. For our "standard" arrays with 127 microlenses we advise using 44 Zernike terms.

2. **Orthogonalization of the basis responses**. Even for aberrations described by orthogonal Zernike polynomials, the corresponding responses of the wavefront sensor may be non-orthogonal. "FrontSurfer" uses singular value decomposition (SVD) algorithm to construct an orthogonal basis [25]. Discarding of those modes having relatively low singular values allows to make reconstruction more steady, especially if the wavefront is approximated by large number of Zernike terms. The range of "good" SVD values can be adjusted by the user. Normally, taking into account modes with singular values larger than 1/100 of the maximum one provides stable reconstruction.

3. **Decomposition** of the tilts over the orthogonalized basis using SVD algorithm; it results in a set of Zernike coefficients representing the wavefront.

4. **Calculation of the wavefront** as a superposition of Zernike polynomials with the coefficients found.

6.3.5 Further information

For further information, please refer to the latest version of the "FrontSurfer" manual, which is available from http://www.okotech.com.

6.4 Measurement schemes for optical shop testing

Optical setup for testing of optical components with the Shack-Hartmann wavefront sensor should satisfy the following conditions:

- The relay optics should re-image the plane of the object to the plane of the Hartmann mask (lenslet array).

- The scheme should scale the beam in such a way that the image of the scaled object (wavefront) is densely filled with Hartmann sub-apertures.

- The optics should allow for calibration. In the general case, it consists of separate measurement of the complete setup aberration with ideal object or a source of ideal wavefront, replacing the one to be tested.

Three typical measurement schemes are considered below.

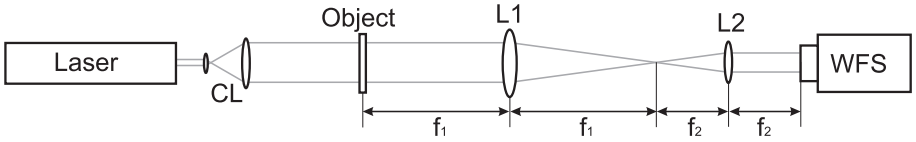

Figure 6.9: *Typical measurement scheme for testing of transparent optics with Shack-Hartmann wavefront sensor. Here CL is a collimator; L_1 and L_2 are lenses with focal distances f_1 and f_2, respectively; WFS is the wavefront sensor.*

6.4.1 Testing of transparent optics

A typical optical setup for measurement of transparent optics with Shack-Hartmann wavefront sensor is shown on Figure 6.9. The object under test should be placed in a collimated laser beam. A telescopic system consisting of two lenses, L_1 and L_2, is used to re-image the aperture of the object to the microlens array (or Hartmann mask) of the wavefront sensor. The system should scale the area to be measured to the aperture size of the wavefront sensor; the scaling factor is equal to f_1/f_2, where f_1 and f_2 are focal distances of the lenses L_1 and L_2, respectively.

Although "FrontSurfer" is able to perform "absolute" wavefront measurement without any reference pattern, it is advisable to switch to the reference mode. It allows to get rid of aberrations of the relay optics, which are always present due to imperfection of the components and misalignment in the system. Reference pattern can be measured with the object removed from the setup.

6.4.2 Testing of reflective optics

A typical optical setup for measurement of reflective optics is shown on Figure 6.10. To facilitate calibration, it is convenient to build it in a similar way to the Twyman-Green interferometer, where a beam splitter divides the incoming beam in two branches. The object is placed the in first branch behind the beam splitter, and the reference (normally a high-quality flat or spherical mirror) in the second one. The beams reflected from the object and reference are then directed to the wavefront sensor. A telescopic system similar to the one from the previous scheme (Figure 6.9) is used to provide conjugation between the object and WFS with proper scaling. One of the branches should always be blocked – the first branch for measurement of the reference pattern, and the second one for testing of the object.

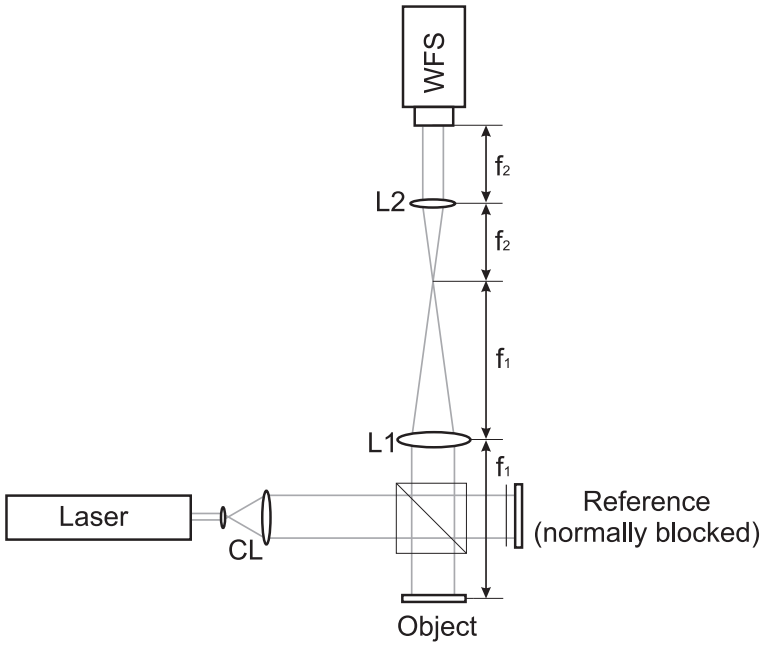

Figure 6.10: *Typical measurement scheme for testing of reflective optics with Shack-Hartmann wavefront sensor. See Figure 6.9 for notations.*

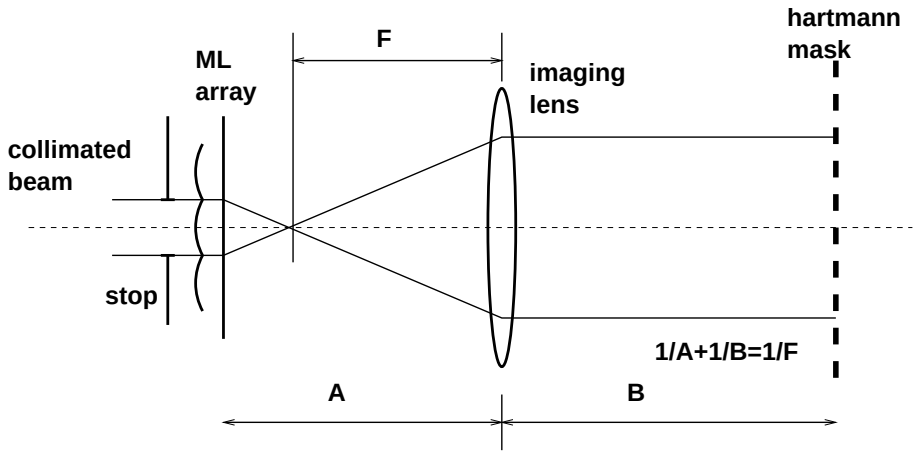

Figure 6.11: *Measurement scheme for testing of a microlens with Shack-Hartmann wavefront sensor.*

6.4.3 Testing of microlenses

An example of a relay system designed to measure the aberrations of a microlens for fiber coupling applications is shown in Figure 6.11. In this case the microlens has a small diameter (1 mm) compared to the Hartmann mask aperture (4 mm). A telescope formed by the microlens itself and the imaging lens is used to couple the microlens aperture to the sensor mask. The Hartmann mask is co-incident with the microlens image.

Calibration of the setup consists of two steps:

1. Obtaining of an ideal reference wavefront.

2. Calibration of the imaging microlens.

In the first step we ensure that the aberration of the illuminating beam is negligible over the aperture of the microlens. In the simplest case this can be achieved by illumination of the microlens with slightly divergent wavefront produced by a remote pinhole source. If there are no optical components between the pinhole and tested microlens, we can be sure the illumination wavefront is close to ideal.

In the second step, we place another pinhole in the focus of the microlens. By doing that we eliminate all aberrations of the setup, except for the aberrations introduced by the imaging lens, to be able to measure the aberration of the relay optics only.

In the last step, we remove the pinhole and measure the total aberration. To obtain the aberration of the microlens, the aberration of the imaging setup measured at step 2 should be extracted from the measurement result.

In this example we have used slightly divergent wavefront instead of collimated. This does not introduce any significant problem if the radius of curvature of the wavefront is much larger than the focal length of the microlens under test. If the lens has focal length of 4 mm and the point source is placed at 1 m from the lens, spherical aberration introduced by "wrong" illumination is negligible. Nevertheless, it is always advisable to check expected aberrations using ray-tracing code.

7

CLOSED-LOOP ADAPTIVE OPTICAL SYSTEMS

OKO Technologies not only produces components for AO systems but also provides integrated solutions based on “FrontSurfer” software, which allows for closed-loop control of a deformable mirror using the measurement data obtained from a (Shack-)Hartmann wavefront sensor. “FrontSurfer” can be integrated not only with the components produced by OKO Technologies but also with custom ones.

7.1 Design of an adaptive optical system

The optical scheme of an adaptive optical system should satisfy the following conditions.

1. The optics should re-image the plane of the mirror to the plane of the Hartmann mask (or microlens array) with proper scaling. An example of such an optical conjugation scheme is shown in Figure 6.10.

2. In a similar way, optical conjugation should be provided between the mirror and the source of aberrations to be corrected.

An important remark should be done regarding the use of micromachined membrane deformable mirrors (MMDM). As the membrane can only be pulled by electrostatic forces but cannot be pushed, if should be biased to provide deformation in both directions (see Figure 2.1). It means that one will get much better results when optimizing the mirror with respect to a sphere than when optimizing it with respect to a flat surface. This sphere should be taken into

account when the mirror is incorporated into the optical setup. The optimum radius of the bias curvature can be evaluated assuming the mirror flexure to be in the middle of the range.

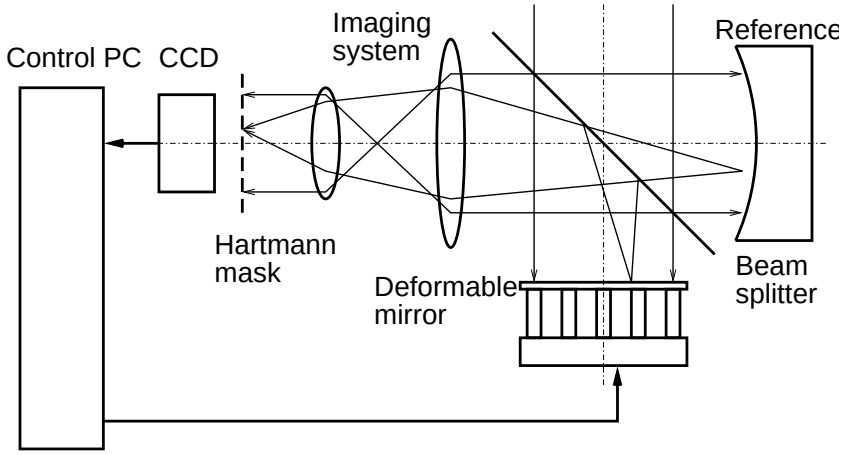

Figure 7.1: *Scheme of typical adaptive optics setup.*

The typical setup for functional feedback loop is shown in the Figure 7.1. A high-quality flat or spherical mirror can be used as a reference. A concave spherical mirror is preferable for the use with MMDM due to its biased operation, and a flat mirror for PDM systems.

7.2 "FrontSurfer" in the closed-loop mode

Closed-loop correction mode is implemented in the version of "FrontSurfer" for deformable mirrors. Overview of the features of this version is described on page 102.

Before starting closed-loop correction with a deformable mirror (DM), the mirror should be properly configured. "FrontSurfer" supports standard OKO's ISA, PCI and USB interface modules for deformable mirrors. Configuration files can be supplied for standard OKO's DM types. It is possible to integrate "FrontSurfer" with a non-OKO DM interface by developing a custom plugin according to our specification.

After the mirror is coupled with the wavefront sensor, it should be calibrated. The calibration consists in measurement of the Shack-Hartmann sensor responses (displacements of spots) caused by consecutive actuating of the mirror's actuators. These responses form the so-called *influence matrix* of

the mirror; we shall denote it as $\mathbf{A}$. Calibration should be restarted after any change in the optical setup.

After calibration, the influence matrix $\mathbf{A}$ is subjected to singular value decomposition (SVD) $\mathbf{A} = \mathbf{USV}^T$ [25]. The columns of the matrix $\mathbf{U}$ make up an orthonormal set of the mirror deformations (modes), and the values of the diagonal matrix $\mathbf{S}$ represent the gains of these modes. Discarding those modes having small singular values improves controllability of the system [26]. The user is able to visualize the modes and singular values and limit the number of modes to be used in wavefront correction. Example singular values and SVD modes for MMDM and PDM can be found in Section 7.4.

"FrontSurfer" perform wavefront correction in a series of iterations. If the residual aberration ϕ_n at the n-th iteration corresponds to the set of actuator signals $\mathbf{X}_n$ then the actuator signals at the next step $\mathbf{X}_{n+1}$ will be determined by expression

$$\mathbf{X}_{n+1} = \mathbf{X}_n - g\mathbf{A}^{-1}\phi_n,$$

where g is the feedback coefficient with value in the range (0..1], $\mathbf{A}^{-1}$ is the pseudo-inverse of $\mathbf{A}$ given by $\mathbf{A}^{-1} = \mathbf{VS}^{-1}\mathbf{U}^T$.

The target wavefront is defined as a combination of Zernike polynomials and can be manually controlled during the correction using arrow keys of the computer keyboard. Examples of Zernike aberrations generated by MMDM and PDM are given in Section 7.4.

7.3 System configuration

OKO Technologies supplies integrated systems, which can be used as a basis for building of applied adaptive optics systems. Applications include scientific instrumentation, astronomy, ophthalmology, laser optics and optical alignment systems.

Our system includes the following components[1]:

- Deformable mirror (MMDM with up to 79 channels or PDM with up to 109 channels).
- PC interface for the deformable mirror (a set of 24-channel PCI DAC boards or 40-channel USB driver modules).
- High-voltage amplifier units for the deformable mirror.
- "FrontSurfer" version for deformable mirrors.
- "FrontSurfer" wavefront sensor; see section 6.2 for available configurations.

[1]The configuration can be customized according to the customer's request

- All necessary cables and documentation.
- Laptop or desktop PC (optional).

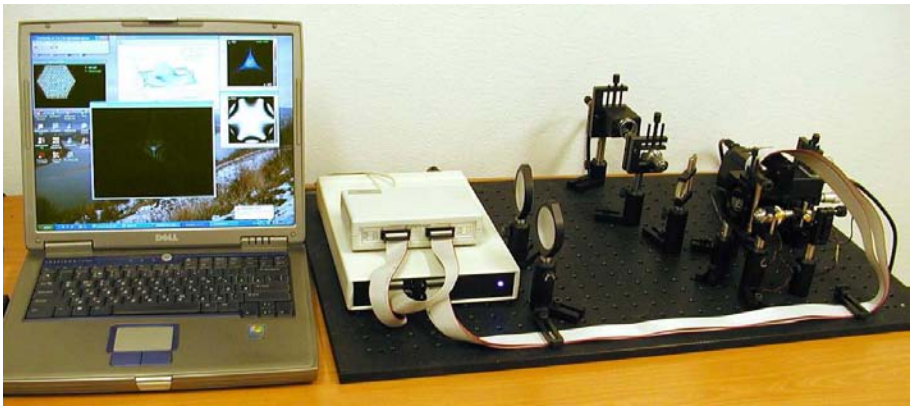

Figure 7.2: *Complete adaptive optical system with a 37-channel PDM.*

OKO Technologies also offers a complete closed-loop adaptive optical system (AOS), which includes all necessary optical and mechanical components (see Figure 7.2). It has a numerical aperture of 1:10 and can be applied for real-time correction of optical aberrations and generation of precision wavefronts. The speed of control depends on the camera and computer; up to 50 frames per second is achieved with a moderately priced camera and a laptop computer.

7.4 AOS testing data

7.4.1 37-channel MMDM system

Experimental singular values for a 37-channel micromachined membrane deformable mirror are given in Figure 7.3; first 20 SVD modes are shown in Figure 7.4.

A flat mirror was used as a reference. Optimization started from the initial shape of the mirror, which was produced by setting all mirror values to zero; this shape is shown in Figure 7.5. As the mirror can be operated only in biased mode, we introduced a bias curvature relative to the reference by adding the Zernike term Z[2,0] with -1 μm amplitude to the target function.

In the first test we generated the spherical wavefront corresponding to the bias curvature - see Figure 7.6. The residual aberrations are shown in Figure 7.7. In the following tests we generated various Zernike aberrations in addition to the bias curvature; the results are shown in Figures 7.8-7.11.

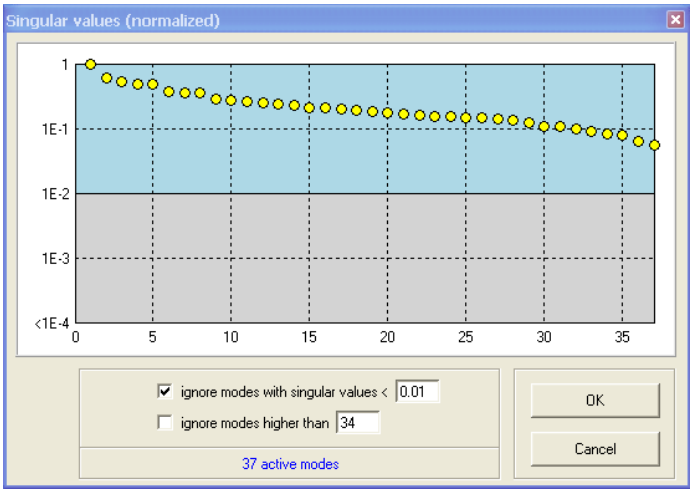

Figure 7.3: *Singular values of a 37-channel MMDM.*

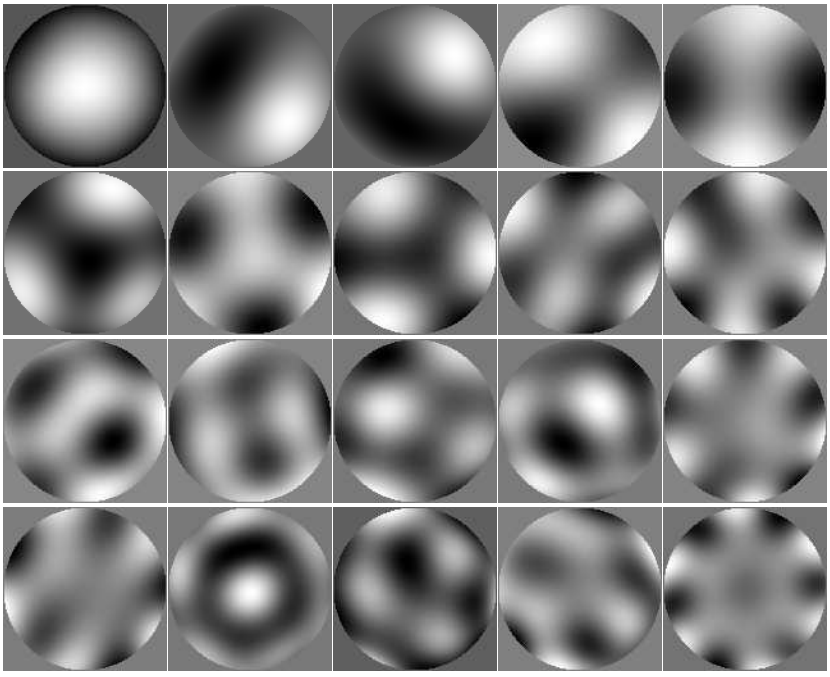

Figure 7.4: *First 20 SVD modes of a 37-channel MMDM.*

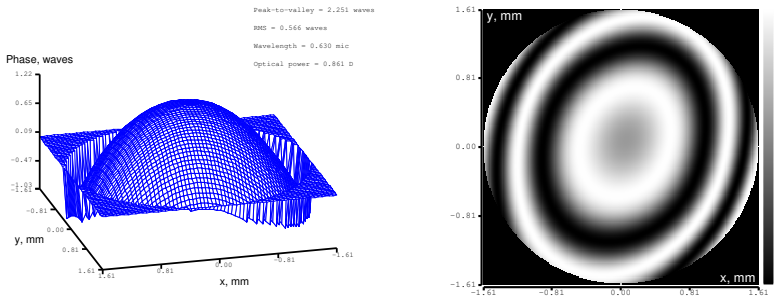

Figure 7.5: *Initial shape of a 37-channel MMDM, which was produced by setting all mirror values to 0.*

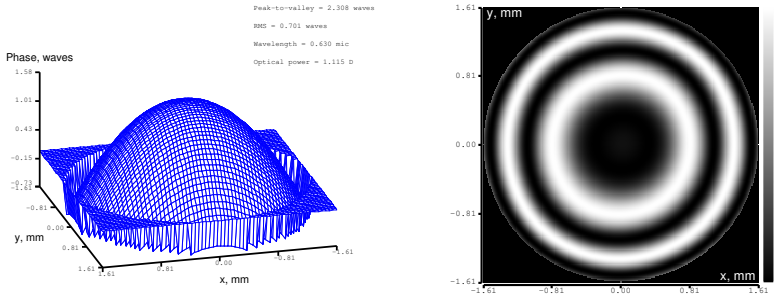

Figure 7.6: *37-channel MMDM; optimization with respect to the reference curvature (Zernike term Z[2,0]=-1 μm).*

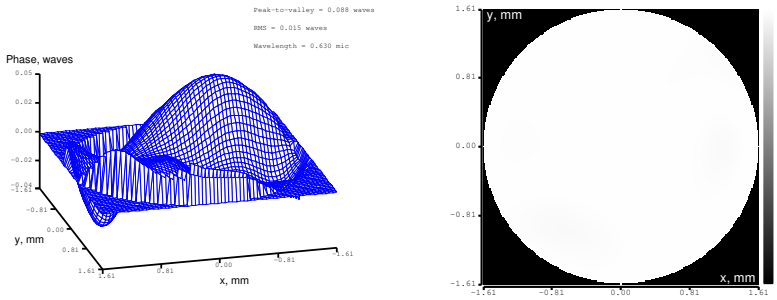

Figure 7.7: *37-channel MMDM, optimization with respect to the reference curvature (Zernike term Z[2,0]=-1 μm); residual aberrations.*

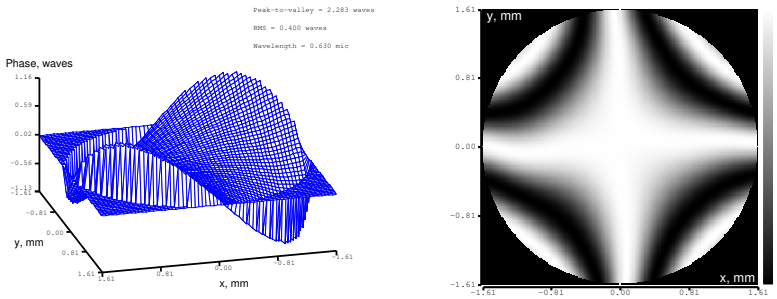

Figure 7.8: *Astigmatism generated by a 37-channel MMDM with respect to the reference curvature, Zernike term Z[2,2], amplitude 1 μm.*

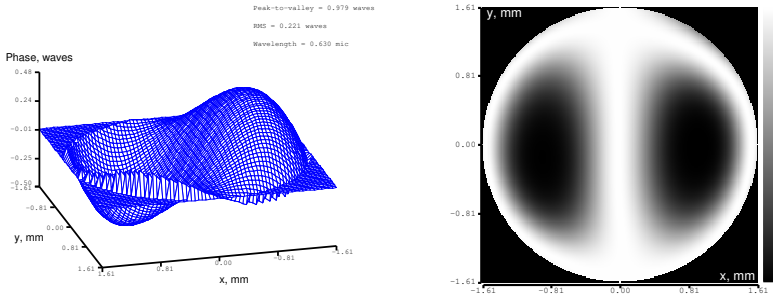

Figure 7.9: *Coma generated by a 37-channel MMDM with respect to the reference curvature, Zernike term Z[3,1], amplitude 0.5 μm.*

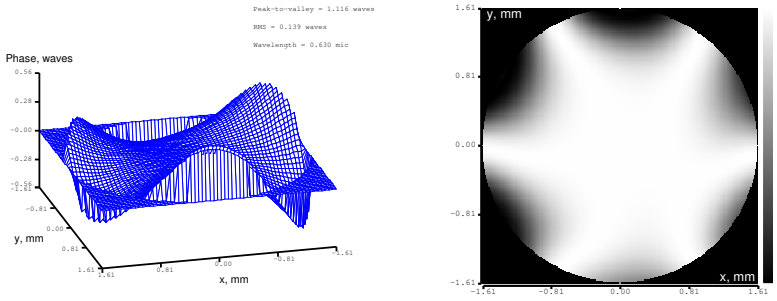

Figure 7.10: *Trifoil generated by a 37-channel MMDM with respect to the reference curvature, Zernike term Z[3,3], amplitude 0.5 μm.*

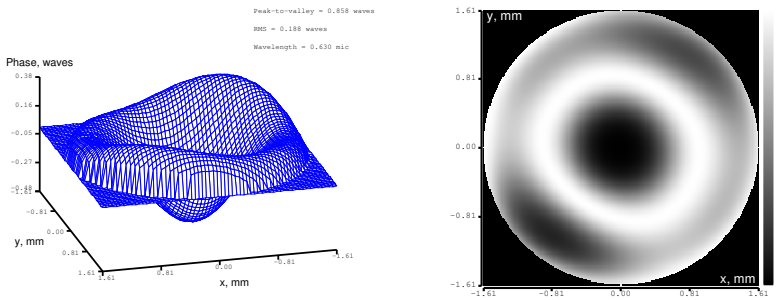

Figure 7.11: *Spherical aberration generated by a 37-channel MMDM with respect to the reference curvature, Zernike term Z[4,0], amplitude 0.3 μm.*

7.4.2 37-channel PDM system

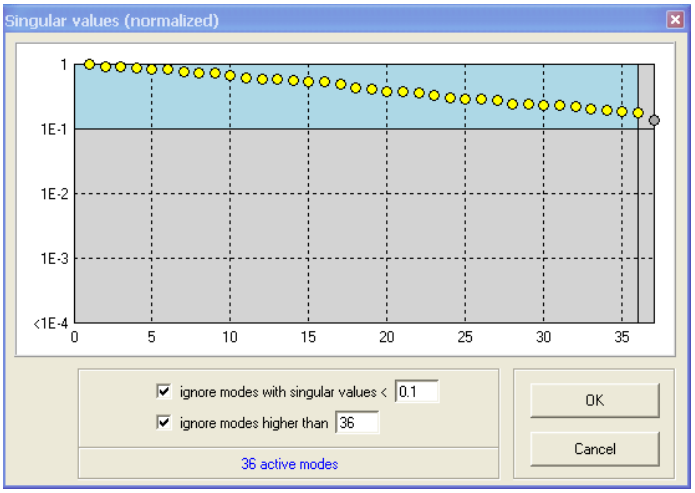

Figure 7.12: *Singular values of a 37-channel PDM.*

Experimental singular values for a 37-channel piezoelectric deformable mirror are given in Figure 7.12; first 20 SVD modes are shown in Figure 7.13.

Flat mirror was used as a reference. Optimization started from the initial shape of the mirror, which was produced by setting all mirror values to zero; this shape is shown in Figure 7.14.

In the first test we optimized shape of the deformable mirror with respect to the reference mirror; residual aberrations are shown in Figure 7.15.

In the following tests we generated various Zernike aberrations in addition

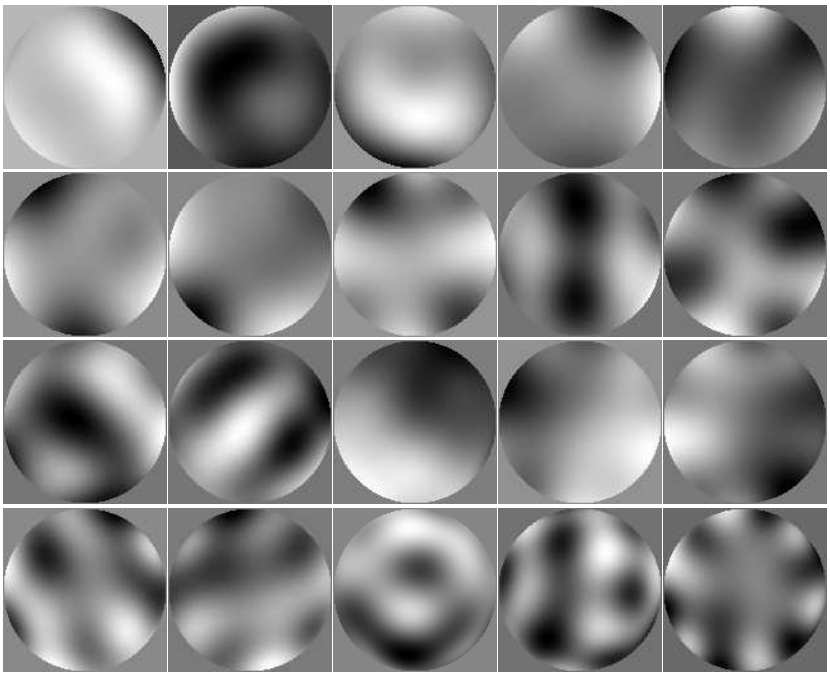

Figure 7.13: *First 20 SVD modes of a 37-channel PDM.*

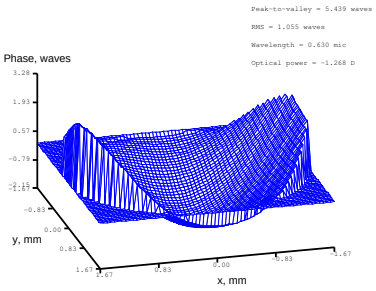

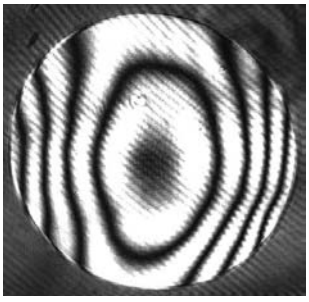

Figure 7.14: *Initial shape of a 37-channel PDM, which was produced by setting all mirror values to 0, with respect to the reference mirror.*

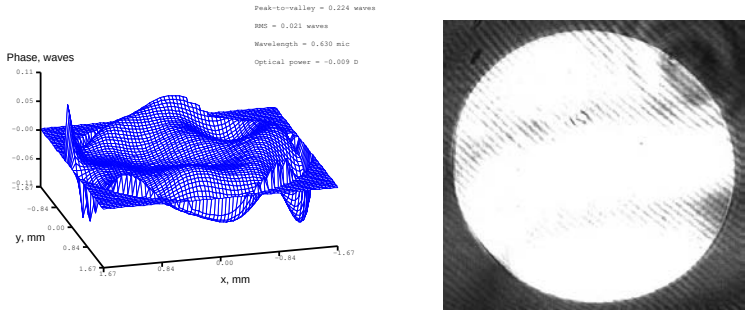

Figure 7.15: *37-channel PDM; optimization with respect to the reference mirror; residual aberrations.*

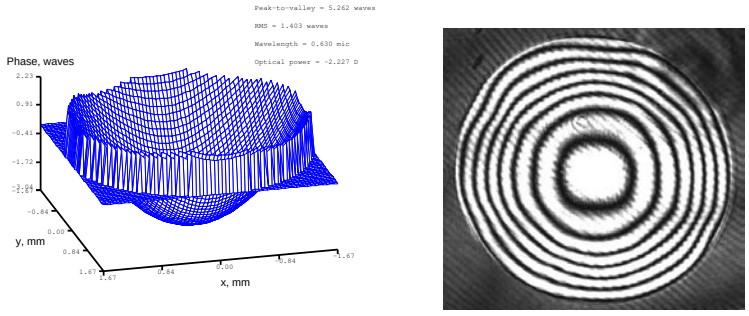

Figure 7.16: *Defocus generated by a 37-channel PDM, Zernike term Z[2,0], amplitude 2 μm.*

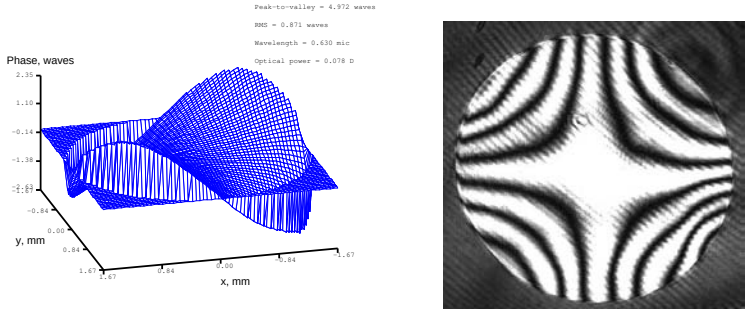

Figure 7.17: *Astigmatism generated by a 37-channel PDM, Zernike term Z[2,2], amplitude 2 μm.*

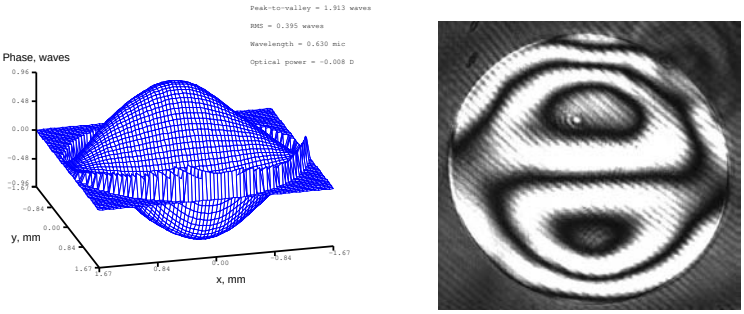

Figure 7.18: *Coma generated by a 37-channel PDM, Zernike term Z[3,1], amplitude 1 μm.*

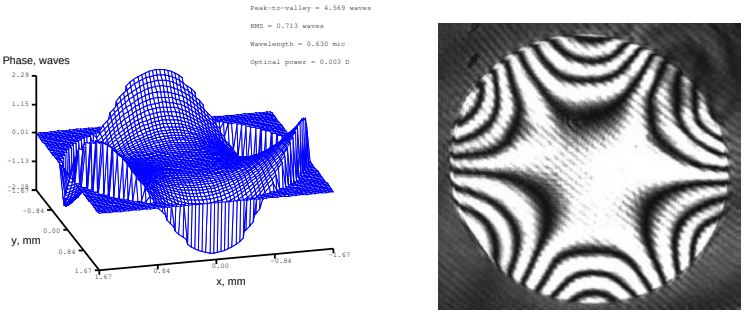

Figure 7.19: *Trifoil generated by a 37-channel PDM, Zernike term Z[3,3], amplitude 2 μm.*

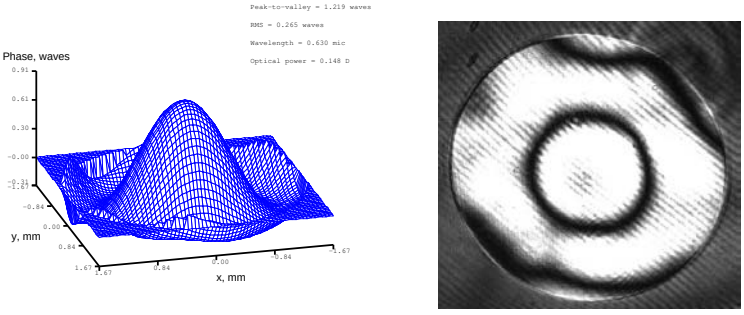

Figure 7.20: *Spherical aberration generated by a 37-channel PDM, Zernike term Z[4,0], amplitude 0.5 μm.*

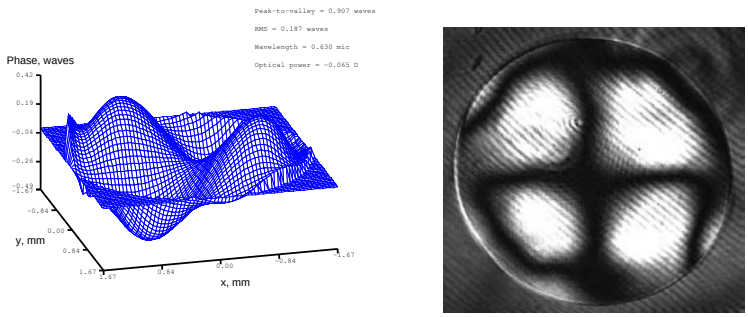

Figure 7.21: *Zernike term Z[4,2] generated by a 37-channel PDM, amplitude 0.5 μm.*

to the bias curvature; results are presented in Figures 7.16-7.21.

8

FREQUENTLY ASKED QUESTIONS

8.1 Deformable mirrors

- *What is MMDM?*

  MMDM stands for "Micromachined Membrane Deformable Mirror".

  MMDMs with 37, 59 and 79 control channels are fabricated by

  > Flexible Optical BV (Okotech), http://www.okotech.com,
  > Röntgenweg 1, 2624 BD Delft, The Netherlands,
  > fax: +31-15-2851548, email: oko@okotech.com.

  MMDM consists of a thin (500 to 700 nm thick) membrane made of silicon nitride. The membrane is coated by a thin layer of aluminum or gold to produce a highly reflective surface. The membrane is fixed to silicon frame and suspended over a number of planar electrodes. When the membrane is electrically grounded and a voltage is applied to one or a number of the electrodes, the membrane is deformed locally changing its shape. Different combinations of voltages applied to different electrodes form different shapes.

- *What is PDM?*

  PDM stands for "Piezoelectric Deformable Mirror". PDMs with 19, 37 and 109 control channels are fabricated by

  > Flexible Optical BV (Okotech), http://www.okotech.com,
  > Röntgenweg 1, 2624 BD Delft, The Netherlands,

fax: +31-15-2851548, email: oko@okotech.com.

- *What is "biased operation"?*

  The MMDM membrane can be deflected only in the direction of the electrode structure because the electrostatic force can be only attractive. The deflected membrane can produce only concave optical shapes. To achieve a bi-directional operation the membrane should be initially deflected towards the actuators and made perfectly spherical by adjusting the actuator voltages. From this state the membrane can be moved to both positive (from the electrode structure) and negative (to the actuator structure) directions by controlling the actuators voltage.

- *How to bias the MMDM?*

  In the simplest case biasing can be achieved by applying a constant voltage to all actuators of the MMDM. Theoretically under the constant bias the MMDM should take a parabolic shape. In practice, MMDM biased with a constant voltage has afigure error of up to 300nm RMS from the nearest perfect parabola. The bias voltages should be adjusted to make the biased surface perfect. The theoretical value of the bias voltage equals to $0.71 \cdot V_{max}$ where V_{max} is the maximum voltage that can be applied to the mirror. This value provides for equal mirror strokes in positive and negative direction from the biased position. For example, with 8-bit digital control (one byte, 0 to 255 per channel) all electrodes should be set to 180. These values should be adjusted to obtain a perfect spherical figure.

- *Is it possible to use MMDM for tilt correction (scanner mode)?*

  The device can be specially calibrated to correct for tilts, preserving the diffraction-limited quality of the reflected beam in the range of about $25\lambda/D$ where Λ is the wavelength and D is the mirror diameter. Using the device in scanner mode will reduce its correction performance for higher order aberrations.

- *How good the mirrors will correct our aberrations?*

  Information about the spatial and temporal spectra of the aberrated wavefronts is required for a good answer to this question. Membrane mirrors in general are good in correcting smooth continuous aberrations. 37-ch MMDM provides high-quality correction of all 3-rd order aberrations and is reasonably good in correcting the 5-th order aberrations. 79-ch MMDM will correct aberrations up to 5th order. PDM with 19 and 37 channels will correct low order aberrations with relatively large amplitude. OKO mirrors can be flattened to produce better than $\lambda/20$

rms reflected wavefronts. Contact OKO with specific questions on the correction performance.

- *How large can be the amplitude of the corrected aberrations?*

  Standard 37-ch 15-mm mirror provides about 20000nm of wavefront deformation for defocus. Third and fifth order aberrations with wavefront amplitudes of up to 3000 nm can be corrected. In general the dynamic range is higher for low spatial frequencies.

  The maximum profile difference between the adjacent actuators reaches 800 nm for MMDM and can be as large as 3 μm for a PDM.

- *How linear is the MMDM response?*

  The displacement of the MMDM surface is proportional to the square of the applied voltage. The mirror response can be linearized using the operation of square root. For 8-bit biased digital control the following expression can be used to convert the control signal CS (in the range -1...1) into the control byte CB applied directly to the digital board controlling the mirror actuator: CB=(int)sqrt(0.5*(CS.))*255.; This formula provides linear correspondence between the control signal CS and the mirror displacement and sets the mirror into theoretical biased position when CS=0. **MMDM features negligible hysteresis**.

- *How linear is the PDM response?*

  OKO piezoelectric mirrors have linear response and feature 7 to 15% hysteresis and up to 2% creep.

- *What is the size of MMDM?*

  As in 2008, OKO Tech fabricates membrane mirrors with diameters of 10, 15, 30, 40 and 50 mm with 1 to 79 channels and linear membrane mirrors with 11x39mm membrane.

- *What is the size of PDM?*

  As in 2008, OKO Tech fabricates 30 mm piezoelectric mirrors with 19 and 37 actuators and 50 mm mirrors with 37, 79, and 109 actuators. Linear configuration with 10x55mm aperture and 20 (2x10) actuators is also available.

- *How good is the initial figure of OKO deformable mirrors?*

  The surface quality of all OKO mirrors is similar to any other solid reflective optics produced by leading manufacturers. It is good enough to work with very low scattering in the whole visible spectrum.

The initial figure of MMDM is flat with RMS deviation from the nearest reference plane better than 400nm. OKO mirror with 37 channels and a diameter of 15mm will have less than 1 fringe of astigmatism averaged over a number of devices. Larger MMDM have 8 adjustment screws that allow to set the initial figure of the mirror. The initial optical quality is very good.

The initial figure of PDM is flat with RMS deviation from the nearest sphere better than 500 nm. The initial surface may have some irregularity due to random hysteresis state of different actuators. These irregularities are always formed as combinations of the mirror influence functions and they are completely correctable by the mirror.

- *What is the power handling ability of OKO DM?*

  Standard 15mm Al-coated MMDM can handle up to 3 W optical load in the visible range. On a special order MMDM can be coated with a special HR metal-dielectric coatings, making them suitable for optical loads of up to 500 W and even 1 kW in some cases.

  Piezoelectric mirrors can be coated with high-power HR coatings, making them suitable for optical load of up to 1 kW and higher - is some special cases.

8.2 Wavefront sensors

- *What is FrontSurfer?*

  FrontSurfer is a wavefront analysis and control system based on Shack-Hartmann wavefront sensors and deformable mirrors from OKO Technologies.

- *What the FrontSurfer system can be applied for?*

  Applications include optical shop testing of transmissive and reflective optics, alignment of optical systems, real-time monitoring and active compensation of optical aberrations.

- *What is included in the FrontSurfer wavefront sensor package?*

  The wavefront sensor package includes FrontSurfer software and a measurement head - Hartmann or Shack-Hartmann wavefront sensor. The Hartmann wavefront sensor consist of a precision Hartmann mask and a CMOS (or CCD) camera. In the Shack-Hartmann sensor, the mask is replaced by a microlens array.

- *Which modifications of FrontSurfer software are available?*

FrontSurfer is available in two modifications - with and without support for deformable mirrors and adaptive optics feedback.

- *How many measurements are required for FrontSurfer to reconstruct a wavefront?*

  One in the absolute measurement mode and two in the reference mode.

- *What is the absolute measurement mode of FrontSurfer?*

  In this mode, the wavefront is reconstructed from one intensity pattern captured by the wavefront sensor. Geometric parameters of the Hartmann mask or microlens array are used as a reference. This mode can only be used with a precision Hartmann mask (or microlens array) having complete hexagonal or square structure of subapertures (for example, see Figure 6.5).

- *What is the reference measurement mode of FrontSurfer?*

  In this mode, the wavefront is reconstructed from two intensity patterns captured by the wavefront sensor. The first one (*main* pattern) is measured in presence of the the aberration to be reconstructed, and the second one (*reference* pattern) is measured for calibration purposes, i.e., with the aberration removed. In this mode, the microlens array (Hartmann mask) can be neither complete nor regular; one can even use an array with random positioning of sub-apertures.

- *What is the sensitivity of FrontSurfer wavefront sensor?*

  Typical configuration of the FrontSurfer wavefront sensor (see parameters in Table 6.1) has a noise-limited sensitivity of about $\lambda/60$ PV (for λ=0.63 μm). The sensitivity can be improved by averaging over multiple frames and using a microlens array with larger focal distance.

- *What is the precision of FrontSurfer wavefront sensor?*

  Typical configuration of the FrontSurfer wavefront sensor (see parameters in Table 6.1) has a precision of about $\lambda/60$ PV (for λ=0.63 μm) in the reference mode and about $\lambda/6$ PV in the absolute measurement mode.

  In the reference mode, the precision is mainly limited by the image sensor noise and can be improved by averaging over multiple frames and using a microlens array with larger focal distance. In the absolute measurement mode, the precision is limited by fabrication errors of the microlens array (or Hartmann mask).

  Please note that the precision is specified for low-order aberrations, when the sampling error can be neglected. It is important that the microlens array (or Hartmann mask) provide sufficient sampling for the aberrations to be measured.

- *Which mask or microlens array can be used with FrontSurfer?*

  In the reference mode, any mask or microlens array with up to several hundred subapertures over the image sensor area can be used. For the absolute measurement mode, a precision array with complete hexagonal or square structure of sub-apertures is required.

- *Which camera can be used with FrontSurfer?*

  FrontSurfer can be interfaced with any camera or frame grabber, but it requires a special video plugin for FrontSurfer. Plugins for Picasso PCI-2SQM framegrabber from Arvoo, DFG/LC1 framegrabber from Imaging Source, A601f/A602f CMOS digital cameras from Basler and UI-2210M/2410M from IDS Imaging are included in the distribution. FrontSurfer manual contains description of the functions that should be included in such a plugin, so that the user can develop his own plugin following these instructions.

- *How to use FrontSurfer wavefront sensor for optical shop testing?*

  Setup for testing of optical components should provide optical conjugation between the component under test and the wavefront sensor with proper scaling. See the section 6.4 for general recommendations and typical measurement schemes.

8.3 Adaptive optical systems

- *What is included in a typical FrontSurfer adaptive optics package?*

  FrontSurfer adaptive optics package includes a deformable mirror with a full set of control electronics and the FrontSurfer wavefront sensor package including FrontSurfer software with adaptive optics enabled.

- *Which deformable mirror can be used with FrontSurfer?*

  FrontSurfer have embedded support of OKO's deformable mirror controllers, including 24-channel ISA and PCI boards and 40-channel USB driver modules. With these features, FrontSurfer can control any mirror from OKO Technologies - MMDM with up to 79 channels and PDM with up to 109 channels - or any custom mirror using the same controllers. Custom controllers can be interfaced to FrontSurfer using external libraries - plugins. FrontSurfer manual contains instructions on development of a custom mirror plugin.

- *How to integrate FrontSurfer adaptive optics package into your application?*

FrontSurfer adaptive optics package can be used for building an adaptive optical system for correction of aberrations. Optical design of the system is dependent on the application and should be made by a specialist. In general, the system should provide optical conjugation between the optical aberrations, deformable mirror and the wavefront sensor with proper scaling.

- *What is the closed-loop correction speed in FrontSurfer?*

  The average correction rate is dependent on the camera and computer. For a PC with AMD Athlon XP1800+ processor and 256 MB RAM, 50 Hz correction rate can be achieved with Basler A602f camera and hexagonal microlens array with 127 subapertures. Using of dual or multi-core processors provides more stable feedback.

- *What is included in a complete adaptive optical system from OKO Technologies?*

  On demand, OKO Technologies can supply a complete closed-loop adaptive optical system (AOS), which includes all necessary optical and mechanical components in addition to the FrontSurfer adaptive optics package. It has a numerical aperture of 1:10 and can be applied for real-time correction of optical aberrations and generation of precision wavefronts. The system is shown in Figure 7.2.

9

WARRANTY AND EXPORT DISCLAIMERS

9.1 Warranty

The equipment is covered by a one-year factory-defect warranty.

We offer separate shipping insurance. The price of the shipping insurance is 2% of the total value of the insured item. Insured items damaged during shipping will be replaced by a similar device within two months. A photo of the damaged device followed by a damage report should be sent to Flexible Optical B.V. (OKO® Technologies) within 5 working days after the damaged device is received.

EXCEPT WHEN OTHERWISE STATED IN WRITING FLEXIBLE OPTICAL B.V. (OKO® TECHNOLOGIES) AND/OR OTHER PARTIES PROVIDE THE EQUIPMENT AND SERVICES "AS IS" WITHOUT WARRANTY OF ANY MERCHANTABILITY AND/OR FITNESS FOR ANY PARTICULAR PURPOSE. THE ENTIRE RISK AS TO THE QUALITY AND PERFORMANCE OF THE EQUIPMENT IS WITH YOU.

IN NO EVENT UNLESS REQUIRED BY APPLICABLE LAW OR AGREED TO IN WRITING WILL FLEXIBLE OPTICAL B.V. (OKO® TECHNOLOGIES) BE LIABLE TO YOU FOR DAMAGES, INCLUDING ANY GENERAL, SPECIAL, INCIDENTAL OR CONSEQUENTIAL DAMAGES ARISING OUT OF THE USE OR INABILITY TO USE THE HARDWARE SOFTWARE AND SERVICES DESCRIBED IN THIS DOCUMENT AND/OR SUPPLIED BY FLEXIBLE OPTICAL BV.

9.2 Export

According to the European export law, a license to export outside the EU should be obtained for any product that matches the definition:

”Deformable mirrors having either continuous or multi-element surfaces, and specially designed components therefor, capable of dynamically repositioning portions of the surface of the mirror at rates exceeding 100 Hz.”

Export inside the EU is free from this restriction. Export to some selected destinations can be or can not be free from this restriction.

Bibliography

[1] R. K. Tyson. *Principles of adaptive optics, second edition*. Academic Press, 1998.

[2] M. C. Roggemann and B. Welsh. *Imaging through turbulence*. CRC Press, 1996.

[3] G. D. Love, editor. *Adaptive optics in industry and medicine*. World Scientific, 2000.

[4] U. Wittrock, editor. *Adaptive optics for industry and medicine*, volume 102 of *Springer Proceedings in Physics*. Springer, 2005.

[5] E. J. Fernandez, I. Iglesias, and P. Artal. Closed-loop adaptive optics in the human eye. *Optics Letters*, 26:746–748, 2001.

[6] O. Albert, L. Sherman, G. Mourou, T. B. Norris, and G. Vdovin. Smart microscope: an adaptive optics learning system for aberration correction in multiphoton confocal microscopy. *Optics Letters*, 25:52–54, 2000.

[7] R. Bartels, S. Backus, E. Zeek, L. Misoguti, G. Vdovin, I. P. Christov, M. M. Murnane, and H. C. Kapteyn. Shaped-pulse optimization of coherent emission of high-harmonic soft x-rays. *Nature*, 406:164–166, 2000.

[8] S. Timoshenko and S. Woinowsky-Krieger. *Theory of plates and shells*. McGraw-Hill, 1953.

[9] A. I. Lourye. Some problems of bending of a thin plate. *Prikladnaja matematika i mehanika (in Russian)*, 4:93–102, 1940.

[10] C. Schwartz, E. Ribak, and S. G. Lipson. Bimorph adaptive mirrors and curvature sensing. *JOSA A*, 11(2):895, 1994.

[11] M. Born and E. Wolf. *Principles of optics*. Pergamon Press, 1993.

[12] Gleb Vdovin, Oleg Soloviev, Alexander Samokhin, and Mikhail Loktev. Correction of low order aberrations using continuous deformable mirrors. *Opt. Express*, 16(5):2859–2866, 2008.

[13] A. Kolmogorov. Dissipation of energy in locally isotropic turbulence. In S. Friedlander and E. Topper, editors, *Turbulence, Classic Papers on Statistical Theory*. Wiley-Interscience, 1961.

[14] J. Y. Wang and J. K. Markey. Modal compensation of atmospheric turbulence phase distortion. *JOSA*, 68:78–87, 1978.

[15] M. Loktev, D. W. De Lima Monteiro, and G. Vdovin. Comparison study of the performance of piston, thin plate and membrane mirrors for correction of turbulence-induced phase distortions. *Optics Communications*, 192:91–99, 2001.

[16] R. J. Noll. Zernike polynomials and atmospheric turbulence. *JOSA*, 66:207–211, 1976.

[17] G. V. Vdovin, N. Kugler, and M. Schacht. Membrane deformable mirrors under cw laser load. *Proceedings of SPIE*, 3762:58–66, 1999.

[18] G. V. Vdovin. Optimization-based operation of micromachined deformable mirrors. *Proceedings of SPIE*, 3353:902–909, 1998.

[19] Gleb Vdovin and Vadim Kijko. Intracavity control of a 200-w continuous-wave nd:yag laser by a micromachined deformable mirror. *Optics Letters*, 26(11):798, 2001.

[20] W. H. Press, S. A. Teukolsky, W. T. Vetterling, and B. P. Flannery. *Numerical recipes in C*. Cambridge University Press, 1997.

[21] A. F. Naumov, M. Y. Loktev, I. R. Guralnik, and G. V. Vdovin. Liquid crystal adaptive lenses with modal control. *Optics Letters*, 23:992–994, 1998.

[22] A. F. Naumov, G. D. Love, M. Y. Loktev, and F. L. Vladimirov. Control optimization of spherical modal liquid crystal lenses. *Optics Express*, 4:344–352, 1999.

[23] M. Y. Loktev. *Modal wavefront correctors based on nematic liquid crystals*. PhD thesis, Delft University of Technology, 2005.

[24] O. Soloviev and G. Vdovin. Hartmann-shack test with random masks for modal wavefront reconstruction. *Optics Express*, 13:9570–9584, 2005.

[25] L. Baker. *C tools for scientists and engineers*. McGraw-Hill, 1989.

[26] C. Paterson, I. Munro, and C. Dainty. A low cost adaptive optics system using a membrane mirror. *Optics Express*, 6:175–185, 2000.

Index